Towards a molecular understanding of the functional role of the Sodium-Potassium Adenosine Triphosphatase in the unconventional secretion of Fibroblast Growth Factor 2

Inaugural dissertation

for

obtaining the doctoral degree

of the

Combined Faculty of Mathematics, Engineering and Natural Sciences

of the

Ruprecht - Karls - University

Heidelberg

Presented by

M.Sc. Jaime Fernández Sobaberas

born in: Madrid, Spain

Oral examination: 2nd March 2026

Towards a molecular understanding of the functional role

of the Sodium-Potassium Adenosine Triphosphatase

in the unconventional secretion of Fibroblast Growth Factor 2

Referees: Prof. Dr. Walter Nickel

Prof. Dr. Sebastian Schuck

Acknowledgments

This acknowledgments is dedicated to the people who formed part and had an influence inside and outside my experience during my doctoral studies.

I would like to thank Prof. Dr. Walter Nickel. Thank you Walter for providing me the opportunity to complete my doctoral studies in the laboratory. This period of my doctoral studies allowed me to experience Science from the first-hand and discover what really Science is all about.

I would like to thank my TAC committee, Prof. Dr. Sebastian Schuck and Prof. Dr. Matthias Mayer. Thank you both for the insightful discussions during meetings. Your input was really appreciated and provided new takes on the project. I would also like to thank Prof. Dr. Michael Brunner, which together with the above mentioned, completes my defense committee.

I would like to thank the Nickel laboratory, including former and current members. You made the lab environment a pleasant and joyful atmosphere to work in. Although there is no formal record or stated direct contribution, that lab environment contributed indirectly to the successes of this project. Always was a pleasure to meet outside of the lab and have fun memories together. Thanks to Annalena and Roberto for introducing me into the group and making the best team fit from the beginning. Thanks to Sabine for the experimental support. Thanks to Julia, Thomas, Fabio and Michael for the scientific feedback and support. Thanks to Ali and Manpreet for the great times and the late stays in the lab. Thanks to Ana Marija for the fun times, and together with Zeynep and Irene for the fortune telling coffee breaks. Thanks to Franzi and Sarah as the best table-partners and having "unconventional" conversations. Thanks to Daniel and Suvi for the nice times together. Thanks to Jutta for the cookie time. Thanks to Anke for the administrative support and socializing organization. Thanks all of you for the enjoyable fun times together.

I would also like to thank the members of the third floor for making the space a pleasurable and supportive environment to work in. I would also like to thank the people involved in the PhD board, with whom I shared great memories throughout the years. It has been a delight to watch our paths develop together and share anecdotes together.

I would like to thank Dr. Eleonora Margheritis and Dr. Katia Cosentino. Thank you both for the magnificent help performing the oligomeric state of FGF2 at the membrane of intact cells.

I would like to acknowledge Dr. Monika Langlotz and the ZMBH Flow Cytometry & FACS Core Facility for facilitating cell line sorting. I would like to acknowledge Dr. Holger Lorenz and the ZMBH Imaging Facility for facilitating access to TIRF microscope. I would like to acknowledge Dr. Hiromi Imamura from Kyoto University for kindly sharing the ATeam sensor.

I would like to thank my girlfriend Valerie. Thank you for accompanying me throughout the master, PhD and beyond. It is so beautiful to share this journey together, with all the great excitements and deepest struggles, always knowing we would be there for each other. Thank you for making this time a wonderful experience. I wonder what will be our next adventures together!

I would like to thank my family. I would like to thank my parents, who supported me throughout my studies. I would have not reached so far without their support. I would like to thank my brother, for the good times we spent growing up together.

And finally, I would like to dedicate this thesis to my mother. Sadly, you left us during the time I was writing this thesis. Now that is finished, this thesis belongs to you…

"Lo único que realmente nos pertenece es el tiempo. Incluso aquel que nada tiene, lo posee."

(Baltasar Gracián)

Abstract

Fibroblast growth factor 2 (FGF2) is exported from mammalian cells via an unconventional secretory pathway that depends on the ability of FGF2 to self-translocate across plasma membranes into the extracellular space. This process is triggered by phosphatidylinositol 4,5-bisphosphate ($PI(4,5)P_2$)-dependent FGF2 oligomerization, inducing the formation of a lipidic membrane pore. The sodium-potassium adenosine triphosphatase (Na^+,K^+-ATPase) participates in the transport of FGF2 into the extracellular space, representing the entry point of this unusual pathway of protein secretion. In this thesis, I contributed evidence for a direct role of the FGF2 residue cysteine 95 (C95) as an essential determinant for membrane-dependent oxidative FGF2 dimerization in a cellular context. This process is further shown to represent a prerequisite for $PI(4,5)P_2$-dependent formation of high-order oligomers, a requirement for FGF2 membrane translocation into the extracellular space. I further show that the Na^+,K^+-ATPase acts as a critical facilitator of this process in a cellular context, as high-order oligomers FGF2 could not be observed under experimental conditions that impair the interaction between FGF2 and the cytoplasmic domain of the α1 subunit of the Na^+,K^+-ATPase. Moreover, I observed that overexpression of a membrane-attached variant of the cytosolic domain of the α1 subunit of the Na^+,K^+-ATPase causes both an increase of FGF2 recruitment at the inner leaflet of the plasma membrane and FGF2 secretion into the extracellular space. My findings suggest that the Na^+,K^+-ATPase enhances the local assembly of FGF2 oligomers and thereby promotes efficient FGF2 membrane translocation to cell surfaces. Together, these findings corroborate the proposed FGF2 secretion mechanism proposed by the group of Prof. Nickel in the recent years. First, FGF2 secretion requires the C95- and $PI(4,5)P_2$-dependent formation of high-order FGF2 oligomers. Second, the Na^+,K^+-ATPase consolidates as the starting point of this unconventional secretory pathway by recruiting and accumulating FGF2 at the inner leaflet of the plasma membrane.

Zusammenfassung

Fibroblast Growth Factor 2 (FGF2) wird in Säugetierzellen über einen unkonventionellen Sekretionsweg in den extrazellulären Raum transportiert. Dieser beruht auf der Fähigkeit von FGF2 in einer Phosphatidylinositol-4,5-bisphosphat ($PI(4,5)P_2$)-abhängigen Weise zu oligomerisieren und eine Membranpore zu bilden. Die Natrium-Kalium-Adenosintriphosphatase (Na^+,K^+-ATPase) ist an der Translokation von FGF2 in den extrazellulären Raum beteiligt und stellt den Startpunkt dieses ungewöhnlichen Sekretionsweges dar. In der vorliegenden Arbeit präsentiere ich Daten, die eine direkte Rolle des FGF2-Restes Cystein 95 (C95) als entscheidenden Faktor für eine membranabhängige oxidative Dimerisierung von FGF2 in Zellen belegen. Diese oxidative Dimerisierung erwies sich in einem zellulären Kontext als notwendige Voraussetzung für die $PI(4,5)P_2$-abhängige Bildung höherer Oligomere, die wiederum essenziell für die Translokation von FGF2 über die Plasmamembran in den extrazellulären Raum sind. Darüber hinaus zeigen meine Ergebnisse, dass die Na^+,K^+-ATPase diesen Prozess in Zellen ermöglicht, da bei Störung der Interaktion zwischen FGF2 und der zytoplasmatischen Domäne der α1-Untereinheit der Na^+,K^+-ATPase, keine Membranporen-bildenden FGF2 Oligomere detektiert werden konnten. Zudem führt die Überexpression einer membrangebundenen Variante der zytosolischen Domäne der α1-Untereinheit der Na^+,K^+-ATPase sowohl zu einer verstärkten Rekrutierung von FGF2 an die Innenseite der Plasmamembran als auch zu einer gesteigerten Sekretion von FGF2 in den extrazellulären Raum. Die Resultate meiner Arbeit unterstützen somit das von der Nickel Arbeitsgruppe in den letzten Jahren erarbeitete Modell des molekularen Mechanismus der FGF2 Sekretion. Auf die initiale Rekrutierung von FGF2 an der Plasmamembraninnenseite durch die Na^+,K^+-ATPase folgt die C95-vermittelte membranabhängige oxidativen Dimerisierung von FGF2 und anschließend dann die von dieser Dimerisierung abhängige Bildung von Membranporen-bildenden höheren FGF2 Oligomeren.

Abbreviations

Table 1. Abbreviations

%	Percent
α1	Alpha 1 subunit of the Na^+,K^+-ATPase
A	Alanine
Å	Angstrom
a-MEM	a-modification of Minimal Essential Medium
ABC	Adenosine trisphosphate-binding cassette
ARF	ADP ribosylation factors
ATP	Adenosine triphosphate
ATP1A1	α-subunit isoform 1, of the Na^+,K^+-ATPase
BMH	Bismaleimidohexane
BMOE	Bismaleimidoethane
bp	Base pairs
BSA	Bovine serum albumin
C	Cysteine
Ca^{2+}	Calcium
CD	Cytosolic Domain
CDB	Cell dissociation buffer
CFTR	Cystic fibrosis transmembrane conductance regulator
CHO cells	Chinese hamster ovary cells
CIP	Calf intestinal phosphatase
cm	Centimeter
CNX	Calnexin
COPI/COPII	Coat protein complex I/coat protein complex II
CRT	Calreticulin
DEAE	Diethylaminoethyl cellulose
DHFR	Dihydrofolate reductase
DMEM	Dulbecco's Modified Eagle's Medium
DMSO	Dimethyl sulphoxide
DNA	Deoxyribonucleic acid
dNTP	Deoxyribonucleotide triphosphate
dox	Doxycycline

DTME	Dithiobismaleimidoethane
DTT	Dithiothreitol
E. coli	Escherichia coli
EDTA	Ethylenediaminetetraacetic acid
EM-CCD	Electron-multiplying charge-coupled device
ER	Endoplasmic reticulum
ERAD	ER-associated degradation
ERES	ER exit site
ERGIC	ER-Golgi intermediate compartment
et al.	Et altera
FACS	Fluorescent activated cell sorting
FCS	Fetal calf serum
FGF	Fibroblast growth factor
FGFR	Fibroblast growth factor receptor
Fig.	Figure
FRET	Förster resonance energy transfer
g	Gravitation
GAG	Glycosaminoglycan
GAPDH	Glycerinaldehyd-3-phosphate-dehydrogenase
GEF	Guanine nucleotide exchange factor
GFP	Green fluorescent protein
Glc	Glucose
GPC	Glypican
GPI	Glycosylphosphatidylinositol
GRASP	Golgi Reassembly-Stacking Protein
GSDMD	Gasdermin D
GSH	Glutathione
GTP	Guanosine triphosphate
GUV	Giant unilamellar vesicle
h	Hour
HCl	Hydrochlorid acid
HEK cells	Human embryonic kidney cells
HeLa cells	Henrietta Lacks cells
HEPES	4-(2-hydroxyethyl)-1-piperazineethanesulfonic acid

HIV	Human immunodeficiency virus
HMW	High molecular weight
HS	Heparan sulfate
HSP	Heat shock protein
HSPG	Heparan sulfate proteoglycan
IL-1β	Interleukin-1β
IHRES	Internal ribosome entry site
K	Lysine
K^+	Potassium
kb	Kilobase
KCl	Potassium chloride
KD	Knock down
kDa	Kilo Dalton
KH_2PO_4	Potassium dihydrogen phosphate
KO	Knock out
LB	Lysogeny broth
LCIS	Live cell imaging solution
L_d or l_o	Liquid ordered or disordered
LMW	Low molecular weight
M	Molar
Man	Mannose
MAPK	Mitogent-activated protein kinase
MATa	a-factor mating pheromone
MCAT	Murine cationic amino acid transporter
$MgCl_2$	Magnesium chloride
mGFP	Monomeric green fluorescent protein
min	Minute
mL	Milliliter
mM	Millimolar
MMLV	Moloney Murine Leukemia Virus
MRA	Mycoplasma removal agent
mRNA	Messenger RNA
ms	Milli-seconds
MVB	Multivesicular body

MW	Molecular weight
n	Number/replicates
Na^+	Sodium
Na_2HPO_4	Sodium hydrogen phosphate
NaCl	Sodium chloride
Na^+,K^+-ATPase	Sodium-potassium ATPase
ng	Nanogram
NLS	Nuclear localization signal/sequence
nm	Nanometer
nM, mM or μM	Nano-, milli- or micro-molar
NP-40	Nonidet P40
P2A	Porcine teschovirus-1 2A
PAGE	Polyacrylamide gel electrophoresis
PAMP	Pathogen-associated molecular patterns
PBS	Phosphate buffered saline
PC	Phosphatidylcholine
PCR	Polymerase chain reaction
Pdf	Probability density function
PDI	Protein disulfide isomerase
PE	Phosphatidylethanolamine
PFA	Paraformaldehyde
PH	Pleckstrin homology
PI	Phosphatidylinositol
$PI(4,5)P_2$	Phosphatidylinositol - (4,5) bisphosphate
$PI(X)P_x$	Phosphatidylinositol phosphate
PLA	Proximity ligation assays
PMPI	N-p-maleimidophenylisocyanate
PVDF	Polyvinylidene fluoride
Q	Glutamine
R	Arginine
RIPA buffer	Radioimmunoprecipitation assay buffer
RNA	Ribonucleic acid
RNAi	RNA interference
rpm	Revolutions per minute

RT	Room temperature
s	Second
SDS	Sodium dodecyl sulfate
SP	Signal peptide
SRP	Signal recognition particle
TANGO1	Transport and Golgi organization protein 1
Tat	Transactivator of transcription
TGN	Trans-Golgi network
TIRF	Total internal reflection fluorescence
TRE	Tet-response element
Tris	Tris[hydroxymethyl]aminoethane
Tween	Polyoxethylene sorbitane monolaureate
U	Units
U2OS cells	Human bone osteosarcoma epithelial cells
UPS	Unconventional protein secretion
v/v	Volume/volume relationship
w/v	Weight/volume relationship
wt	Wild-type
Y	Tyrosine
β	Beta
ΔHS	HS chains removed (via hepIII digest)
µl	Microliter
µm	Micrometer

Amino acids are abbreviated in conventional three letter or single letter code following IUPAC-IUB guidelines[1].

Table of Contents

Table of Contents

List of Figures

List of Tables

Introduction

Protein secretion

Protein localization is crucial for the correct functionality of a cell. In eukaryotic cells, around 30 % of the genome encodes transmembrane proteins and around 10 % of the genome encodes secreted proteins. Secreted proteins follow mainly the classical secretory pathway for the correct localization[2–5]. In recent years, alternative pathways bypassing the classical route have been described, known as unconventional protein secretion (UPS)[6].

Classical secretory pathway

The classical secretory pathway is the main mechanism for protein transport into the extracellular space (Fig. 1). It involves the transport through the organelles endoplasmic reticulum (ER), Golgi apparatus, and the intermediate compartments, including the ER exit sites (ERES), the ER to Golgi intermediate compartment (ERGIC), the Golgi complex and post Golgi network[7].

In order for proteins to follow the classical secretory pathway, proteins must carry a signal peptide. The signal peptide is a specific 16-30 amino acids sequence, containing 6-12 hydrophobic amino acids flanked by positively charged residues. The signal peptide locates at the amino terminus of the nascent polypeptide chain. The signal peptide is recognized during the nascent polypeptide translation, which leads to the recruitment of the protein synthesis complex to the ER[8].

The ER is a net-structured organelle. ER is subdivided into rough and smooth ER. While the rough ER shows an interconnected cisternae complex, the smooth ER presents tubular structures.

The rough ER is specialized in protein synthesis, with ribosomes attaching to the outer face. The smooth ER is specialized in lipid synthesis and carbohydrate metabolism[9].

The signal recognition particle (SRP), a ribonucleoprotein complex of six proteins and an RNA scaffold, recognizes the signal sequence. The SRP holds transiently the elongation, until the SRP binds to the SRP receptor at the ER. The SRP receptor recruits the translocon, a protein-forming channel that serves as a gateway for proteins to be moved across or inserted into the membrane. The translocon is classically formed by the protein complex of Sec61 α1/ß/γ proteins[10]. Once recruited, SRP is released[11]. The SRP and Sec61 complex positioning allow the polypeptide chain to be translocated co-translationally into the lumen of the rough ER. A signal peptidase removes the signal peptide in the lumen[12]. Transmembrane domains contain a stop-transfer-sequence, which opens Sec61α subunit and allows the peptide chain to access the membrane lipid bilayer[13–15]. Multiple transmembrane domains proteins contain several internal signal and stop-transfer sequences, based on the number of the transmembrane domains[16]. Chaperones bind to the nascent polypeptide to facilitate folding, like BiP[17].

At the ER lumen, post-translational modification can be initiated, including glycosylation and disulfide-bridge formation. Glycosylation is the enzymatically-mediated conjugation of a carbohydrate to a protein. Glycosylation can be divided according to the functional group to which the glycan is attached. N-glycosylation attaches the glycan to amino groups, like in asparagine or arginine. O-glycosylation attaches the glycan to hydroxyl groups, like in serine, threonine or tyrosine. Glycans can also be attached to phosphate groups. Glycans can also serve as a linker to bind lipids, as in glypiation, which incorporates a glycosylphosphatidylinositol (GPI) anchor to a protein[18].

Glycosylation is essential for protein folding and quality control in the ER. The mature glycosylation pattern allows the lectins calnexin (CNX) and calreticulin (CRT) to be recruited and promote folding. Finally proteins will be transported to the Golgi apparatus for further processing[19]. Oppositely misfolded proteins are prevented to continue the secretory pathway. The ER-associated degradation (ERAD) pathway recognizes misfolded proteins. The ERAD induces retranslocation into the cytoplasm, where misfolded proteins are ubiquitylated and degraded via the proteasome[20].

Disulfide bridge formation occurs in the ER, which is key for correct protein folding[11]. The ER presents an oxidizing environment, in comparison to the reductive environment of the cytoplasm. The redox environment is established by the glutathione (GSSG : GSH) ratio in these compartments. Protein disulfide isomerases (PDI) and endoplasmic reticulum oxidoreductases regulate disulfide bridge formation in the ER lumen[21]. Also, non-native or folding intermediate disulfide bridges are isomerized by PDI into the correct bond.

After the ER processing, proteins are transported to the following compartments, leaving the ERES to the ERGIC and Golgi complex. Coat protein complex II (COPII) vesicles mediate vesicle formation and facilitate anterograde vesicle transport[22,23]. COPII assemble around the vesicle in two layers: an inner layer of Sar1, Sec23, and Sec24; surrounded by an outer coat of Sec13, and Sec31. Vesicle formation is initiated by the small GTPase Sar1[24]. Sec12, an ER-bound guanine nucleotide exchange factor (GEF), activates Sar1 (Sar1-GDP to Sar1-GTP). Sar1 inserts itself into the ER membrane[23,25], and recruits the heterodimer Sec23/Sec24. Sec23/Sec24 mediate cargo selection[26]. Once the inner coat is formed, Sec13/Sec31 heterodimer is recruited and forms the outer layer, driving vesicle budding[23].

COPII vesicles are 60-90 nm in diameter. Larger cargos require additional auxiliary proteins, such as TANGO1 and cTAGE5[27,28].

Luminal proteins are recruited by binding to cargo receptors, including ERGIC-53 family, Erv family or p24 family[29]. Transmembrane proteins are recruited into vesicles by Sec24. COP II-vesicles bud from the ERES and are received in the ERGIC. The ERGIC is exclusively present in mammalian cells while absent in other eukaryotic cells, reaching the Golgi apparatus directly[30]. Vesicles travel through the microtubule between the organelles[31].

The Golgi apparatus consists of stacked flattened cisternae. The cisternae present a progressive polar display, which translates into both structure and function. Cisternae are subdivided into cis-, medial-, and trans-Golgi cisternae, according to their functionality and location. The cis-Golgi faces the ER and receives ER-vesicles. The trans-Golgi faces the plasma membrane and sorts out the destination of proteins[32,33].

The Golgi apparatus finalizes glycan maturation and sorts proteins trafficking. Additional post-translational modifications can occur in the Golgi apparatus, such as sialic acid addition and tyrosine sulfation[34].

The Golgi apparatus carries protein sorting, which is achieved through vesicular transport. Intra-Golgi transport ensures the correct distribution of protein within the stacked cisternae. Retrograde transport brings proteins from the Golgi apparatus back to the ER. Retrograde transport is mediated by COPI vesicles[4]. COPI complex consists on seven subunits, α, β, β', γ, δ, ε and ζ, which form coatomers around the vesicle[35].

Arf1, a small GTPase of the Ras family, initiates COPI vesicle biogenesis. ARF is post-translationally modified at the N-terminus by the addition of the fatty acid myristate.

Arf1 is activated by the GEF GBF1 (Arf1-GFP to Arf1-GTP). In the GTP-bound form, ARF conformation changes, exposing the myristate, and associates with the membrane. Arf1 inserted into the membrane and recruits the coatomers to the membrane[36].

Luminal proteins that follow the retrograde transport contain the signal peptide KDEL[37]. KDELR recognizes these motifs, binds to an Arf-GEF, and induces vesicle formation[38]. Transmembrane proteins that follow the retrograde transport contain the motifs KKXX or KXKXX. These motifs are recognized by α-COP and β'-COP subunits[37,39].

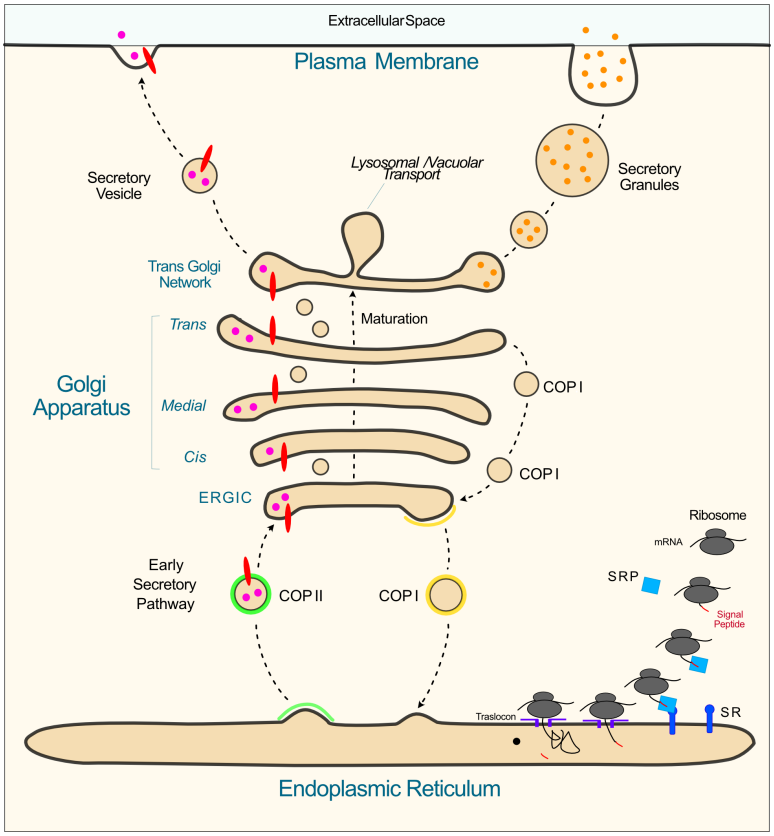

Figure 1. Schematic representation of the conventional secretory pathway.

Proteins that follow the classical secretory pathway are translocated in the ER lumen through the translocon. Proteins undergo the corresponding post-transductional modifications and are properly folded. Subsequently proteins are packaged in COPII vesicles and delivered to the Golgi apparatus. Proteins are sorted and delivered to the extracellular space. *Adapted from Viotti,* 2016 [43].

The trans-Golgi sorts and directs proteins to different cellular compartments, including plasma membrane, endosomes, and secretory granules[40]. Simultaneously, the trans-Golgi receives proteins form the endocytic pathway, like clathrin-mediated endocytosis. Sorting is mediated by the recognition of protein export motifs, post-translational modifications, protein complex formation, and membrane partitioning[40].

In the case of secretion to the extracellular space, two different pathways appear: constitutive and regulated secretion. Constitutive secretion represents a constant flow of vesicles to the plasma membrane, which releases the content to the extracellular space[41]. Regulated secretion consists on the formation of granule vesicles, which restricts the secretion in a localized compartment of the membrane, and is triggered in a signal-dependent manner[42].

Unconventional protein secretion (UPS)

In the recent decades, exceptions to the classical secretory pathway have progressively appear. This includes secreted proteins lacking the signal peptide, bypassing the Golgi apparatus, or translocating directly across the membrane. These alternative pathways are defined as unconventional protein secretion (UPS)[44–46] (Fig. 2). UPS pathways are insensitive to inhibitors of the classical secretory pathway, such as Brefeldin A, Monesin or Nocodazole[47–49]. Around 20 % of the human proteome is estimated to enter the secretory pathway[50].

There are four types of UPS, type I to IV. UPS Type I, II and III consist of soluble cytoplasmic proteins without signal peptide that are transported to the extracellular space. Secreted proteins are active after secretion outside the cell. UPS Type IV consists on transmembrane proteins or signal peptide-containing proteins that reach the ER, but bypass the Golgi apparatus in order to reach be secreted [45,51].

UPS Type I Secretion

UPS Type I consists on the direct translocation across the plasma membrane. This involves pore formation at the plasma membrane.

Fibroblast Growth Factor 2 (FGF2) and the Trans-activator of transcription of the Human Immunodeficiency Virus (HIV-Tat) proteins are two examples following UPS Type I. These proteins interact with phosphatidylinositol 4,5-bisphosphate ($PI(4,5)P_2$) at the plasma membrane and self-oligomerize, leading to a membrane pore with a toroidal structure[45,52,53]. Both proteins also interact with the Na^+,K^+-ATPase at the plasma membrane, having a distinct role in the secretion process[54,55]. After translocation, these proteins bind to heparan sulfate proteoglycans (HSPGs) at the extracellular space[45,56–59].

UPS Type I can also be triggered by inflammation. Interleukin-1β (IL-1β) is an example, which can follow UPS Type I or Type III depending on the cell type. IL-1β follows UPS Type I in pathogen-activated macrophages[60]. After exposure to immunogenic stimuli, including pathogen- or damage- associated molecular patterns (PAMPs and DAMPs, respectively), caspase-1 is activated. Caspase-1 cleaves the inactive synthesized precursor pro-IL-1β into the active form[61]. Caspase-1 also cleaves gasdermin D (GSDMD) into two fragments [62]. The N-Terminal fragment binds to $PI(4,5)P_2$ at the plasma membrane, where it oligomerizes and forms a pore. These GSDMD pores facilitate cytokine release, including IL-1β[63,64].

Tau is another example that can follow different UPS pathways, including type I, III and IV. Tau binds to $PI(4,5)P_2$ at the plasma membrane as well and disrupt the lipid bilayer[65,66]. Tau also binds

to HSPGs at the extracellular space[67,68]. Cholesterol and sphingomyelin also have a role in Tau secretion from cells, as it does in FGF2 secretion[66,69].

Other examples of proteins following UPS Type I are FGF1, FGF12 Annexin A1, Galectin-1 and TG2[51,70].

UPS Type II Secretion

UPS Type II is mediated by ATP-binding cassette (ABC) transporters. ABC-transporters are a family of transmembrane proteins that actively transport proteins across both leaflets of the plasma membrane[71]. ABC transporters consist of two transmembrane domains and two ATP-binding domains[72].

Acetylated apurinic endonuclease-1/redox factor-1 (AcAPE1/Ref-1) is an example of UPS Type II. ABCA1 mediates the secretion, which has a decremental effect on proinflammatory responses[73].

The mating pheromone a-factor (MATa) of *S. cerevisiae* is another example of UPS Type II. Mat a is matured by undergoing post-translational modifications, including carboxymethylation and prenylation. Mat a is exported by Ste6p ABC transporter[74]. The M-factor of *S. pombe* is also secreted via UPS Type II. After S-farnesylation and carboxymethylation, the protein is exported by MAM1 ABC transporter[75].

Other examples of proteins following UPS Type II are Leishmania hydrophilic acylated surface protein B (HASPB) and macrophage migration inhibitory (MIF)[74,76,77].

UPS Type III Secretion

UPS Type III consists on secretion through vesicular intermediates. Some proteins come from endosomes or autophagosomes, which fuse with the plasma membrane and release the content outside[45,78].

Multivesicular bodies (MVBs) are acidic vesicular organelles defined by numerous luminal vesicles. MVBs derive from the endocytic pathway, where plasma membrane and TGN content concentrates and undergoes fission into luminal vesicles. The luminal vesicles are later sorted to the final destination, including the secretory pathway[79]. Proteins can be released to the extracellular space or be secreted in vesicles outside as exosomes[80].

IIL-1β, as described previously (see section *UPS Type I Secretion*), can follow UPS Type I and III. IL-1β follows UPS Type III upon starvation. IL-1β is introduced into the endosome or lysosome, where it matures. The vesicle fuses with the plasma membrane, where active IL-1β is released[81–83]. In other cell types, IL-1β is secreted through the Golgi apparatus reassembly-stacking protein (GRASP) proteins and multi-vesicular-body (MVB) formation[83]. Defects in or inhibition of autophagy prevents IL-1β secretion in these cases[83,84].

In macrophages, transmembrane emp24 domain-containing protein 10 (TMED10) is responsible for the translocation of IL-1β across the membrane. TMED10 locates in the ERGIC and oligomerizes to form a peptide channel. TMED10 requires peptides to be unfolded in order to be translocated (similar mechanism as the ER translocon). TMED10 interacts with unfolded IL-1β in the presence of the cytoplasmic chaperon HSP90A. After exposure to immunogenic stimuli DAMPs and/or PAMPs, HSP90A unfolds IL-1β to be translocated into the ERGIC by TMED10.

In the ERGIC lumen, HSP90B1 folds IL-1β back to the active form. TMED10 knock down and knock out reduced IL-1β secretion[85].

Exosomes have been described to have a strong influence on immune response regulation. Several immune cells, cancer cells, among other cell types, shed exosomes that effect in proliferation of the immune system.[80]

UPS Type IV Secretion

UPS Type IV take proteins synthesized at the ER but secreted bypassing the Golgi complex. As a consequence, these proteins keep the ER glycosylation pattern, with high unprocessed mannose oligosaccharides content[86].

UPS Type IV is induced by ER stress. Cystic fibrosis transmembrane conductance regulator (CFRT) is an example following UPS Type IV. GRASP55 is relocated to the ER upon ER stress, and mediates the vesicular transport of CFRT to the membrane[87,88]. Pendrin also follows UPS Type IV, where HSP70 escorts the bypass of the Golgi complex[89].

UPS Type IV is also induced by mechanical stress. Integrins bypass the Golgi apparatus in Drosophila upon mechanical stress. This is mediated by the GRASP orthologue[45,90,91].

Fibroblast Growth Factor

Fibroblast growth factor family

The fibroblast growth factor (FGF) family is a group of 24 signaling proteins with a mitogenic function involved in development. FGFs present a molecular weight range of 17-34 kDa in size. FGF members share a conserved core that folds into a β-trefoil structure from three 4-stranded

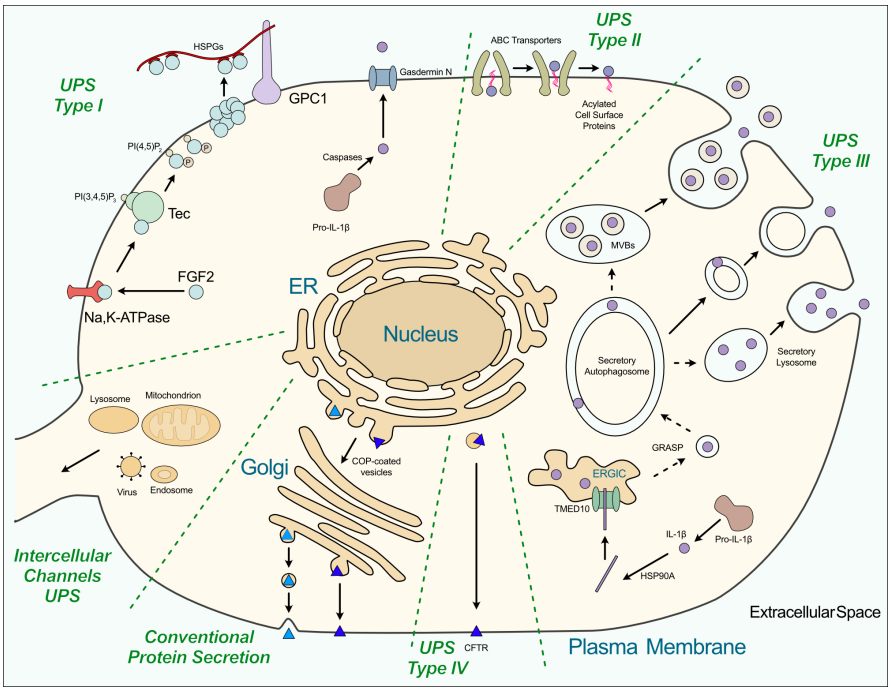

Figure 2. Schematic representation of unconventional secretory pathways.

There are four types of unconventional protein secretion. UPS type I consists on direct protein translocation across the plasma membrane. UPS Type II consists on plasma membrane translocation mediated by ABC transporters. UPS Type III compromises transport through the endocytic compartments. UPS type IV consists on secretion bypassing the Golgi apparatus during transport to the plasma membrane. *Adapted from Pallotta and Nickel, 2020* [6].

β-sheets. This region contains 120-130 amino acids showing 16-65 % sequence similarity[92,93]. FGFs are characterized for their high affinity towards heparin and heparan sulfate proteoglycans (HSPGs). A positively charged binding site within the β1 and β2 loop is responsible for this interaction[94]. The different functionality of FGFs members rely on the high variability of the C- and N-terminus regions[95]. FGFs generally mediate paracrine or autocrine signaling, usually mediated by HSPGs. FGFs binding to HSPGs also protect FGFs from proteolytic degradation[96].

24 members form the FGF family. Only 22 FGF family members are known in humans: FGF1-14 and FGF16-23[97].

The first FGF member was purified from the pituitary glands as a mitogen inducing DNA synthesis[98]. Its high isoelectric point (pI) granted it the name basic FGF (bFGF). Another mitogen

with similar function was later discovered, termed acidic FGF (aFGF) due to its low pI[99–101]. Today aFGF and bFGF are known as FGF1 and FGF2 respectively. FGF1 and FGF2 share another peculiarity. Both lack a N-terminal secretory signal peptide. Still, both are secreted following UPS[102].

Within the FGF2 family, the FGF11-FGF14 form a subfamily, the fibroblast homology factors (FHFs). FHFs are not secreted and do not bind to FGF receptors, although they retain the high affinity toward heparin. Instead, FHFs interact with and regulate voltage-gated sodium channels[103–105]. However, a recent study showed that FGF12 can be unconventionally secreted, potentially following a UPS Type I like FGF2[70].

FGF15/19, FGF21 and FGF23 form another subfamily (FGF15/19 subfamily). These members signal in an endocrine-manner in comparison to the rest of the FGFs[105].

FGF9, FGF16 and FGF20 form another subfamily (FGF9 subfamily). These FGFs follow the classical secretory pathway although they do not contain a classical N-terminal signal peptide. Instead, these FGF members contain an internal non-cleaved hydrophobic sequence, which is crucial for translocation into the ER[106].

Fibroblast growth factor receptor family

FGF members bind to fibroblast growth factor receptors (FGFRs). FGFRs belong to the tyrosine kinase receptors family and contains 4 members (FGFR1-4). FGFRs structure contains an extracellular receptor domain, composed of 3 immunoglobulin-like domains; a transmembrane domain; and an intracellular split tyrosine kinase domain[107,108]. The Ig-like domains and the linker

between dictate FGF binding: I and III regulate ligand binding specificity; I and II inhibit ligand binding[109,110].

FGF/FGFR signaling complex is stabilized by the heparan sulfate chains (HS) of heparan sulfate proteoglycans (HSPGs) at the extracellular matrix. This is known as the ternary signaling complex[111]. The ternary complex is required for FGFs to bind FGFRs. Cells mutants for HS chains expression lack FGF binding to the receptor[112]. Indeed, HS chains enhance FGFs affinity towards the receptors tenfold[113,114]. The main reason is that FGFs at the HS chains resolve as a dimer, which is also the functional conformation for binding the receptor[115].

Upon FGF binding, FGFR undergo full dimerization. The cytosolic domains cross-phosphorylate each other, which recruits proteins containing Src homology-2 (SH2) or phosphotyrosine binding (PTB) domains. FGFR can signal through the RAS/MAP kinase, PI3 kinase/AKT and the phospholipase C-γ (PLC-γ) pathways. Overall these pathways lead to gene expression, cell growth and differentiation, cell survival or apoptosis[116]. Alternatively, FGF signaling disruptions is present in several diseases and cancers[117,118]. Dysregulation of the FGF signaling drives tumorigenesis, both by promoting cell growth, induce epithelial-mesenchymal transition (EMT), and protecting against cell death.

Fibroblast growth factor 2 (FGF2)

Fibroblast growth factor 2 (FGF2) is a strong apoptosis inhibitor and angiogenesis inducer, as well as crucial for embryogenesis and wound repair[119–123]. FGF2 can be translated into 5 isoforms in humans. The low molecular weight (LMW) FGF2 isoform contains 155 amino acids. The LMW FGF2 is translated from the conventional Kozak AUG start codon. This sequence is conserved in all isoforms, and represents the C-terminus for all 5 isoforms. The higher molecular weight (HMW)

isoforms are translated from upstream in-frame CUG codons, which represent alternative translational start sites. The LMW FGF2 molecular weight is 18 KDa; while the HMW FGF2 isoforms weight 34 kDa, 24 kDa, 22,5 kDa and 22 kDa[123].

The C-terminal contains a nuclear localization signal (NLS), hence present in all isoforms. The HMW isoforms additionally contain a classical N-terminal NLS, formed by Glu/Arg repeats. The 34 kDa FGF2 isoform has a third Arg-rich NLS[124–126]. That is the reason leading to the nuclear localization of FGF2 isoforms, especially HMW. The LMW FGF2 isoform localizes both in nucleus and cytoplasm[125]. LMW FGF2 can reach the nucleus by direct translocation or by internalized after receptor binding. In regards with functionality, gene transcription is stronger stimulated upon FGFR activation[127].

LMW FGF2 contains 12 antiparallel β-sheets, folding into a β-trefoil structure (Fig. 3). The complex FGF2/FGFR1/heparin has been crystalized, showing a 2:2:2 stoichiometry[111,128]. FGF2 binds preferentially to FGFR1, although it can also bind to FGFR2 and FGFR4 as well[121].

FGF2 unconventional secretion

The low molecular weight fibroblast growth factor 2 (from now on just referred as FGF2) undergoes unconventional protein secretion type I[6].

The group of Prof. Nickel is pioneer in unrevealing extensively FGF2 secretion pathway. The current-state model on FGF2 unconventional secretion is the following (Fig. 4): FGF2 is expressed in the cytosol in a folded state. FGF2 interacts with the α1 subunit of the sodium-potassium ATPase (Na^+,K^+-ATPase) at the inner leaflet of the plasma membrane[54,130]. FGF2 subsequently binds to the plasma membrane, specifically to the phosphatidyl inositol phospholipids $PI(4,5)P_2$.

FGF2 undergoes self-oligomerization based on disulfide bridge formation. FGF2 oligomerization induces membrane curvature and remodeling until forming a toroidal pore. This membrane structure allows FGF2 to translocate from the inner to the outer leaflet of the plasma membrane. At the outer leaflet of the plasma membrane, heparan sulfate proteoglycans (HSPGs) attract FGF2 and resolves them into FGF2 dimers. The FGF2 dimer can later exert the signaling function in an autocrine- or paracrine- manner[111,128]. FGF2 unconventional secretion in cells is a dynamic and fast process, where translocation takes place within ~200 ms[131].

FGF2 secretion was firstly reconstituted in vitro using affinity-purified plasma membrane inside-out vesicles[132]. In this experiment FGF2 was introduced into the lumen of the inside-out vesicles, while FGF2 was absent in right side-out vesicles. This was the first evidence that FGF2 undergoes direct translocation across the membrane. This translocation is unidirectional, dependent on the correct asymmetric display of the export machinery.

Conventionally, in order for proteins to translocate though biological membranes, proteins require to be in an unfolded state. As discussed during classical secretion (see section *Classical secretory pathway*), proteins are translocated by Sec61 into the ER lumen during translation, while the new peptide has not acquired any folding structure yet[133]. The same remains true for mitochondrial protein transport[134]. Hence, the question whether FGF2 undergoes unfolding for translocation was addressed using FGF2-GFP-DHFR[135]. Dihydrofolate reductase (DHFR) is an enzyme whose folded three-dimensional structure is stabilized by aminopterin[134,136]. FGF2 secretion remained unaltered upon cell treatment with aminopterin. This experiment was evidence that FGF2 remains folded during unconventional secretion.

There have been multiple evidences throughout decades suggesting the role of the α1 subunit of the sodium-potassium ATPase (Na^+,K^+-ATPase) in FGF unconventional secretion. The first

evidences that the Na^+,K^+-ATPase played a role in FGF2 secretion involved experiments with ouabain, an inhibitor of the Na^+,K^+-ATPase, which could prevent FGF2 secretion. Overexpression of ouabain-resistant Na^+,K^+-ATPase rescued FGF2 secretion. However, ion gradient perturbation had no effect on FGF2 secretion[137–139]. Although posterior studies showed that ouabain prevents FGF2 and Na^+,K^+-ATPase interaction[54].

A genome-wide RNAi screen identified the α1 subunit of the Na^+,K^+-ATPase as a component in FGF2 secretion. The α1 subunit of the Na^+,K^+-ATPase was the strongest hit in the screen, while other isoforms of the α subunit of the Na^+,K^+-ATPase or other subunits like the β subunit appeared as negative hits[130].

FGF2 interacts with the α1 subunit of the Na^+,K^+-ATPase at the inner leaflet of the plasma membrane[54]. Specifically, FGF2 binds to the cytosolic domain of the Na^+,K^+-ATPase, in a sub-domain within the third intracellular loop of the Na^+,K^+-ATPase called sub-CD3 (for sub-domain of the Cytoplasmic Domain 3)[54,130]. This sub-CD3 is necessary and sufficient for the interaction with FGF2. Using total internal reflection fluorescence (TIRF) microscopy, α1 was proven to directly recruit FGF2 to the inner leaflet of the plasma membrane. Indeed, the amino acids

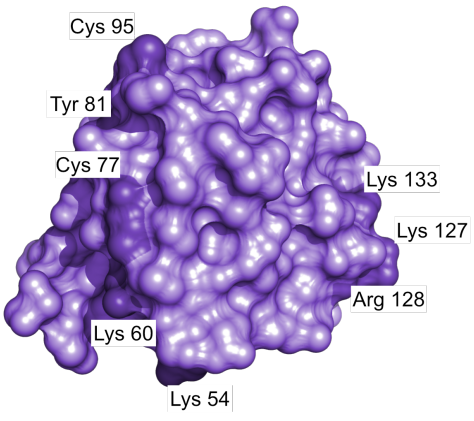

Figure 3. Fibroblast growth factor 2 structure.

The most important amino acids involved in FGF2 UPS are highlighted in a dark colour. These include the residues cysteine 95, involved in FGF2 oligomerization; lysines 54, 60 and cysteine 77, involved in FGF2 interaction with the Na^+,K^+-ATPase; and lysines 127, 133 and arginine 128, involved in FGF2 interaction with $PI(4,5)P_2$ and HSPG. These residues are also refered as cis-elements in FGF2 secretion. *Adapted from PDB structure 1BFF* [129].

involved in this interaction were determined, including the lysine residues K54 and K60 in FGF2 (Fig. 3). This interaction contributes to FGF2 secretion[54].

FGF2 is phosphorylated by Tec kinase at Y81[140]. Interestingly, Tec kinase inhibition decreases FGF2 secretion. Although this indicates a possible role of the Tec kinase in FGF2 unconventional secretion, the function remains unclear[140,141].

FGF2 binds to the inner leaflet of the plasma membrane, specifically through the phosphoinositide $PI(4,5)P_2$[52,142]. FGF2 binds lipids at the plasma membrane, but it was able to discriminate between different PIPs in membrane-like liposomes. FGF2 binds $PI(4,5)P_2$ with the highest affinity[142]. Additionally FGF2 binding to $PI(4,5)P_2$-containing liposomes is promoted by cholesterol- and sphingomyelin- mediated clustering of $PI(4,5)P_2$[142]. The amino acids involved in this interaction include the lysine and arginine residues K127, R128 and K133. K133 is additionally essential for binding to HSPGs[142] (Fig. 3).

At the outer leaflet of the plasma membrane, FGF2 binds to HSPGs[139,143]. FGF2 binding to HSPGs is important for both FGF2 signaling and secretion. Inhibition of HS sulfation in cells using $NaClO_3$ treatment reduced FGF2 secretion[131,143]. FGF2 interaction with HSPGs is mediated by the lysine residue K133[144] (Fig. 3). Recently, Glypican 1 (GPC1) was identified as the HSPGs provider to drive FGF2 translocation[145].

The interaction between FGF2 and $PI(4,5)P_2$ and HSPGs is crucial for FGF2 cell export. $PI(4,5)P_2$ induces FGF2 oligomerization, which remodels the plasma membrane into lipidic pores. The pore-forming capacity of FGF2 was reconstituted in vitro using giant unilamellar vesicles (GUVs)[52,144].

The second factor crucial for FGF2 export is disulfide bridge formation. Both cysteine residues C77 and C95 are important for disulfide bridge formation and FGF2 oligomerization[146]. Indeed, when these residues were substituted (C77A, C95A), FGF2 secretion is impaired.
Neither the α1-subunit of the Na^+,K^+-ATPase nor the Tec kinase are required for the core secretion process. However, a hypothesis evaluated in this thesis suggests that FGF2 dimerization occurs between cysteine residues 95 at the α1 subunit of the Na^+,K^+-ATPase.

FGF2 directionality in the secretory pathway is achieved by the differences in affinity between FGF2 towards the different components of the secretory machinery. FGF2 has higher affinity interaction with heparan sulfates (KD ~ 100 nM) than with $PI(4,5)P_2$ (KD ~ 5-15 μM); and binding is mutually exclusive since both factor share the interaction pocket[142,144,145]. Finally, FGF2 binds to the FGFRs, to which FGF2 has an even higher affinity (KD ~ 20 pM)[147,148].

FGF2 secretion kinetics is established by the correct localization of the different components of the secretory machinery. The kinetics of FGF2 membrane translocation in cells is fast, within ~200 ms[131]. The asymmetric distribution of the components of the plasma membrane enhances the rapid kinetics of FGF2 membrane translocation into the extracellular space[149].

Sodium-potassium ATPase

The sodium-potassium ATPase (Na^+,K^+-ATPase) is an enzymatic active ion antiporter located at the plasma membrane in eukaryotic cells. The Na^+,K^+-ATPase imports two ions of potassium (K^+) and exports three ions of sodium (Na^+) for every ATP molecule consumed. Eukaryotic cells present a high concentration of K^+ and a low concentration of Na^+ intracellularly. This ion gradient is known as the membrane potential. The membrane potential is achieved by the action of the Na^+,K^+-ATPase[150]. The membrane potential is crucial for cell homeostasis, cellular volume,

membrane transport. In specific cell types, like muscles and neurons, is also responsible for the nerve impulse and electrical excitability. The Na^+,K^+-ATPase was first described in 1957[150] and its discovery and enzymatic mechanism study was rewarded with the Nobel prize of Chemistry in 1997.

Na^+,K^+-ATPase belongs to the P-type ATPase family, being the first discovered member of this superfamily[151]. The P-type family can transport ions and phospholipids, being the largest family of ions transporters[152]. The P-type family consists of ATP-dependent transporters, which require a self-phosphorylation step in the mechanism of action[151]. Additionally, P-type ATPase family members interconvert between at least two conformations[153]. P-type ATPases consist of two subunits: the catalytic subunit α, which binds ATP at the cytosolic side; and the regulatory subunit β.

Structure of the Na^+,K^+-ATPase

The Na^+,K^+-ATPase consists of three subunits: the catalytic subunit α, the regulatory subunit β, and the modulatory subunit γ (Fig. 5). Each subunit has several isoforms. For example, there are four isoforms of the α subunit. α1 is expressed ubiquitously, α3 is specific for neurons.

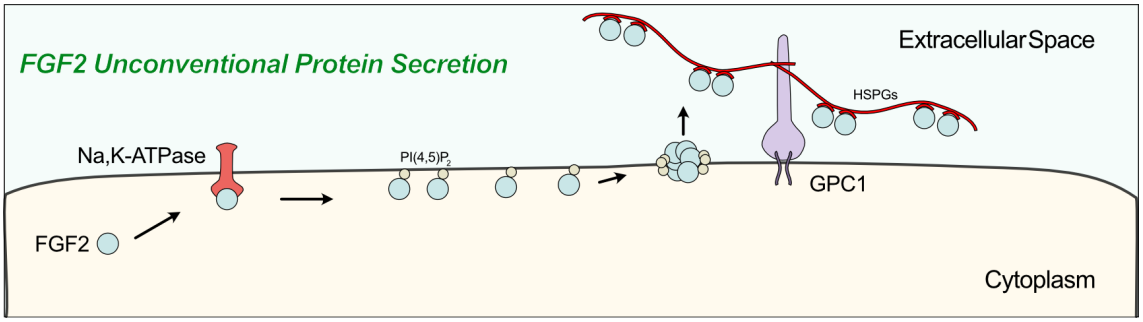

Figure 4. Schematic representation of FGF2 unconventional secretory pathway.

FGF2 is secreted by direct translocation across the plasma membrane. The secretion is dependent on the sequential interactions with Na^+,K^+-ATPase and $PI(4,5)P_2$ at the inner leaflet of the plasma membrane. FGF2 undergoes self-oligomerization and translocates by the formation of a toroidal membrane pore. Cell surface HSPGs capture FGF2 at the outer leaflet of the plasma membrane. *Adapted from Pallotta and Nickel, 2020* [6].

The α1 weighs approximately 110 kDa and consists of mainly transmembrane and cytosolic domains, with a small extracellular portion. The transmembrane portion consists of ten transmembrane helices (M1 to M10). The binding sites for ligands are located between the helices. The cytosolic domains are composed by the extracellular loops between the transmembrane helices, defining three domains: a first N-terminal domain 1, M2-M3 domain 2 and M4-M5 domain 3. The remaining interhelical loops are short and have mainly structural function.

The cytoplasmic region contains additionally three characterized functional domains: an actuator domain (A), a nucleotide-binding domain (N), and a phosphorylation domain (P). The phosphorylation domain contains the canonical DKTGT phosphorylation motif with an aspartic residue (conserved among all P-type ATPases), which is phosphorylated during the pump activity[154]. The nucleotide-binding domain contains the ATP-binding pocket, pointing towards the P-domain, and acts as kinase of the P-domain. The actuator domain dephosphorylates P domain[155]. Additionally, it occludes the ligands-bindings sites. It also transfers the energy from ATP hydrolysis into the transmembrane transport of ligands[156].

The β subunit is expressed as several isoforms as well, from which β1 is expressed ubiquitously. The β1 weights 35 kDa and consists of mainly a transmembrane helical domain and an extracellular domain[157]. The β subunit is glycosylated, and is required for correct folding and membrane localization[158,159]. Oppositely, when the β subunit is palmitoylated and/or glutathionylated, the modification destabilizes the interaction with the α subunit and reduces the pump activity[160,161]. The β subunit associates with the α subunit between M7 and M8 helices with a 1:1 stoichiometry[162]. The β subunit is required for the proper folding, regulation and trafficking of the whole Na^+,K^+-ATPase[163,164], as a functional Na^+,K^+-ATPase pump is composed of an heterodimer[165–169].

The γ subunit consists of a single 8 kDa membrane span, which contains a FXYD motif, a conserved motif between channel modulatory proteins[170]. The γ subunit has a regulatory function, being capable of modifying Na^+,K^+-ATPase affinity towards Na^+, K^+ and ATP[171–174].

α subunit of the Na^+,K^+-ATPase

The existence of several α subunit isoforms was first discovered by their affinity towards ouabain. Ouabain titrations on mouse brain preparation showed biphasic curves on the ATPase activity[175]. While ouabain affinity towards α1 is in the range of mM, ouabain affinity towards α3 is in the range of μM.

The α subunits isoforms 1, 2 and 3 share about 87 % homology, while the α4 isoform shares about 78 % homology with the other isoforms[176]. The α1 isoform is ubiquitously expressed. The α2 isoform is predominantly expressed in the heart, skeletal muscles and brain. α2 has high sensitivity to membrane potential and a reduced affinity for potassium in complex with β2 chain[177]. In combination with the Na^{+3}/Ca^{2+} exchanger, the α2/β2 complex regulate calcium concentration in the heart[178]. The α3 isoform is expressed in neurons, at the dendrites, and hence also highly expressed in the brain[179]. The α3 isoform has a lower affinity towards sodium compared to α1 (25-50 mM vs 10 mM)[180]. That is crucial for α3 role to keep correct sodium concentration during neuronal activity. The α4 isoform is found exclusively spermatozoa cells[181]. Lack of α4 isoform result in male sterile mice[182].

Mechanism and regulation of the Na^+,K^+-ATPase

For each catalytic cycle of the Na^+,K^+-ATPase undergoes two conformational changes, named E1 and E2. The initial conformation E1 state is open towards the cytosol, allowing both ATP and

Na^+ binding. Full Na^+ recruitment to the Na^+,K^+-ATPase induces a conformational change, which leads to ATP hydrolysis at the N domain[183]. The subsequent phosphorylation of the P domain leads to another conformational change, allowing Na^+ export[184]. This consolidates the E2 state, open towards the extracellular space. E2 allows the binding of K^+. After full K^+ recruitment, the dephosphorylation of the P domain follows. The dephosphorylation leads to a conformational change, allowing K^+ import and returning back to the E1 state[185,186]. Hence, a new cycle can start. During each catalytic cycle, the phosphorylation of the aspartate provides the energy to transport ions against the concentration gradient[156].

Cardiotonic steroids (CTS), also known as cardiac glycosides (CG), can interact with the Na^+,K^+-ATPase and inhibit its activity. CTS are natural steroids, mainly found in plants from the genus *Digitalis*. Congestive heart failure patients, which suffer an impairment in the heart's ability to pump, were treated with extracts of these plants already in the 18th century[187].

CTS have a conserved mechanism of action. CTS bind the α subunit at a highly conserved binding-site between the M1/M2, M3/M4 and M5/M6 loops[188–190]. CTS stabilize the Na^+,K^+-ATPase in an E2 intermediate state, which prevents the release of Na^+ ions[191].

The use of CTS against congestive heart failure is due to the relationship between Na^+ and Ca^{2+} ion transport. The Na^+/Ca^{2+} antiporter imports Na^+ and exports Ca^{2+} at the plasma membrane, in favor of concentration gradient. Na^+,K^+-ATPase inhibition upon CTS disrupts the cellular ion transport flow. Ca^{2+} export is prevented due to indirect inhibition of the Na^+/Ca^{2+} antiporter. This increases the intracellular concentration of Ca^{2+}, which also increases the concentration of Ca^{2+} in the sarcoplasmic/endoplasmic reticulum[192]. Upon cardiac stimulation, high concentration of Ca^{2+} is released, which increases the contractility of myocytes, which contributes to overcome congestive heart failure. Therapeutic CTS use is performed at low concentrations. Higher concentrations lead to complete ion flow disruption and hence cardiac arrest.

CTS treatment also can affect other cellular functions related to the Na^+,K^+-ATPase activity, including cellular volume, membrane potential, and Na^+ symport with glucose, amino acids, nucleotides and inorganic phosphate[193].

Interestingly, rodents have adapted to the presence of CTS. Approximately 100-fold concentration is required to reach similar inhibition levels in comparison to other mammals. Two substitutions in the rodent Na^+,K^+-ATPase, glutamine 111 arginine and asparagine 122 aspartate, are responsible for reducing sensitivity towards CTS[194].

Recently complementary functions of the Na^+,K^+-ATPase have been described beyond the main activity as an ion pump. These functions involve ouabain-mediated signaling transduction, where the Na^+,K^+-ATPase act as a signaling scaffold[195–197]. Signaling is mediated by multiple possible

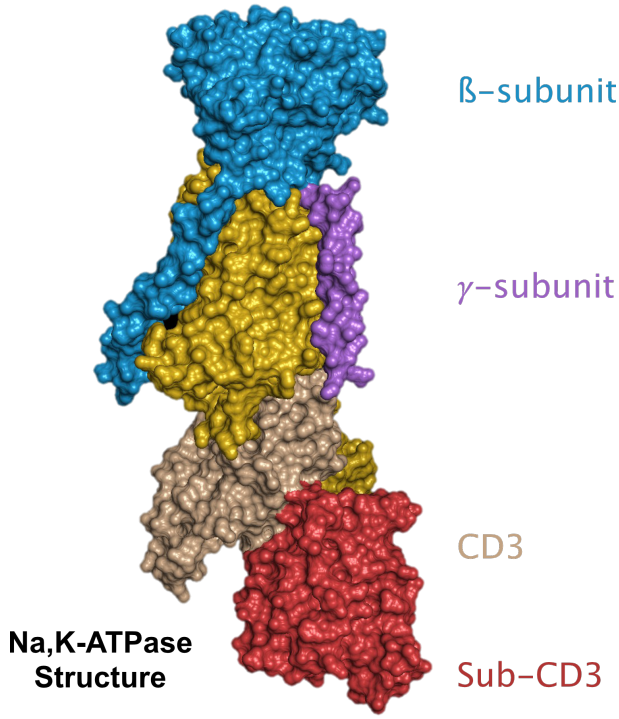

Figure 5. Sodium-potassium ATPase structure.

The sodium-potassium ATPase (Na^+,K^+-ATPase) consists of three subunits: the catalytic subunit α, the regulatory subunit β, and the modulatory subunit γ. The cytosolic domains (CD) of the Na^+,K^+-ATPase can be divided into subdomains, including the CD3 and subCD3 regions, which have a relevant function in FGF2 UPS. *Adapted from Legrand et al., 2020* [54].

downstream effectors, including SRC kinase, inositol 1,4,5-triphosphate receptor (IP3R), caveolin and epidermal growth factor receptor (EGFR)[195–200]; and regulating cellular functions like cell proliferation[201] and apoptosis[202].

Low concentration CTS-binding induces a conformational change, which activates SRC kinase and recruits IP3 and phospholipase C (PLC)[203]. The IP3/IP3R interaction allows the Na^+,K^+-ATPase interact with the ER, inducing the release of Ca^{2+} to the cytoplasm[197,204]. The transient increase in Ca^{2+} activates the transcription factor nuclear factor-κB (NF-κB). NF-κB enhances gene expression promoting cell proliferation and apoptosis inhibition[205]. SRC kinase can also phosphorylate and activate EGFR. EGFR mediates downstream signaling through the Ras-RAF-MAPK signaling cascade, which induces cell proliferation and differentiation[206]. Additionally, ouabain inhibition induces the production of reactive species of oxygen (ROS) via Na^+,K^+-ATPase/Src signaling in a Ras-dependent3 manner[207]. ROS can as well directly alter conformation of the α1 subunit[208–210].

Ultimately, this CTS-mediated signaling transduction function of the Na^+,K^+-ATPase is independent of the ion antiport activity[211]. Finally, binding of CTSs leads to pump endocytosis and degradation in lysosomes[212].

Plasma membrane

Cell membranes are a crucial structure for biological processes. Involves functions like physical support, signaling, substrate transport, protection, among others[213–215]. Biological membranes are composed of lipid bilayers with amphipathic character, which contain a hydrophilic head and hydrophobic hydrocarbon tails. These lipids include glycerophospholipids, sphingolipids and sterols[213].

Phospholipids are the main component of biological membrane. Phospholipids provide the general physical and chemical characteristics to the membrane[216]. Phospholipids are composed of a hydrophilic headgroup and two hydrophobic fatty acids, which differ in headgroup chemistry, fatty acid chain length, and unsaturation number and position. Most known phospholipids include phosphatidic acid (PA), phosphatidyl choline (PC), phosphatidyl ethanolamine (PE), phosphatidyl serine (PS), and phosphatidyl inositol (PI).

$PI(4,5)P_2$ is a rare phospholipid in the plasma membrane of eukaryotic cells, around 1 % of the total phospholipid content in the inner leaflet of the plasma membrane[217]. Still, $PI(4,5)P_2$ plays an important role in the biological process taking place at the plasma membrane. $PI(4,5)P_2$ is crucial for membrane trafficking, cytoskeletal organization, signaling, among other processes[218–223]. Special significance has $PI(4,5)P_2$ contribution in membrane curvature, key for many biological processes, including FGF2 UPS. Also important, $PI(4,5)P_2$ has an asymmetric trans-bilayer distribution, located at the inner (cytoplasm-facing) leaflet of the plasma membrane[224].

Cholesterol is one of the most abundant lipid species. Cholesterol makes up to 25-50 % of the plasma membrane lipids[213,225–227]. Cholesterol possesses a plate-like structure, orientating the polar hydroxyl group towards the end of the lipid bilayer[228]. Cholesterol forms complexes with other lipids at the plasma membrane. These include sphingomyelin and phospholipids[229,230].
Cholesterol modulates plasma membrane physical properties. Cholesterol makes lipid bilayers more rigid, less deformable, decreasing fluidity and permeability[231–233]. Alternatively, at low temperature, highly rigid lipid bilayers; cholesterol increases fluidity. Cholesterol is often found in liquid-ordered domains, in complex with SM and GPI-anchored proteins[234].

Sphingolipids contain sphingosine as a backbone, an amino-alcohol with an eighteen-carbon unsaturated chain[235]. Sphingolipids are divided into ceramides, sphingomyelins (SMs), and glycosphingolipids (GSLs). Ceramides result from the N-acylation of sphingosine. SMs result from the esterification of ceramides with a phospho-choline or phospho-ethanolamine molecule. Sphingomyelin represent the most abundant sphingolipid in mammalian calls. GSLs attach a sugar to the ceramide instead. Depending on the sugar, GSLs are classified as cerebrosides, if a single monosaccharide (glucose or galactose) is attached[236,237]; or gangliosides, if three monosaccharide are attached, one being sialic acid[238]. GSLs are present at the outer leaflet of the plasma membrane, and act as cell antigens.

Cellular membranes are asymmetric, with a different lipid composition between the two leaflets. Cell membranes are fluid, where lipids and proteins rapidly diffuse within the layer. The organization must respond to the dynamic functions required by the cell. PC and SM are more abundant in the outer leaflet; while PS, PE, and PI are present more in the inner leaflet[239]. Consequently, the net charge of the two plasma membrane leaflets differs: while the outer leaflet is positively charged, the inner leaflet is negatively charged.

Nanodomains

Membranes must be organized to respond to the dynamic functions required by the cell. This is achieved by the compartmentalization into membrane domains, which can be classified according to the composition and physical properties. In the plasma membrane there are liquid-disordered phase (l_d) and liquid-ordered phase (l_o). L_d domains are composed of unsaturated lipids, and are highly fluid. l_o domains are composed of high-order, saturated sphingolipids (mainly sphingomyelin) and cholesterol, are less fluid, and are non-ionic detergent-resistant at cold

temperatures[240–244]. L_o domains are present in both leaflets of the plasma membrane. They range in size from 20 to 100 nm, and can reach up to 200 nm[245].

L_o domains or nanodomains are formed following the subsequent model. The high presence of sphingolipids, which have an inverted cone-like shape (head groups occupy a larger area than fatty acid chains), creates voids. The voids are filled by cholesterol molecules, which have cone-like shape. This generates close-packed cholesterol-sphingolipid clusters[246].

Nanodomain formation is not only lipid-dependent, certain proteins can characterize plasma membrane domains. Proteins can associate permanently or transiently to l_o domains. The mechanisms of association l_o domains include hydrophobic transmembrane domains, a hydrophobic protein tail modification, protein-protein interactions and protein-lipid interactions. Among the tail modifications, some relevant modifications include glycophosphatidylinositol (GPI)-anchor (like GPC1)[247–249], N-myristylation (for cytosolic proteins, like SH4 domain-containing proteins)[250] and S-palmitoylation (for integral and peripheral membrane proteins)[251,252]. Caveolin is an example of permanently associated l_o domain protein, which serves as scaffold to recruit other proteins. PI(4,5)P_2 is an example of lipid present in l_o domains, which can recruit other proteins containing Pleckstrin homology (PH) domains[252].

L_o domains are important for signaling and spatial organization. Nanodomains spatial compartmentalization favors signaling transduction for example[234].

Aim of the Thesis

The machinery involved in UPS of FGF2 can be classified as core and auxiliary factors. Auxiliary factors include the Na^+,K^+-ATPase[130,137,138,140] and Tec kinase[52,140,141]. These auxiliary factors mediate the initial steps of the pathway. FGF2 interacts directly with the Na^+,K^+-ATPase[54]. However, the relevance of this interaction is still unknown. Na^+,K^+-ATPase could serve as a landing platform for FGF2 at the inner leaflet of the plasma membrane. An alternative hypothesis suggests that Na^+,K^+-ATPase interaction is required for the maintenance of the plasma membrane potential during FGF2 membrane translocation[253,254].

After the interaction with the Na^+,K^+-ATPase, FGF2 interacts with the $PI(4,5)P_2$ lipids at the plasma membrane, where oligomerization is triggered[52,144,146]. However, the mechanism leading to the transition from the Na^+,K^+-ATPase to $PI(4,5)P_2$ is not well characterized.

Additionally, disulfide bridge formation is crucial for FGF2 oligomerization, pore formation and translocation[51,144,255]. However, the specific contribution of the cysteine residues C77 and C95 to disulfide bridge formation remains unknown. Furthermore, FGF2 oligomerization is triggered at $PI(4,5)P_2$, but the formation of oligomeric intermediates is unknown. Extremely relevant is understanding at what point of the UPS the FGF2 dimer forms. A hypothesis suggests that the Na^+,K^+-ATPase facilitates FGF2 dimer formation. Moreover, the FGF oligomeric size functional for pore formation and translocation is unclear.

In this thesis, I aim to deepen the understanding on the role of the Na^+,K^+-ATPase in FGF2 UPS. Complementarily, I investigate FGF2 oligomerization and the dependance to the secretory machinery, in particular to the Na^+,K^+-ATPase and the $PI(4,5)P_2$ lipids. Additionally, I provide

evidence to identify the functional role of the residues C77 and C95 and the contribution to disulfide bridge formation, together with further observations from other members in the group of Prof. Nickel[256]. I further show that the Na^+,K^+-ATPase acts as a critical facilitator of the PI(4,5)P_2-dependent formation of high-order oligomers in a cellular context. And finally, I studied FGF2 recruitment at the inner leaflet of the plasma membrane and FGF2 secretion into the extracellular space in the context of the overexpression of a membrane-attached variant of the cytosolic domain of the α1 subunit of the Na^+,K^+-ATPase.

All together, the work in this thesis provides further evidences to the current understanding of FGF2 UPS, specifically providing new insights on FGF2 recruitment to the inner leaflet of the plasma membrane, studying the role of the Na^+,K^+-ATPase in FGF2 UPS, refining the function of FGF2 cysteine residues, and characterizing the oligomerization process as FGF2 follows throughout the secretion pathway.

Materials and Methods

Materials

Consumables

Table 2. Consumables

Product	Supplier	Reference number
2 mL Amber Screw Top glass vials	Supelco	507628
Beakers	Schott	-
Cell culture plate 6-, 12-, 24-, 48-, 96- well	Greiner Bio-one	-
Cell culture plates 60, 100, and 150 mm	Greiner Bio-one	-
Cell scraper	Serva	99004
Cryotubes CryoS	Greiner	122263
Falcon tube 15 ml	Greiner Bio-one	188271
Falcon tube 50 ml	Greiner Bio-one	227261
Glass beads 2,85-3,3 mm	Carl-Roth	A557.1
Glass bottom dishes 35mm No 1,5, poly-d-lysine coated	MatTek	P35GC-1,5-10-C
Glass Pasteur pipettes	Brand	747715
Immobilon-FL PVDF Transfer Membrane	Millipore	IPFL00010
LUNA Cell counting slides	Logos Biosystems	L12001
Mobicol filters	MoBiTec	M1003
Nitrile gloves	Starguard	SG-C-L
NuPAGE 4-12 % Bis-Tris gels 1mm x 10 well	Invitrogen	NP0321
NuPAGE 4-12 % Bis-Tris gels 1mm x 15 well	Invitrogen	NP0323
NuPAGE 4-12 % Bis-Tris gels 1mm x 17 well	Invitrogen	NP0323
PCR tubes	Kissler	S0141
Pipette 5 ml	Greiner Bio-one	606180
Pipette 10 ml	Greiner Bio-one	607180
Pipette 25 ml	Greiner Bio-one	760180
Pipette tips (with filter)	Greiner Bio-one	-
Pipette tips filtered (for cell culture)	Greiner Bio-One	-

Pipette tips	Sarstedt	70.3030.XXX
Pipette tips	Sarstedt	70.3030.XXX
Reaction tube 1,5 ml	Sarstedt	72.690.001
Reaction tube 2 ml	Greiner Bio-one	623201
Robust nitrile gloves	TouchNTuff	92-600
Round-bottom polystyrene tubes 5 mL, with cell strainer	Falcon	352235
Round-bottom polystyrene tubes 5 mL	Falcon	352003
SafeSeal 1,5 mL tubes	Sarstedt	72.706
SafeSeal 2 mL tubes	Sarstedt	72.695.500
Syringe filters 0,20 μm Whatmann	Cytiva	10462200
Syringe filters 0,45 μm Whatmann	Cytiva	10462100
Syringes 10 mL	BD Plastikpak	300912
Syringes 50 mL	BD Plastikpak	300865
Vacuum filter	Qpore	500022
Whatman paper 3 mm	Cytiva	742118
μ-Slide 8 well glass bottom dishes	Ibidi	80827

Chemicals and biological reagents

Table 3. Reagents

Product	Supplier	Reference number
1-Ethyl-3-(3-dimethylaminopropyl) carbodiimide (EDC)	Thermo Fisher	22981
1 kb DNA ladder	NEB	N3232
100 bp DNA Ladder	NEB	N3231
2-Bromohexadecanoic acid	Sigma-Aldrich	21604
2-deoxyglucose (2DG)	Sigma-Aldrich	D8375
2-mercaptoethanol	Merck	8.05740
4-succinimidyloxycarbonyl-alpha-methyl-alpha (2-pyridyldithio)toluene (SMPT)	Thermo Fisher	21558
Acetic acid (AcOH)	Sigma-Aldrich	33209
Agarose	Invitrogen	16500-500

Amido black 10 B	Serva	12310.01
Ampicillin sodium salt	Gerbu Biotechnik	1046
Bacto Agar	Becton Dickinson	214010
Bacto Yeast extract	Gibco	80705
Biotin	Sigma-Aldrich	B4501
Bismaleimidohexane (BMH)	Thermo Fisher	22330
Bismaleimidoethane (BMOE)	Thermo Fisher	22323
Blasticidin [10 mg/ml]	ChemCruz	SC-495389
Bovine Serum Albumin (BSA), fraction V	Carl-Roth	8076
Bromophenol blue-NA-salt	Serva	11447413
Calcium chloride ($CaCl_2$)	Sigma-Aldrich	31307
Cell dissociation buffer (CDB)	Gibco	13151-014
Chloroform	Sigma-Aldrich	32211-M
Collagen R (0,2 %)	Serva	47254.01
Complete EDTA-free Protease Inhibitor Cocktail	Sigma-Aldrich	54925800
$CuSO_4$	Sigma-Aldrich	61245
DEAE-dextran	Sigma-Aldrich	78816
Deoxynucleotide (dNTP) Solution Mix	NEB	N0447S
Dimethyl sulfoxide (DMSO)	Sigma-Aldrich	D8418
Disodium hydrogen phosphate dihydrate (Na_2HPO_4)	AppliChem	T877.1
Disuccinimidyl glutarate (DSG)	Thermo Fisher	20593
Dithiobismaleimidoethane (DTME)	Thermo Fischer	22335
DMEM high glucose	Sigma-Aldrich	D6429
DMEM low glucose	Sigma-Aldrich	D6046
Doxycycline	Clontech	564-25-0
Ethanol absolute (EtOH)	Sigma-Aldrich	32205-M
Ethylenediaminetetraacetic acid (EDTA)	Honeywell	34549
EZ-Link-Sulfo-NHS-SS-Biotin	Thermo Fischer	21331
FACS clean buffer	Becton Dickinson	340346
FACS flow buffer	Becton Dickinson	342003
FACS rinse buffer	Becton Dickinson	340345
Fetal Calf Serum (FCS)	Biochrom AG	S0615
G418	Sigma-Aldrich	G8168
Gel Loading Dye, Purple, no SDS (6x)	NEB	B7025S

GFP Booster-AlexaFluor 647	Chromotek (Proteintek)	gb2AF647
Glycerol	Sigma-Aldrich	15523
Glycine	Labochem Int. (neoLAB)	LC-4522.2
HaloTag Oregon Green Ligand	Promega	G2801
Heparinase III	NEB	P0737
HEPES	Sigma-Aldrich	3375
Hoechst 33342 stain	Thermo Fischer	62249
Hydrochloric acid (HCl)	Merck	258148
Isopropanol p.A.	Merck	278475
Kanamycin monosulfate	Sigma-Aldrich	25389-94-0
L-glutamine	Gibco	25030081
Live Cell Imaging Solution (LCIS)	Thermo Fischer	A14291DJ
Magnesium chloride (MgCl2)	Sigma-Aldrich	63068
MEM-Alpha modification	Sigma-Aldrich	M8042
Methanol (MeOH)	Honeywell	32213
Milk powder	Carl Roth	T145.2
Monosodium phosphate (NaH_2PO_4)	Sigma-Aldrich	S0751
Mycoplasma Removal Agent (MRA)	MP Biomedicals	3050044
N-p-maleimidophenylisocyanate (PMPI)	Thermo Fisher	28100
N-succinimidyl 3-(2-pyridyldithio) propionate (SPDP)	Thermo Fisher	21857
Nonidet P-40 (NP-40)	Sigma-Aldrich	492016
NuPAGE 20x MES SDS Running buffer	Invitrogen	NP0002
NuPAGE 20x MOPS SDS Running buffer	Invitrogen	NP0001
OptiMEM	Gibco	11058021
Ouabain oxtahydrate	Sigma-Aldrich	O3125
PageRuler prestained protein ladder	Thermo Fischer	26617
Paraformaldehyde (PFA) 16 % solution	Electron Microscopy Sciences	15710
PBS	Sigma-Aldrich	D8537
Penicillin-streptomycin	Biochrom AG	P06-07050
Pierce Streptavidin UltraLink Resin	Thermo Fischer	53114
Potassium chloride (KCl)	Sigma-Aldrich	31248
Potassium cyanide (KCN)	Sigma-Aldrich	207810
Potassium dihydrogen phosphate (KH_2PO_4)	AppliChem	P018.2
Protease inhibitor mix M	Serva	39102.02

Protease inhibitors	Roche	54925800
Q5 High GC Enhancer	NEB	B9028
Q5 High-Fidelity DNA Polymerase	NEB	M0491S
Q5 Reaction Buffer Pack	NEB	B9027S
Quick-Load Purple 1 kb DNA Ladder	NEB	N0552
QuickExtract DNA Extraction Solution	Lucigen	QE0905T
RedSafe nucleic acid staining solution	iNtRON Biotechnology	21141
Saccharose	Carl-Roth	4621.1
Saponin	Sigma-Aldrich	47036
SDS (sodium dodecyl sulfate)	Bio-Rad	1610301
Sodium azide (NaN_3)	Carl Roth	K305
Sodium chloride (NaCl)	Labochem	LC-59321
Sodium hydroxide (NaOH)	Sigma-Aldrich	30620
Sodium-deoxycholate	Sigma-Aldrich	30970
Streptavidin Sepharose beads	Cytiva	17511301
Triethanolamine	Sigma-Aldrich	90278
Tris base	Carl-Roth	4855.2
Triton X-100	Sigma-Aldrich	T8787
Trypsin-EDTA (0.05 %)	Gibco	25300
Tween-20	Sigma-Aldrich	P9416

Kits and Assays

Table 4. Kits

Product	Supplier	Reference number
DNA Ligation kit	Takara	6022
FuGENE HD Transfection Reagent	Promega	E2311
MBS Mammalian Transfection Kit	Agilent Technologies	200388
NucleoBond Xtra Midi Plus	Macherey-Nagel	740410
NucleoSpin Plasmid Mini Prep kit	Macherey-Nagel	740588
QIAquick Gel Extraction Kit	Qiagen	28704
QIAquick PCR Purification Kit	Qiagen	28106

Zero Blunt® PCR Cloning Kit	Invitrogen	K270020

Antibodies

Table 5. Antibodies

Product	Supplier & Ref. number	WB Dilution
anti-ATP1A1 (α1) Mouse monoclonal	Abcam Ab7671	1:200
anti-ATP1A1 (α1) Rabbit	Affinity purified antibody or unpurified serum	1:500
anti-FGF2 Mouse monoclonal	Thermo Fischer MA1-24682	1:500
anti-FGF2 Rabbit polyclonal	Custom made, Pineda Antibody Service	1:500
anti-GAPDH Mouse monoclonal	Thermo Fisher AM4300	1:20000
anti-GFP Rabbit polyclonal	Custom made, Pineda Antibody Service	1:500
anti-mouse AlexaFluor 488 IgG Goat	Invitrogen A11029	1:500
anti-mouse AlexaFluor 546 IgG Goat	Invitrogen A11030	1:500
anti-mouse AlexaFluor 647 IgG Goat	Invitrogen A21235	1:500
anti-mouse Secondary AlexaFluor680 Goat	Thermo Fisher A21057	1:10000
anti-rabbit AlexaFluor 488 IgG Goat	Invitrogen A11034	1:500
anti-rabbit AlexaFluor 546 IgG Goat	Invitrogen A11035	1:500
anti-rabbit AlexaFluor 647 IgG Goat	Invitrogen A21244	1:500
anti-rabbit Secondary IRDye 800CW Goat	LI-COR Biosciences 926-32211	1:10000

Plasmids

Table 6. Original plasmids

Plasmid	Source
pREV TRE2 FGF2(WT)-Halo	Nickel lab, BZH
pREV TRE2 FGF2(WT)-P2A-GFP	Nickel lab, BZH
pRev TRE2 FGF2(WT)-mGFP	Nickel lab, BZH

TetOn TMD-mGFP	Cosentino lab, CellNanOs
pcDNA(-) ATeam1.03_NL	Imamura lab, Kyoto University

Table 7. Created plasmids

Plasmid
pRev TRE2 Halo
pRev TRE2 FGF2(C77A)-Halo
pRev TRE2 FGF2(C95A)-Halo
pRev TRE2 FGF2(C77A/C95A)-Halo
pRev TRE2 FGF2(K54E/K60E)-Halo
pRev TRE2 FGF2(K127Q/R128Q/K133Q)-Halo
pRev TRE2 FGF2(K54E/K60E/K127Q/R128Q/K133Q)-Halo
pRev TRE2 mGFP
pRev TRE2 TMD-mGFP
pRev TRE2 FGF2(C95A)-mGFP
pRev TRE2 FGF2(K54E/K60E/C77A)-mGFP
pRev TRE2 FGF2(K127Q/R128Q/K133Q)-mGFP
pRev TRE2 FGF2(K54E/K60E/C77A/K127Q/R128Q/K133Q)-mGFP
pRev TRE2 FGF2(K54E/K60E/C77A/C95A/K127Q/R128Q/K133Q)-mGFP
pRev TRE2 SH4-mCherry-CD1-3
pRev TRE2 SH4-mCherry-CD3
pRev TRE2 SH4-mCherry-subCD3
pRev TRE2 SH4-mCherry
pRev TRE2 FGF2(C77A)-P2A-GFP
pRev TRE2 FGF2(C95A)-P2A-GFP
pRev TRE2 FGF2(C77A/C95A)-P2A-GFP
pRev TRE2 FGF2(K54E/K60E)-P2A-GFP
pRev TRE2 FGF2(K54E/K60E/C77A)-P2A-GFP
pRev TRE2 FGF2(K127Q/R128Q/K133Q)-P2A-GFP

pRev TRE2 FGF2(K54E/K60E/K127Q/R128Q/K133Q)-P2A-GFP
pRev TRE2 FGF2(K54E/K60E/C77A/K127Q/R128Q/K133Q)-P2A-GFP

Cell Lines

Table 8. Original cell lines

Cell line	Source
HEK EcoPack 2-293	Clontech
CHO K1 MCAT TAM/CD2	Nickel lab, BZH
CHO 745 MCAT TAM/CD2	Nickel lab, BZH
U2OS MCAT TAM/CD2	Nickel lab, BZH
HeLa S3 MCAT TAM/CD2	Nickel lab, BZH
HeLa S3 FGF2(WT)-IRES-GFP	Nickel lab, BZH
HeLa S3 FGF2(WT)-GFP	Nickel lab, BZH
CHO K1 FGF2(WT)-GFP	Nickel lab, BZH

Table 9. Created cell lines

Cell line
CHO K1 TMD-mGFP
CHO K1 FGF2(WT)-mGFP
CHO K1 FGF2(C95A)-mGFP
CHO K1 FGF2(K54E/K60E/C77A)-mGFP
CHO K1 FGF2(K127Q/R128Q/K133Q)-mGFP
CHO K1 FGF2(K54E/K60E/C77A/K127Q/R128Q/K133Q)-mGFP
CHO K1 FGF2(K54E/K60E/C77A/C95A/K127Q/R128Q/K133Q)-mGFP
CHO 745 TMD-mGFP
CHO 745 FGF2(WT)-mGFP
CHO 745 FGF2(C95A)-mGFP
CHO 745 FGF2(K54E/K60E/C77A)-mGFP

CHO 745 FGF2(K127Q/R128Q/K133Q)-mGFP
CHO 745 FGF2(K54E/K60E/C77A/K127Q/R128Q/K133Q)-mGFP
CHO 745 FGF2(K54E/K60E/C77A/C95A/K127Q/R128Q/K133Q)-mGFP

U2OS TMD-mGFP
U2OS FGF2(WT)-mGFP
U2OS FGF2(C95A)-mGFP
U2OS FGF2(K54E/K60E/C77A)-mGFP
U2OS FGF2(K127Q/R128Q/K133Q)-mGFP
U2OS FGF2(K54E/K60E/C77A/K127Q/R128Q/K133Q)-mGFP
U2OS FGF2(K54E/K60E/C77A/C95A/K127Q/R128Q/K133Q)-mGFP

U2OS Halo
U2OS FGF2(WT)-Halo
U2OS FGF2(C77A)-Halo
U2OS FGF2(C95A)-Halo
U2OS FGF2(C77A/C95A)-Halo
U2OS FGF2(K54E/K60E)-Halo
U2OS FGF2(K127Q/R128Q/K133Q)-Halo
U2OS FGF2(K54E/K60E/K127Q/R128Q/K133Q)-Halo

Hela S3 P2A-GFP
Hela S3 FGF2(WT)-P2A-GFP
Hela S3 FGF2(C77A)-P2A-GFP
Hela S3 FGF2(C95A)-P2A-GFP
Hela S3 FGF2(C77A/C95A)-P2A-GFP
Hela S3 FGF2(K54E/K60E)-P2A-GFP
Hela S3 FGF2(K54E/K60E/C77A)-P2A-GFP
Hela S3 FGF2(K127Q/R128Q/K133Q)-P2A-GFP
Hela S3 FGF2(K54E/K60E/K127Q/R128Q/K133Q)-P2A-GFP

CHO K1 FGF2(WT)-mGFP + SH4-mCherry-CD1-3
CHO K1 FGF2(WT)-mGFP + SH4-mCherry-CD3
CHO K1 FGF2(WT)-mGFP + SH4-mCherry-subCD3

CHO K1 FGF2(WT)-mGFP + SH4-mCherry

CHO 745 FGF2(WT)-mGFP+ SH4-mCherry-CD1-3
CHO 745 FGF2(WT)-mGFP+ SH4-mCherry-CD3
CHO 745 FGF2(WT)-mGFP+ SH4-mCherry-subCD3
CHO 745 FGF2(WT)-mGFP+ SH4-mCherry

U2OS FGF2(WT)-mGFP+ SH4-mCherry-CD1-3
U2OS FGF2(WT)-mGFP+ SH4-mCherry-CD3
U2OS FGF2(WT)-mGFP+ SH4-mCherry-subCD3
U2OS FGF2(WT)-mGFP+ SH4-mCherry

Equipment

Table 10. Equipment

Device	Supplier
Agarose gel chamber	Biorad
Analytical Balance CP64	Satorius
Centrifuge 5404R	Eppendorf
Centrifuge 5417R	Eppendorf
Centrifuge Megafuge 16R	Thermo Fisher Scientific
CO_2-incubator steri-cycle	Heraeus
FACSCalibur Flow Cytometer	Becton Dickinson
Gel Doc XR	BioRad
Heraeus Megafuge 4oR	Thermo Fischer Scientific
Incubation Shakers Infors HT	Multitron
Incubator for bacteria plates	Heraeus
Infinite F50 plate reader	Tecan
Laminar flow hood, Herasafe KS12	Thermo Fisher Scientific
LSM 800 Confocal microscope	Zeiss
LUNA Automated Cel Counter	Logos Biosystems
Magnetic stirrer MR 3000	Heidolph
Microcentrifuge	Neolab

Mini Gel Tank Electrophoresis System	Invitrogen
Mini Trans-Blot® Cell	Biorad
Mini-Trans-Blot system	Biorad
Nanodrop ND-100	Thermo Fischer Scientific
Odyssey CLx Imaging system	LI-COR Biosciences
Olympus xCellence TIRF/Scanner FRAP	Olympus
PCR Thermocycler FG-TC01	FastGene
PCR Thermocycler primus 25	peQLab
PCR Thermocycler primus 96	peQLab
pH-meter 766 Calimatic	Calimatic Knick
Pipets (P2, P10, P20, P200, P1000)	Gilson
Pipette (P2, P10, P200, P1000)	Eppendorf
PowerPac™ HC Power Supply	Biorad
Sonication bath	Bandelin
StepOne Real-Time PCR System	Applied BiosystemsTM
Vortex mixer	Heidolph

Software

Table 11. Software

Product	Supplier
Affinity Designer	Serif Europe Ltd
ApE (A plasmid Editor)	M. Wayne Davis[257]
Benchling	Benchling
Fiji	Schindelin, 2012 [258]
Image Studio Lite	LI-COR Biosciences
Microsoft Office	Microsoft
Olympus xCellence	Olympus
Prism 10	GraphPad
SnapGene	Dotmatics
ZEN (blue edition)	Zeiss
Zotero	Zotero

Methods

Molecular biology methods

E. coli DNA transformation

Calcium competent DH5α *E. coli* cells were aliquoated. 10 % DNA (v/v) was added and mixed together. After incubation at 4 °C for 30 min, bacteria were heat-shocked at 37 °C for 20 s. inmediatly after, bacteria were cooled down at 4 °C for 2 min. 400 µL LB medium (5 g/L NaCl, 10 g/L Tryptone and 5 g/L yeast extract) was added to the bacteria and then incubated (400 rpm 37 °C for 1 h).

Afterwards, transformed bacteria were submitted to selection. If bacterias were transformed in order to expand the DNA, a Miniprep or Midiprep culture was prepare. Bacteria were transferred into a 15 mL tube (for Miniprep) or 250 mL Edenmyer (for Midiprep). 5 mL (for Miniprep) or 100 mL (for Midiprep) LB medium with the specific selection marker antibiotic (25 µg/mL kanamycin or 100 µg/mL ampicillin) was added. Cultures were incubated shaking at 37 °C overnight.

If bacterias were transformed with a mixtrue of DNA to be selected, bacteria were plated on agar plates (LB + 16 g/L agar) containing the specific selection marker antibiotic (25 µg/mL kanamycin or 100 µg/mL ampicillin). Plates were incubated at 37 °C overnight. The next day, single colonies were picked and transferred into a 15 mL tube. 5 mL LB medium with the specific selection marker antibiotic (25 µg/mL kanamycin or 100 µg/mL ampicillin) was added. Cultures were incubated shaking at 37 °C overnight.

In either option, overnight culture is followed by plasmid DNA isolation the next day.

Plasmid DNA isolation

Overnight bacteria cultures were pelleted down at 4000 xg RT for 10 min. Plasmid DNA isolation was performed using NucleoSpin Plasmid Kit for Minipreps or the NucleoBond MIDI Kit for Midipreps (Macherey-Nagel) following manufacturer's instructions. Final DNA elution was performed with 30 µL Tris buffer or water. After isolation, DNA concentration was measured with the spectrophotometer Nanodrop ND-1000 by measuring absorbance at 260 nm (A260). Plasmid DNA from single-colonies selection were sequenced at Microsynth Seqlab. DNA was stored at -20 °C for long-term storage.

Polymerase chain reaction

Polymerase chain reaction (PCR) was used to amplify discrete DNA fragments from existing vectors. Generally, PCR was used to amplify the gene of interest and add restriction enzyme sites. Fragment was after used for the corresponding cloning strategies. PCR fragment was purified by checking the expected size fragment.

PCR reaction was prepared at 4 °C following the protocol below:

Table 12. PCR Mix

Reagent	Volume (µl)
DNA Template (50-100 ng)	-
dNTP mix (10 mM each dNTP)	4
Forward primer (10 pmol/µl)	5
Reverse primer (10 pmol/µl)	5
Q5 5X Reaction Buffer	10
Q5 High GC Enhancer	10
Q5 High-fidelity DNA Polymerase	0,5
H_2O	Until 50 µl final volume

Table 13. PCR Protocol

Step	Temperature (°C)	Duration	Cycles
Initial Denaturation	98	1 min	x 1
Denaturation	98	10 s	
Annealing	60 (adjustable)	20 s	x 30
Extension	72	10 s	
Final Extension	72	2 min	x 1
Cooling	8	∞	x 1

Restriction enzyme digestion

For cloning expression vectors, DNA plasmid was digested with restriction enzyme (RE) (NEB). Purified DNA (5 µg) was mixed in CutSmart buffer (NEB) with 1 µL of RE and water to a final reaction volume of 25 µL. Digestion was performed at 37 °C for 1 h. Vector sample was additionally treated with Quick calf intestinal phosphatase (QuickCIP) at 37 °C for 30 min to dephosphorilate and avoid religation. DNA molecules were purified by gel electrophoresis.

Agarose gel electrophoresis

1 % Agarose gel were prepared in 1x TAE buffer (40 mM Tris, 20 mM acetic acid, 1 mM EDTA). The mixture was solubilized by microwave heating. After cooling and before solidification, RedSafe dye was added. The solution was poured into the gel caster chamber with combs and let solidify. Agarose gel were stored at 4 °C for long-term storage.

DNA samples were prepared by mixing a sample aliquot with 6x purple gel loading dye (NEB). Samples were loaded together with the 1 Kb DNA ladder (NEB). Agarose gel elctrophoresis ran

in 1x TAE buffer at 120 V RT for 15 min. DNA visualization was performed with the Gel Doc 200 system (Bio-Rad).

Desired DNA molecules were purified by cutting the gel band with a sterile scalpel and isolated using the QIAquick Gel Extraction Kit from (Qiagen) following manufacturer's instructions. DNA was eluted in water and stored at -20 °C for long-term storage.

DNA ligation

Ligation reactions were performed using the following proportion:

$DNA\ quantity_{vector}$ (ng) / $DNA\ length_{vector}$ (bp) = $DNA\ quantity_{insert}$ (ng) / $DNA\ length_{insert}$ (bp)

An insert : vector ratio of 3 : 1 and 50 ng of vector were employed. All reagents were added together and ligated using the Takara DNA Ligation Kit at 16 °C for 30 min. As a control for vector self-ligation, a mixture without insert was additionally prepared. Ligation samples were transformed into competent *E. coli* DH5α cells.

Cell biology methods

Cell line maintenance

Chinese Hamster Ovary (CHO) K1 and CHO 745 cells were cultured in Minimal Essential Medium Eagle (α-MEM), Human Embryonic Kidney (HEK) EcoPack 2-293 and Hela S3 were cultured in Dulbecco's Modified Eagles Medium (DMEM) low Glucose (1 g/L) and human bone osteosarcoma epithelial cells (U2OS) cells were cultured in DMEM high Glucose (4,5 g/L). Mediums were supplemented with 10 % heat inactivated Fetal Calf Serum (FCS), 100 U/mL penicillin, and 100 µg/mL streptomycin. α-MEM was further supplemented with 2 mM glutamine.

Cell lines were grown at 37 °C with 5 % CO_2 and with 95 % humidity. Cells were split every 2-3 days. Cells were detached using Cell Disassociation Buffer (Gibco) or Trypsin (U2OS mainly). If necessary, cells were cultivated in collagen-coated dishes. Dishes were filled with a 0,02 % Collagen R (Serva) solution and left air drying under a laminar flow hood.

If cells expressed transgenic constructs under doxycycline-operated promoter, 1 μg/mL doxycycline was added 24 h prior to experiments in order to induce gene expression. Excepcionally, TIRF-based experiments were performed without doxycicline addition.

Cell line freezing and thawing

2X Freezing medium contained 40 % growth medium, 40 % FCS, and 20 % DMSO. Freezing medium was freshly prepared and filtered sterile (0,2 μm).

10 cm plate confluent cells were detached and pelleted down. Cells were resuspended in growth medium and 750 μL were transfered to each cryovial. 750 μL of freezing medium was added and mixed together. Cryovials were stored at -80 °C for a few days, and then transferred into a liquid nitrogen tank for long-term storage.

For thawing, cryotubes were taken from the liquid nitrogen tank and quickly thawed in warm water. Thawed cells were tranfered into 15 mL tubes containing 7 mL of the appropriate growth medium. Cells were pelleted at 1000 rpm RT 3 min and resuspended in 10 mL of growth medium. Cells were transferred into a 10 cm plate and a small aliquot into a 6-well plate. The 10 cm plate was grown for stock freezing, while the 6-well plate was treated with Mycoplasma Removal Agent (MRA) for a week prior to performing any experiment.

Transient transfection

Cells were transfected in 6-well plates or 8-well μ-slide Ibidi chambers. DNA plasmid was diluted in OptiMEM (Gibco) with FuGENE (Promega) in a 1:3 ratio. The mixture was laid RT for 10 min and added dropwise to cells. Transfected cells were studied 24 or 48 h post-transfection according to the experiment.

Stable cell line generation

Stable cell line generation was based on a retroviral transduction system of Moloney Murine Leukemia Virus (MMLV)[139]. HEK EcoPack 2-293 cell line was used for virus production. This cell line was integrated in its genome with the pVPack-Eco packaging system, which stably expressed the retroviral packaging proteins (MMLV Gag, Pol and Env proteins). The gene of interest was cloned into retroviral vectors: pFB-Neo for constitutive expression; or pRev TRE2 for doxycycline-dependent induction.

Retrovirus production was performed based on the modified bovine serum (MBS) Mammalian Transfection Kit (Agilent). On the first day HEK EcoPack 2-293 cells were plated in a 10 cm collagen-coated plate. On the second day, 30 min prior transfection, cell medium was replaced with 6 mL MBS-containing medium (DMEM + 7 % modified bovine serum + 20 μM chloroquine). 9 μg vector DNA diluted in 450 μL sterile deionized water was mixed with 50 μL Solution I and 500 μL Solution II. The mixture was laid RT for 10 min and added dropwise to cells. After 3 h, medium was replaced with growth medium supplmented with 25 μM chloroquine. After 6 h, medium was replaced with 6 mL of growth medium. Growth medium was replaced once again the next morning. 48-72 h post-transfection, the medium supernatant containing retroviral particles was harvested, filtered through a 0,45 μm filter.

Transduction target cells expressed the Tet-On transactivator rtTA2-M2[259] and the murine cationic amino acid transporter MCAT-1[260], which enables cell viral transduction and doxycicline-dependent gene expression respectively[139,259,260].

2,5 mL of filtered virus-containing supernatant was directly added to the target cells. DEAE-dextran was added to target cells to reach a final concentration of 10 µg/ml. 3 h post-transduction, medium was added and incubated for 72 h with viral particles.

Fluorescent-tagged constructs were used to sort positve-cells after 3 consecutive rounds of fluorescence-activated cell sorting (FACS). The first and last sortings were performed under doxycycline expression to select positive-expressing cells, while the second sorting was performed in the absence of doxycycline to remove non-regulated expression in cells.

Halo Tag expressing cell lines were preincubated with the Halo Ligand before FACS sorting following manufacturers´s guidelines.

Ouabain treatment

Ouabain was resuspended in DMSO into the desired concentration (generally 50 µM treatment). U2OS cell line stably expressing tagged FGF2 in a doxycycline-dependent manner were incubated with ouabain for the desired time period in the corresponding growht medium (generally 6 h). TIRF-based experiments were performed without doxycicline addition. Mock condition was treated with the same DMSO concentration (0,1 %) as experimental conditions.

2-bromopalmitate treatment

2-bromopalmitate (2BP) was resuspended in DMSO into the desired concentration (50 µM treatment). Cells were incubated with 2BP in growth medium for 4 h or overnight. TIRF-based

experiments were performed without doxycicline addition. Mock condition was treated with the same DMSO concentration (0,1 %) as experimental conditions.

Biochemical methods

Whole cell lysis

Cells from 6-well confluent plates were detached and transferred to 1,5 mL tubes. Cells were pelleted by centrifugation 500 xg RT 5 min and resuspended in RIPA buffer supplemented with protease inhibitors (Roche). The mixture was incubated at 4 °C for 30 min. Afterwards, samples were centrifuged at 20000 xg 4 °C 10 min and supernatant was collected in a fresh 1,5 mL tube. Samples were mixed with 4x SDS sample buffer and boiled generally at 60 °C for 10 min. After tubes cool down and spin down, samples were either submitted to SDS-PAGE or stored at -20 °C for long-term storage.

SDS-PAGE and Western blot

SDS-Poli-acrylamide gel electrophoresis (SDS-PAGE) was performed using NuPAGE Bis-Tris gels (Invitrogen) with a 4-12 % gradient polyacrylamide concentration. After boiling, samples were loaded together with the Pre-stained PageRuler (Thermo Fisher) protein ladder as molecular weight marker. Gels were run in MOPS SDS Running Buffer (Thermo Fisher) at 200 V for 55 min.

After the SDS-PAGE run, electrotransfer from gel to a PDVF membrane was performed at 100 V for 1 h in blot buffer (40 mM glycin, 25 mM Tris base, and 20 % methanol, final pH 8,4) under cooling. PVDF membrane was activated in methanol for about a minute prior the electrotransfer.

After the electrotransfer, membrane was blocked in 5 % milk PBS (137 mM NaCl, 2,7 mM KCl, 10 mM Na_2HPO_4, 2 mM KH_2PO_4 pH 7,4) RT for 1h or at 4 °C overnight. Antibodies were prepared in PBS-T supplemented with with 3 % BSA and 0,02 % Na-azide. Antibody solutions were stored either at 4 °C or at -20 °C longer-term. Membrane was washed three times with PBS supplemented with 0,05 % Tween-20 (PBS-T). Then primary antibody incubation took place, RT 1 h or 4 °C overnight. Another three washes with PBS-T were performed after. Then secondary antibody incubation was performed RT 30 min. Again three washes with PBS-T were performed prior imaging with the LI-COR Odyssey CLx imaging system. Images were analyzed with Image Studio Lite Software (Version 5.0.21, LI-COR Biosciences).

Cell Surface Biotinylation Assay

FGF2-expressing cells were grown in 6-well plates and treated with doxycycline for 24 h.
Cells were washed with PBS calcium/magnesium (1 mM MgCl2, 0,1 mM CaCl2), and then incubated in the shaker with the biotinylation reagent (600 µl of 1 mg/ml EZ-Link-Sulfo-NHS-SS-Biotin) in cold incubation buffer (150 mM NaCl, 10 mM Triethanolamine pH 9, 2 mM $CaCl_2$) at 4 °C for 30 minutes on ice. Surface proteins were biotinylated with a membrane impermeable biotinylation reagent. The reagent was freshly prepared, dissolved in a basic biotinylation buffer. Afterwards cells were washed once with a glycine-based quenching buffer (100 mM glycine in PBS-Ca/Mg), and then incubated in the shaker with the same quenching buffer at 4 °C for 20 min. Then cells were washed with PBS and incubated at 37 °C for 10 min with 300 µL biotinylation lysis buffer. This is a Nonidet P-40-based lysis buffer (1 % Nonidet P-40, 50 mM Tris-HCl pH 7,5, 62,5 mM EDTA pH 8, 0,4 % sodium-deoxycholate), supplemented with Protease inhibitors (Roche). Cells were scraped and transferred to 1,5 mL tubes. Lysates were sonicated for 3 min in the sonication bath. Then tubes were laid RT for 15 min, with intermittent vortexing every 5 min. Lysates were centrifuged at 20000 xg 4 °C 10 min and supernatant was collected in a fresh 1,5 mL

tube. An aliquot of the supernatant was taken as input, generally 5 % of the volume. The input was mixed with SDS sample buffer and boiled at 95 °C prior to storage.

60 µL Pierce Streptavidin UltraLink Resin per sample were equilibrated with biotinylation lysis buffer three times. Supernatant was mixed with the beads and incubated RT for 1 h. Afterwards, beads were spined down at 3000 xg 1 min and washed with washing buffer. Washing buffer consists of biotinylation lysis buffer supplemented with 0,5 M NaCl. Then three washes were performed using washing buffer with 0,1 % NP-40 (instead of the previous 1 %). Biotinylated proteins were eluted in SDS sample buffer and boiled at 95 °C.

Samples were analyzed using western blot. α-GFP and α-GAPDH antibodies were used, the former to detect FGF2 variants, the latter as loading and cellular integrity control. Signal intensities were adjusted based on loading volume and original sample volume.

Cross-linking experiments

Cells were seeded on six-well plates. FGF2 variants were expressed, either by transtient expression of plasmid transfection or induced expression of stably transduction. Cross-linking experiments were performed as described in my co-authored publication[256].

"Following 48 h of further incubation, whole cell lysates were prepared in a detergent-containing buffer (50 mM HEPES [pH 7,4], 1 % Nonidet P-40, 0,25 % sodium deoxycholate, 50 mM NaCl, 10 % Glycerol, Halt Protease and Phosphatase Inhibitor Cocktail [Thermo Fisher]).

Lysates were incubated on ice for 30 min followed by centrifugation at 20000 ×g for 10 min at 4 °C. Supernatants were subjected to cross-linking reactions using (i) BMH, (ii) PMPI, or (iii) BMOE that were prepared in DMSO and further diluted to a final concentration of 0,2 mM. Following incubation for 30 min at room temperature in the dark, excess amounts of cross-linkers were quenched for 15 min with 50 mM dithiothreitol (DTT). FGF2 cross-linking products were

separated by SDS-PAGE and quantified by western analysis using anti-FGF2 polyclonal rabbit antibody (Custom made, Pineda Antibody Service) and goat anti-rabbit IRDye 800CW (LICOR Biosciences) as secondary antibody[132,135,139]. The ratio of monomeric versus dimeric species of FGF2 was quantified using a LICOR Odyssey imaging system."[256].

Microscopy methods

Confocal fluorescence microscopy

Immunofluorescence staining

Cells were seeded either on 35 mm Glass bottom plates (MatTek) or 8-well, glass bottom µ-slide plates (Ibidi). If necessary, cells were incubated with 1 µg/mL doxycycline 24 h prior imaging. Cells were washed 3 times with PBS and fixed with 4 % PFA for 20 min. Cells were permeabilized with 0,05 % Saponin in PBS for 10 min. Cells were then washed 3 times again with PBS. Samples were blocked with 1 % BSA in PBS for 30 min. Antibodies were prepared in 1 % BSA-PBS. Primary antibody was incubated for 1 h. After three washes, secondary antibody was incubated for 30 min. Finally, cells were wahsed three times again. If nuclei were stained, cells were incubated with Hoechst staining, followed by three washes.
Cells were imaged in PBS on a Zeiss LMS800 confocal microscope. Image processing and analysis was performed with Fiji[258].

Adenosine triphosphate sensor

Cells were seeded either on 35 mm Glass bottom plates (MatTek) or 8-well, glass bottom µ-slide plates (Ibidi). Cells were transiently transduced with pcDNA AT1.03NL to express the adenosine triphosphate (ATP) sensor[261,262]. 24 h post-transfection, cells were washed with PBS three times.

For monitoring real-time the concentration of ATP, cells were imaged live. Prior to imaging, medium was replaced with Live Cell Imaging Solution (Thermo Fisher). Cells were monitored every 30 s for 25 min. Mock or treatment was added by replacing the medium with the indicated treatment.

For longer time-periods monitoring, cells were treated with ouabain (see section *Ouabain treatment*). After the incubation, cells were washed with PBS three times and fixed with 4 % PFA for 20 min. Finally, cells were washed three times again and imaged.

Cells were imaged live on a Zeiss LMS800 confocal microscope. Image processing and analysis was performed with Fiji[258].

Single-molecule total internal reflection fluorescence microscopy

Plasma membrane recruitment assay

FGF2 recruitment was performed using single-molecule total internal reflection fluorescence (TIRF) microscopy[54,131,263]. An Olympus IX81 xCellence inverted TIRF microscope equipped with an Olympus PLAPO ×100/1.45 Oil DIC objective lens and a Hamamatsu ImagEM Enhanced (C9100-13) camera was used. Images were exported in the Tagged Image File Format (TIFF) and analyzed with Fiji[54,131,258].

Cell lines used in real-time single-molecule TIRF recruitment assay were CHO K1 expressing FGF2-mGFP in a doxycycline-dependent manner and the corresponding SH4-mCherry-α1 CD variant in a stable manner. Cells were seeded on 8-well, glass bottom µ-slide plates (Ibidi) 24 h before imaging without doxycycline induction. Cells were washed three times with Live Cell Imaging Solution (Thermo Fisher) and left in this medium during imaging. TIRF images were acquired as time-lapse videos using an Olympus 488 nm, 100 mW diode laser to excited GFP

fluorescence. Widefield images were acquired with an MT 20 illumination system to select frames of cells.

FGF2-mGFP recruitment efficiency at the inner leaflet of the plasma membrane was quantified and normalized to both cell surface area (μm^2) and FGF2-mGFP (or mGFP) expression level (average intensity with average background subtraction). FGF2-mGFP expression level corresponded to the quantified expression of the first frame of TIRF time-lapse video. The Fiji plugin TrackMate with Log G detector[264] was used to quantify single fluorescent particles using a blob diameter of 0,7 µm. Data was normalized to wild-type cells or mock conditions. The plotted data correspond to the average value from minimum three independent experiments, each with a minimum of 20-30 cells analysed per experiment.

Determination of the oligomeric size distribution of FGF2-mGFP by single particle brightness analysis

FGF2 stoichiometry at the plasma membrane was deterimined based on brightness analysis using monomeric GFP (mGFP = eGFP-A206K) as a standard[265–267]. GFP A206K substitution was used to ensure FGF2 oligomerization was not triggered by GFP dimerization.

Cell lines used expressed stably either TMD-mGFP or FGF2-mGFP variants in a doxycycline-dependent manner with/without the corresponding SH4-mCherry-α1 variant in a stable manner. Cells were detached and seeded on glass microscopy chips without doxycycline induction. Cells were washed 3 times with PBS before and after being fixed in 4 % PFA for 20 min. Chips were maintained in PBS, stored at 4 °C and used for imaging within 24 hours.

Single-particle brightness stoichiometry analysis was performed as described in my first-authored preprint[268].

"Cells with low levels of FGF2-GFP expression were selected to maintain a single-molecule imaging regime and properly focused using a region of interest (ROI) of 256 x 256 pixels. Imaging

was subsequently conducted in a region adjacent to the one used for selection, ensuring it had not been previously exposed to avoid measurements being compromised by bleaching. All samples were imaged on a custom-designed TIRF microscope[269] for a total of 1500 frames under a 50 ms exposure time. Excitation from a 488 nm laser at about 200 W/cm2 (Sapphire, Coherent) was coupled into a single mode polarization maintaining fiber to a TIRF module connected to an Olympus IX83 inverted microscope with a hardware autofocus system (IX3-ZDC, Olympus) and a 100x oil-immersion objective (UPLAPO100xOHR). Images were additionally magnified by 1,6x (IX3-CAS, Olympus) to obtain a final magnification of 160x and a pixel size of 100 nm. Fluorescence was filtered by a four-line polychroic mirror (zt405/488/561/640rpc, Chroma, 3 mm) and rejection band filter (zet405/488/561/647 TIRF, Chroma), and the emission was focused on an iXon Ultra EM-CCD Camera (Andor Technologies).”[268].

“The calibration dataset necessary to calculate the intensity of monomeric GFP was obtained by sampling TMD-mGFP expressing cells. Images obtained from TIRF microscopy were analysed through a single-molecule brightness analysis utilizing the Stoichiometry Analysis Software (SAS)[270]. Briefly, bright spots were automatically detected using an implementation of the Difference of Gaussians method combined with thresholding. The selected particles were defined using a ROI with a defined pixel size and were fitted to two-dimensional (2D) Gaussian models. The background was subtracted by defining a second ROI around the particle’s ROI with a larger pixel size. The brightness value for each detected spot was then provided by the algorithm. To avoid overlapping ROIs or multiple particles in the same ROI, localized particles were filtered based on the distance between two ROIs. The distribution of all the brightness values was plotted as a kernel probability density function (Pdf). The mean monomer intensity and standard deviation, calculated in the calibration phase from monomers of the GFP dataset, were used to define the theoretical intensity of possible higher-order oligomeric species. This approach generated a linear combination of Gaussians, which was then used to fit the experimental Pdf. Percentages of occurrence of oligomeric species of FGF2 were calculated from the area of each fitted Gaussian.

Values were corrected for partial fluorescence efficiency of GFP. Detection parameters were configured as follows in SAS: camera pixel size (nm): 100, camera quantum efficiency: 95, camera offset: 170, camera EM gain (counts per photoelectron): 65,4, maximum sigma: 200. Analysis parameters were set as: labeling efficiency (for GFP): 70, maximum Gaussian mixtures: 30 (max).”[268].

The plotted data correspond to the average value from minimum three independent experiments, each with a total of 40-50 cells and a minimum of a total of 1500 particles being analysed per experiment. Data was corrected for partial fluorescence of GFP in particles, 70 % folding efficiency was considered[266,267].

The experiments and analysis for the determination of the oligomeric state of FGF2-mGFP were performed in collaboration with Dr. Eleonora Margheritis from the group of Prof. Katia Cosentino at the Department of Biology/Chemistry and Center for Cellular Nanoanalytics (CellNanOs) from the University of Osnabrück.

Statistical analysis

Statistical analyses were performed using GraphPad Prism version 10. Data representation and statistical analysis was adjusted to the experimental conditions. The data representation and statistical analysis used in each experiment was specified in the legend of each figure, as well as the number of replicates (n). Generally, data was shown as mean ± SD, with statistical significance indicated as follows: non-significant (ns) $p > 0,05$; * $p \leq 0,05$; ** $p \leq 0,01$; *** $p \leq 0,001$; **** $p \leq 0,0001$.

Results

The residue C95 is essential for the formation of FGF2 dimer

The cross-linking assay is established to measure FGF2 dimer formation in cells

FGF2 secretion is dependent on oligomerization. FGF2 oligomerization is driven by the formation of disulfide bridges. Disulfide bridges require the presence of cysteine residues, the only biological amino acid containing a thiol side chain. Particularly, FGF2 residues cysteine 77 and 95 are known to play a role in FGF2 secretion. Substitution of cysteine residues 77 and 95 into alanines (C77/95A) leads to impair secretion of FGF2[255]. However, additional data suggest different roles of the different cysteine residues.

Previous evidences indicate that the FGF2 dimer is the predominant oligomer form at the inner leaflet of the plasma membrane[131]. And I hypothesized that the dimer is the building block to form high-number oligomer species. Hence, it is crucial to understand the structure of the FGF2 dimer. However, cysteine residues 77 and 95 contribution to the formation of disulfide bridges and FGF2 dimers in a cellular context remains unknown.

One approach to discriminate the role of the cysteine resdiues 77 and 95 in FGF2 oligomer formation and secretion is to determine their role in dimer formation. To study the potential roles of the residues C77 and C95 in FGF2 oligomerization, I decided to conduct FGF2 cross-linking experiments in cells. Cross-linking experiment allow the stabilization and visualization of the crosslinked dimer from the extracted cell lysates.

In order to perform these experiments, I had to establish a cross-linking protocol and optimize the conditions for the reaction in cell lysates. The first approach was to use the combination of

the cross-linkers bismaleimidohexane (BMH) and dithiobismaleimidoethane (DTME). Both cross-linkers contain two maleimide groups separated by a 13 Å length spacer. However, DTME cross-link can be reversed: the spacer arm contains a disulfide bridge, which can be broken by the reduction of the thiol groups. This provided an elegant method to stabilize and identify dimers by cross-linking, and consuming the dimers into monomeres by the addition of reducing agents, such as 2-mercaptoethanol (β-ME).

For that purpose, I selected Hela S3 expressing FGF2 as a FGF2-IRES-GFP. The internal ribosome entry site (IRES) allows the tranlsation into a protein with a 5' cap-independent initiation, allowing policistronic RNAs to be translated into independent peptide chains[271]. Hence, these cells expressed FGF2 untagged from GFP. Cells were lysed and cross-linked with BMH and DTME. The corresponding aliquotes were mixed with sample buffer with addition or absence of 2-mercaptoethanol and analyzed by western blotting (Fig. 6A). Under optimized conditions, I was able to visualize the FGF2 monomer (18 kDa, labeled with '#') and FGF2 dimers (36 kDa, labeled with '##') only in the presence of cross-linker. The FGF2 dimer was robustly present when cross-linked with BMH in the presence and absence of 2-mercaptoethanol. Meanwihle the FGF2 dimer was sublimely present when cross-linked with DTME in the absence of 2-mercaptoethanol and was missing in the presence of 2-mercaptoethanol. This result provides clear evidence FGF2 dimer formation in cells could be stabilized with the use of cross-linkers for experimental analysis.

Another aspect to consider that can influence the efficiency of the cross-linking reaction is the presence of reporter tags fused to FGF2. For that reason I decided to perform the cross-linking reaction in various cell lines expressing FGF2 with differently tagged versions.

I studied Hela S3 FGF2-IRES-GFP, CHO K1 FGF2-GFP and U2OS FGF2-Halo upon cross-linking (Fig. 6.B). GFP and Halo Tag have different structural and electrostatic properties.

Independently, FGF2 dimers were identified in the western blot in the presence of cross-linker, while no dimer was present in the absence of cross-linker. Although dimer formation was similar within the three cell lines, the untagged FGF2 showed a clearer dimer band compared to the tagged version.

The cross-linker screening optimizes the experimental conditions for the assay

Once confirmed that using cross-linkers to visualize and analyze FGF2 dimer formation was a viable approach, I continued to optimize the experimental protocol by varying different

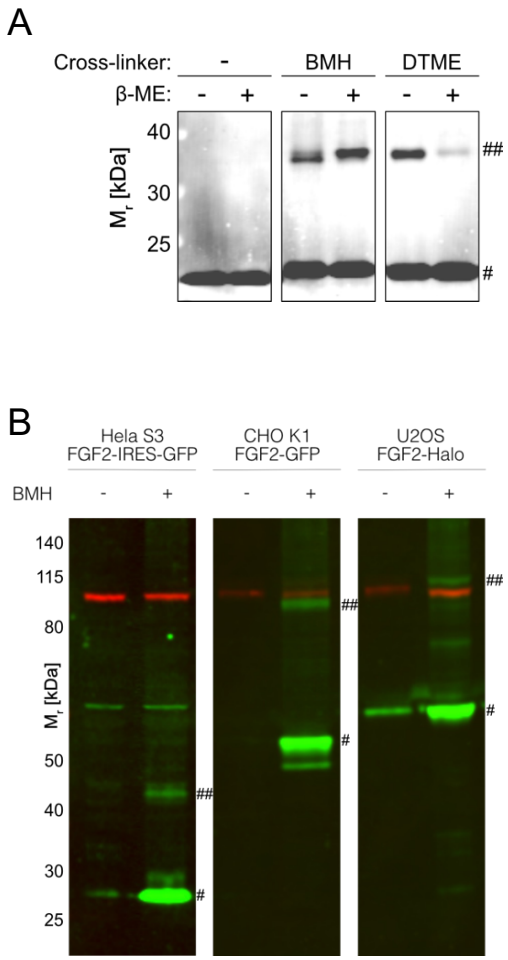

Figure 6. Chemical cross-linkers allow to analyze Fibroblast growth factor 2 (FGF2) dimer formation in cells.

A. FGF2 dimer formation was analyzed by chemical cross-linking in cellular lysates. FGF2 was expressed as a FGF2-IRES-GFP construct, which results in the translation of FGF2 untagged. FGF2 oligomers were analyzed by western blotting using polyclonal anti-FGF2 antibody. Two cross-linkers were used: bismaleimidohexane (BMH) and dithiobismaleimidoethane (DTME). Both cross-linkers contain two maleimide groups separated by a 13 Å length spacer. However, DTME cross-link can be reversed by the reduction of the disulfide bridge in the middle of the space arm. FGF2 monomers (18 kDa) are labeled with '#', FGF2 dimers (36 kDa) with '##' (n=3).

B. FGF2 dimer formation was analyzed by chemical cross-linking in cellular lysates. FGF2 was expressed in several tagged versions, including FGF2-IRES-GFP, FGF2-GFP and FGF2-Halo. FGF2 oligomers were analyzed by western blotting against FGF2 (in green) and α1 subunit (in red). Bismaleimidohexane (BMH) was used to cross-link preformed dimers. FGF2 (tag and untagged) monomers are labeled with '#', FGF2 (tag and untagged) dimers with '##' (n=3).

parameters. Lysis buffer, cross-link reaction among other parameters in the protocol were tested (Fig. 7). A cross-linker screen highlighted bismaleimidohexane (BMH) and N-p-maleimidophenylisocyanate (PMPI) as the best cross-linkers. Cross-linker conditions were optimal with 1 h at 4 °C incubation. These conditions showed maximum FGF2 dimer abundance in a reliable manner across replicates.

Hela FGF2-P2A-GFP mutant cell lines are generated for the cross-linking assay

As mentioned previously, my goal was to discriminate the role of the cysteine residues 77 and 95 in FGF2 dimer formation. And for this purpose, my approach was the use of cross-linking experiments in cells to stabilize and analyze the FGF2 dimer. For that reason, various FGF2 cysteine residues variants had to be studied using cross-linking experiments. In particular, the substitution of FGF2 residues cysteine 77 into alanine (C77A), cysteine 95 into alanine (C95A) and the combination of both (C77/95A).

Considering the results shown above, I decided that the use of untagged versions of FGF2 best suited the optimal conditions for cross-linking experiments. Hence, I proceeded to generate Hela S3 cell lines expressing untagged FGF2 (Fig. 8). Since a reporter still was required for the correct selection, I chose to express FGF2 as an FGF-P2A-GFP construct. The porcine teschovirus-1 2A (P2A) sequence induces ribosomal skipping during translation[272]. Upon expression, this leads to the translation of FGF2 and GFP as independent peptides but in equal stoichiometric ratios. This is a useful property for cell selection based on reporter expression. Additionally, the FGF2-P2A-GFP construct was under the control of a tetracycline-controlled Tet-On promoter, which regulates gene in a doxycycline-dependent manner.

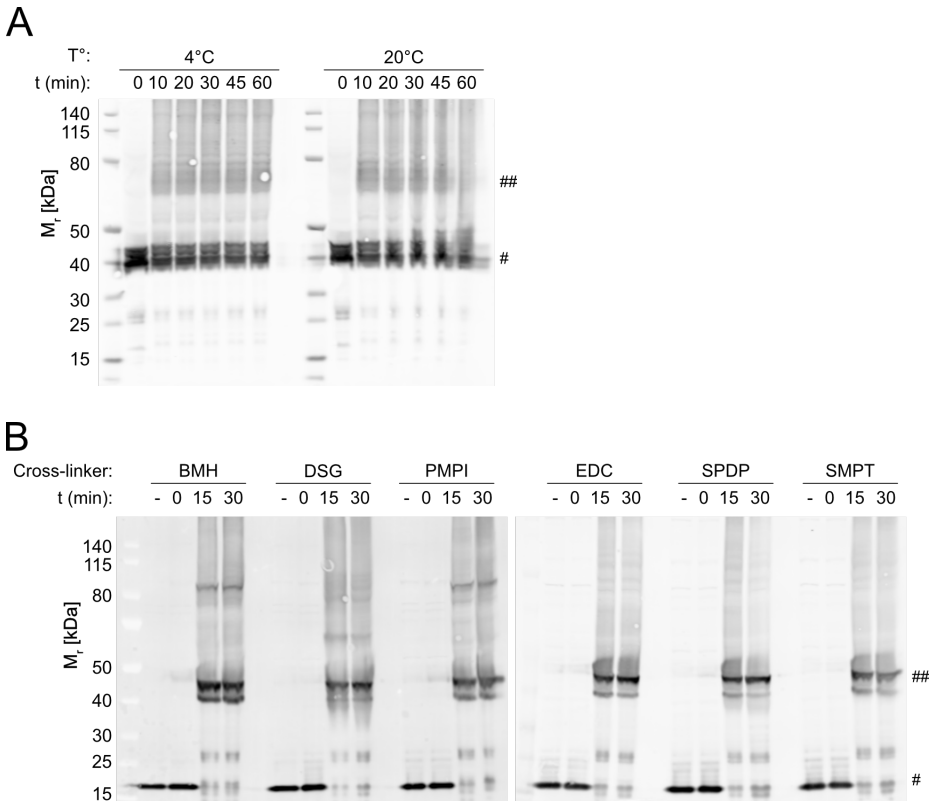

Figure 7. Chemical cross-linkers allow to analyze Fibroblast growth factor 2 (FGF2) dimer formation in cells.

A. FGF2-GFP dimer formation was analyzed by chemical cross-linking in cellular lysates. FGF2-GFP oligomers were analyzed by western blotting using polyclonal anti-FGF2 antibody. Bismaleimidohexane (BMH) was used to cross-link preformed dimers under two conditions, 4 °C or 20 °C. Cross-linking reaction was stopped at different time points (0 ,10, 20, 30, 45, 60, min). FGF2-GFP monomers are labeled with '#', FGF2 dimers with '##" (n=3).
B. Several cross-linkers were screened to optimize the experimental protocol. FGF2 oligomers were analyzed by western blotting using polyclonal anti-FGF2 antibody. Cross-linkers with different chemical properties were used: bismaleimidohexane (BMH), disuccinimidyl glutarate (DSG), N-p-maleimidophenylisocyanate (PMPI), 1-Ethyl-3-(3-dimethylaminopropyl) carbodiimide (EDC), N-succinimidyl 3-(2-pyridyldithio) propionate (SPDP), 4-succinimidyloxycarbonyl-alpha-methyl-alpha(2-pyridyldithio)toluene (SMPT). For every cross-linker, the reaction was performed at 4°C and stopped at different time points (0 ,15, 30 min). FGF2 monomers (18 kDa) are labeled with '#', FGF2 dimers (36 kDa) with '##' (n=3).

FGF2 dimer formation in cells depends on the residue C95 as revealed by chemical cross-linking

Finally, I used the cross-linking approach to discriminate the role of the cysteine residues 77 and 95 in FGF2 dimer formation. For that purpose, Hela S3 cell lines were studied, which expressed the WT and various variants of cysteine residues substitutions: FGF2 WT, FGF2 C77A, FGF2

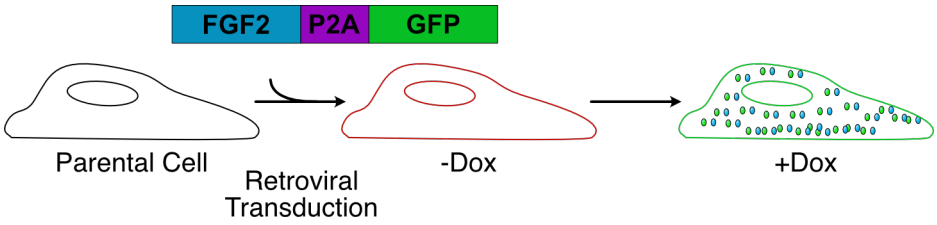

Figure 8. Schematic representation of the generation of the reporter cell lines Hela S3 FGF2-P2A-GFP and their biological characteristics.

Hela S3 cells were transduced with different mutant versions of FGF2 fused to ribosomal-skipper sequence P2A and the fluorescent reporter GFP. FGF2-P2A-GFP is expressed in a doxycycline-dependent manner. Upon expression, FGF2 and GFP are translated as independent peptides but in equal stoichiometric ratios.

C95A, and FGF2 C77/95A. Chemical cross-linkers with different spacer lengths between functional groups and different chemical functional groups were used. Specifically, these cross-linkers were: N-p-maleimidophenylisocyanate (PMPI), bismaleimidoethane (BMOE) and bismaleimidohexane (BMH). These cross-linkers contain maleimide groups, both BMOE and BMH (bifunctional), as well as PMPI (monofunctional), which form covalent bonds through sulfhydryl groups. The rationale to use these cross-linkers, additionally to their previously tested efficiency, was that the cross-linkers would only bind FGF2 subunits into dimers when the functional cysteine residues are present, hence replacing the natural disulfide bridge through the covalent link mediated by the cross-linker.

The crosslinked dimers were visualized by western blotting (Fig. 9). Homogeneous results were observed among the different cross-linkers regardless the differences in spacer length and chemical functionality, and showing differences exclusively between the substitutions in cysteine residues. FGF2 C77A showed similar levels of FGF2 dimer formation as FGF2 WT. On the contrary, FGF2 C95A, as well as FGF2 C77/95A showed severe reduction in dimer formation. This result supports that FGF2 dimer formation is mediated by C95-C95 disulfide bridge FGF2 dimer interface.

The cross-linking results support the hypothesis towards the distinct roles of the cysteine residues 77 and 95 in FGF2 secretion. Additional experimental data from the group of Prof. Nickel, including all *in silico, in vitro* and *in cellullo* experimental approaches, provided further support to this model. All these approaches, including the above cross-linking experiments, were collected and published in *Lolicato and Steringer, 2024* [256]. Specifically, the residue C95 has been identified to play a crucial role in FGF2 dimer formation. FGF2 dimer is established by the disulfide bridge formation between C95-C95 FGF2 monomers. The C95-C95 dimer is the building block to form high-order FGF2 oligomers, which are functional for pore formation and translocation across the lipid membrane. Additionally, the C95-C95 dimer constitutes potentially the primary ligand for FGF2 signaling complexes at the cell surface[273,274]. Oppositely, the residue C77 has been identified to form the interface between FGF2 and the α1 subunit of the Na^+,K^+-ATPase, in coordination with the previously described FGF2 residues lysines 54 and 60[54]. This model is consistent with former studies on FGF2 secretion[144,255].

FGF2 high-order oligomer formation is dependent on FGF2 cis-elements

FGF2 dimer formation in cells depends on cis-elements as revealed by chemical cross-linking

FGF2 secretion involves several factors of the secretory machinery. The main factors at the inner leaflet of the plasma membrane are the Na^+,K^+-ATPase and the $PI(4,5)P_2$ lipids[54,144]. These two factors must facilitate FGF2 dimerization and oligomerization. These factors should allow the development into functional oligomers for pore formation and membrane translocation. The first step is consequently dimer formation. In the previous section I established a successful assay using cross-linkers to visualize FGF2 dimer formation. Hence, I continued to further assess the FGF2 variants that are deficient for the binding of the different factors of the secretory machinery at the inner leaflet of the plasma membrane; in particular, the variants binding-deficient for the Na^+,K^+-ATPase and $PI(4,5)P_2$ lipids.

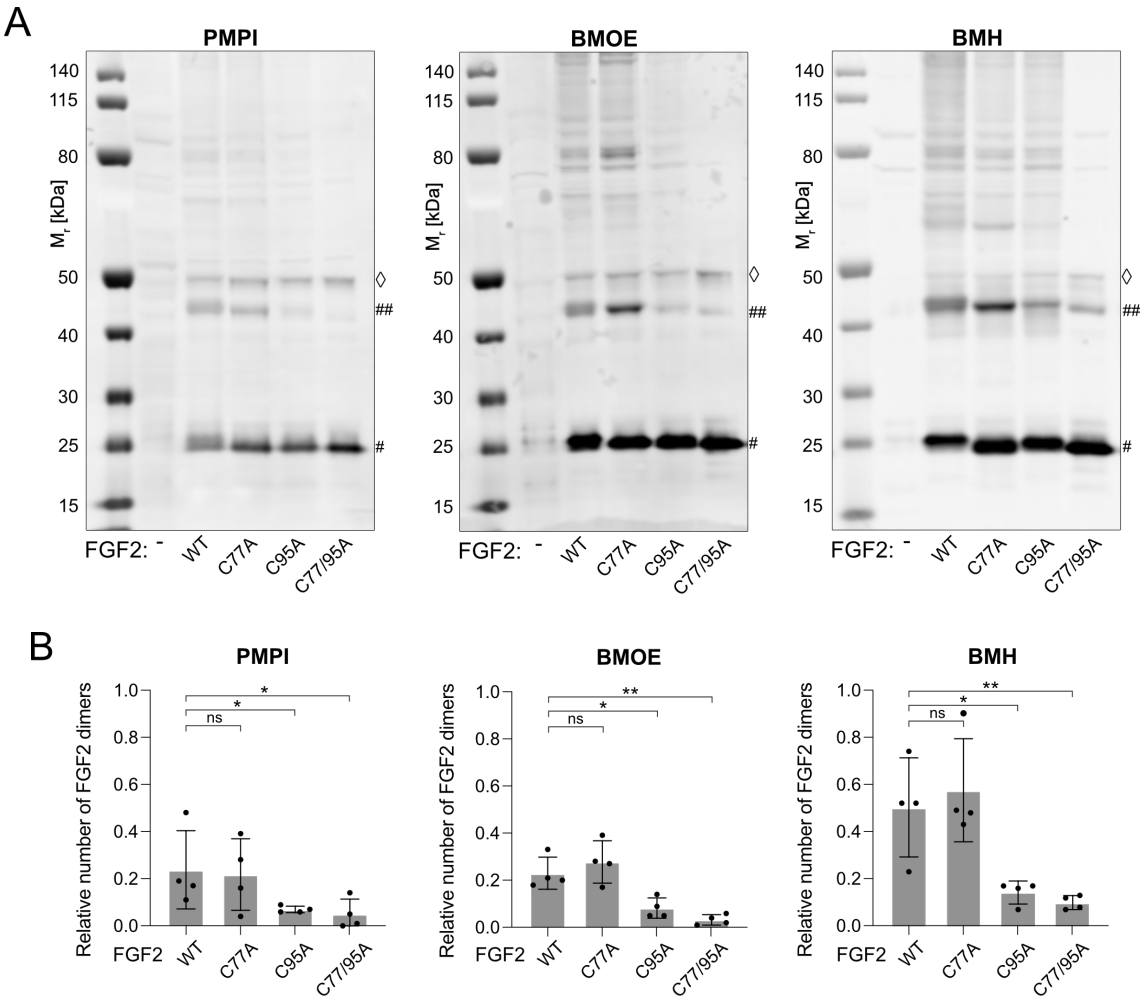

Figure 9. Fibroblast growth factor 2 (FGF2) dimer formation in cells depends on the residue C95 as revealed by chemical cross-linking.

FGF2 dimer formation was analyzed by chemical cross-linking in cellular lysates. FGF2 was expressed as a FGF2-P2A-GFP construct, which results in the translation of untagged FGF2. FGF2 oligomers were analyzed by western blotting using polyclonal anti-FGF2 antibody. Different FGF2 variants, including cysteine residues variants, were studied: WT, C77A, C95A and C77/95A. Three cross-linkers were used. N-p-maleimidophenylisocyanate (PMPI) contains a 8,7 Å length spacer between a maleimide (links to sulfhydryl groups) and isocyanate (links to hydroxyl groups) chemical groups. Bismaleimidoethane (BMOE) contains two maleimide groups separated by a 8 Å length spacer. Bismaleimidohexane (BMH) contains also two maleimide groups separated by a long 13 Å spacer.

A. Representative western blots for each cross-linkers (PMPI, BMOE, BMH). FGF2 monomers (18 kDa) are labeled with '#', FGF2 dimers (36 kDa) with '##' and small amounts of monomeric full-length FGF2-P2A-GFP (~50 kDa) with '◊'.

B. Quantification of FGF2 dimer to FGF2 monomer ratios. The FGF2 dimer to monomer ratios were shown as mean ± SD (n = 4), not significant (ns) $p>0,05$; *$p\leq0,05$; **$p\leq0,01$. The statistical analysis was based on a one-way ANOVA test. Data distribution was assumed to be normal, but this was not formally tested.

Data present in Lolicato and Steringer, 2024 [259].

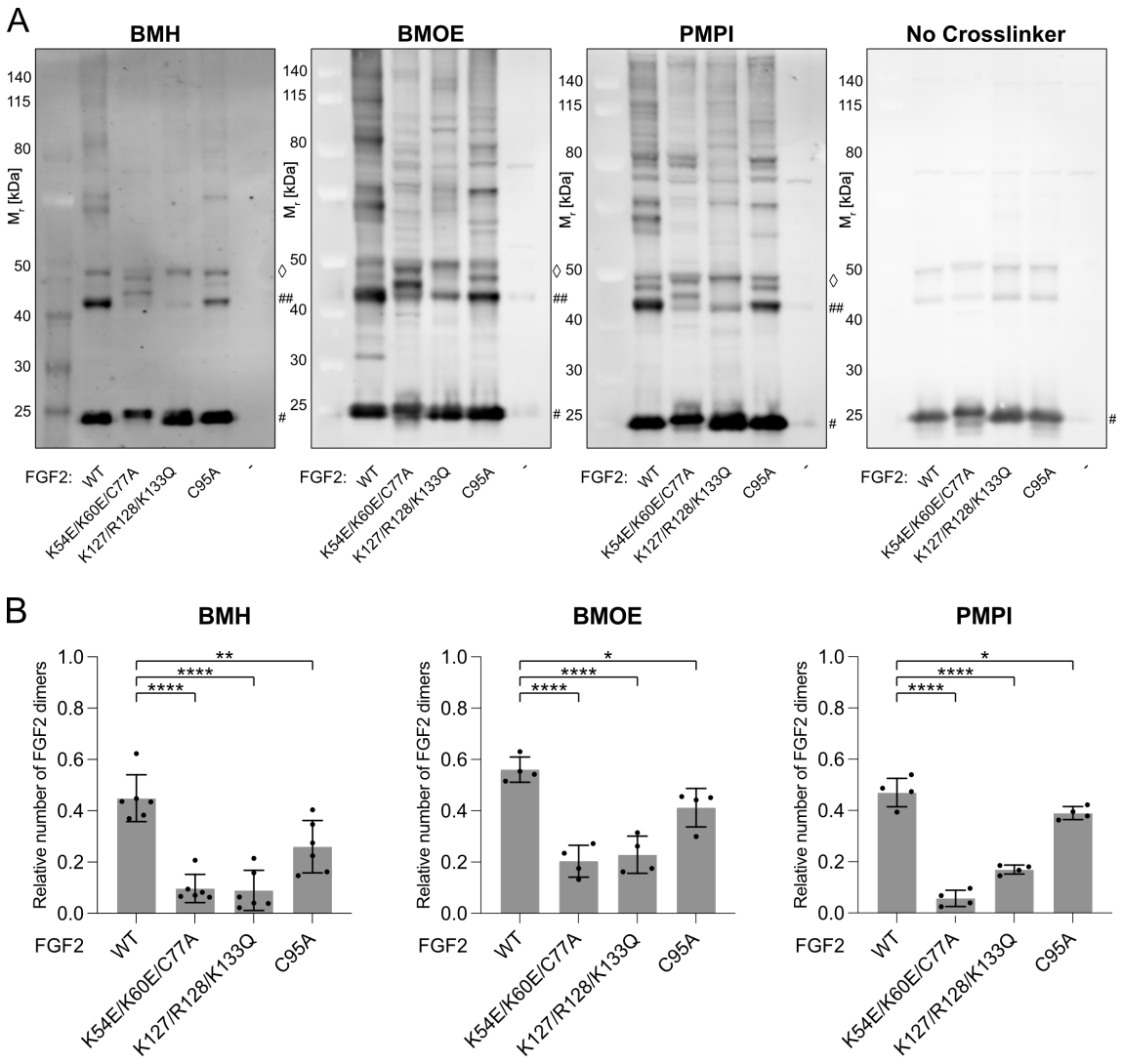

Figure 10. Fibroblast growth factor 2 (FGF2) dimer formation in cells depends on cis-elements as revealed by chemical cross-linking.

FGF2 dimer formation was analyzed by chemical cross-linking in cellular lysates. FGF2 was expressed as a FGF2-P2A-GFP construct, which results in the translation of untagged FGF2. FGF2 oligomers were analyzed by western blot using polyclonal anti-FGF2 antibody. Different FGF2 variants were studied: WT, K54E/K60E/C77A, K127/R128/K133Q and C95A. Three cross-linkers were used. N-p-maleimidophenylisocyanate (PMPI) contains a 8,7 Å length spacer between a maleimide (links to sulfhydryl groups) and isocyanate (links to hydroxyl groups) chemical groups. Bismaleimidoethane (BMOE) contains two maleimide groups separated by a 8 Å length spacer. Bismaleimidohexane (BMH) contains also two maleimide groups separated by a long 13 Å spacer.

A. Representative western blots for each cross-linkers (PMPI, BMOE, BMH). FGF2 monomers (18 kDa) are labeled with '#', FGF2 dimers (36 kDa) with '##' and small amounts of monomeric full-length FGF2-P2A-GFP (~50 kDa) with '◊'.

B. Quantification of FGF2 dimer to FGF2 monomer ratios. The FGF2 dimer to monomer ratios were shown as mean ± SD (n = 4), *p≤0,05; **p≤0,01; ****p≤0,0001. The statistical analysis was based on a one-way ANOVA test. Data distribution was assumed to be normal, but this was not formally tested.

FGF2 dimer formation was assessed using the cross-linking assay (Fig. 10). BMH, BMOE and PMPI were used to cross-link and visualize the FGF2 dimer formation. Homogeneous results were observed across all cross-linkers. FGF2 variants binding-deficient for both Na^+,K^+-ATPase and PI(4,5)P_2 lipids presented diminished FGF2 dimer formation. FGF2 dimer levels were even lower than the FGF2 dimer-deficient variant C95A. These results support that the inner leaflet secretory machinery is directly involved in FGF2 dimerization.

FGF2-mGFP variant expressing cell lines are generated for the FGF2 oligomeric distribution determination

A crucial step for FGF2 secretion is oligomerization. FGF2 needs to form high-order oligomers (oligomers with more than 2 monomers) functional for pore formation and translocation of membrane lipids. However the minimal number of FGF2 units required is unknown. Substitution of cysteine residues 77 and 95 into alanines (C77/95A) leads to impair secretion of FGF2[255], and the group of Prof. Nickel and I provided evidence supporting that FGF2 dimer forms through the C95-C95 disulfide bridge[256]. These observations suggest that high-order oligomers are generated based on the FGF2 dimer as the building block. However, this has not been formally tested. Previously, FGF2 oligomers were observed *in vitro* in the presence of GUVs containing PI(4,5)P_2[255]. Nevetheless, the highest size of oligomers observed in cells was the FGF2 dimer[131].

I previously established a protocol based on chemical cross-linking to study the FGF2 dimer formation and be visualized by western blotting. Although successful for FGF2 dimer analysis, it presented limitations for the analysis on FGF2 oligomers. Hence, I dedided to use single brightness stoichometric analysis to determine the oligomeric size distributions of FGF2 in cells. This method precisely quantifies a molecule oligomer size based on the fluorescent brightness. Hence, cells must express FGF2 fused to a fluorescent reporter, which cannot oligomerize by itself. One example is

monomeric GFP (mGFP)[265]. For that purpose, I generated CHO K1, CHO 745 and U2OS cell lines expressing FGF2-mGFP (Fig. 11). Both CHO and U2OS cells present a morphology with extended shape, which is ideal for imaging. The expression of FGF2-mGFP was under a Tet On promoter, which allowed inducing FGF2 expression in low amounts, required for this method.

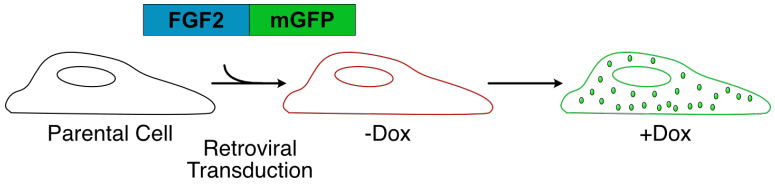

Figure 11. Schematic representation of the generation of the reporter cell lines expressing FGF2-mGFP and their biological characteristics.

U2OS, CHOK1 and CHO745 cells were transduced with different mutant versions of FGF2 fused to the fluorescent reporter monomeric GFP. Reporter is expressed in a doxycycline-dependent manner.

FGF2 high-order oligomer formation in cells depends on cis-elements as revealed by single brightness stoichiometric analysis

FGF2 secretion involves the interaction of FGF2 with the secretory machinery. The machinery includes the Na^+,K^+-ATPase and the phosphatidylinositol-4,5-bisphosphate $PI(4,5)P_2$ in the inner leaflet of the plasma membrane[54,144]. Simultaneously, FGF2 secretion requires the oligomerization of FGF2. However, how these elements contribute to the oligomer formation of FGF2 is unclear. The oligomerization process was studied *in vitro* using GUVs containing $PI(4,5)P_2$[52,144].

I decided to study the role of the secretory machinery at the inner leaflet of the plasma membrane on FGF2 oligomerization. I used single brightness stoichiometric analysis to determine FGF2 oligomeric size distribution (Fig. 12) in collaboration with Dr. Eleonora Margheritis from the group of Prof. Katia Cosentino at the University of Osnabrück. FGF2 variants were explored, including variants deficient for the interaction with the secretory machinery (Na^+,K^+-ATPase and $PI(4,5)P_2$), as well as deficient for dimerization (C95A substitution). Cells were imaged using total internal reflection fluorescence (TIRF) microscopy[263], which uses the evanescent field to excite

only the molecules in close proximity to the slide, hence discriminating only for the FGF2 molecules at the plasma membrane. After imaging, the cells were analyzed using the Stoichiometry Analysis Software[269,270], providing the fluorescence intensity distribution and the oligomeric species occurrence for every FGF2 variant studied.

Interestingly, several observations could be obtained from this analysis. FGF2 WT showed a wide-spread intensity distribution, indicating that a diverse set of oligomers were present. The detailed stoichiometry analysis showed the presence of high-order oligomers (oligomers with more than 2 monomers), including dimers, trimers, tetramers and hexamers. The tetramers population represented the predominant population (approx. 40 %) in comparison to the remaining oligomeric sizes (approx. 20 % each). This is the first evidence of FGF2 high-order oligomers in cells, and first experimental data showing the existence of tetramers and hexamers in cells. Additionally, it is worth highlighting the absence of FGF2 monomers. In contrast, FGF2 C95A showed a narrow intensity distribution, which indicated the absence of high-order oligomers. The detailed stoichiometry analysis showed the absence of high-order oligomers: only monomers (approx. 20 %) and dimers (approx. 80 %) were present.

These results support the relevance of the residue C95 in FGF2 oligomerization. The introduction of the C95A substitution in FGF2 led to the absence of high-order oligomers. This correlates inversely with the increase in FGF2 dimers and FGF2 monomers. Hence, residue C95 is crucial for FGF2 high-order oligomers to develop. These high-order oligomeric species, tetramers and hexamers, most likely represent oligomeric intermediates, which advance into functional oligomers for pore formation and translocation across the membrane, required for unconventional secretion of FGF2. Another aspect to highlight is the observation of FGF2 dimers in the FGF2 C95A. As mentioned previously, experimental observations from the group of Prof. Nickel and presented in this thesis showed that the FGF2 dimer is formed by the disulfide bridge C95-C95. Instead, this

experiment showed the formation of the FGF2 dimer independent of the C95-C95 disulfide bridge.

Additional observations could be obtained from the analysis on the variants deficient for the interaciton with the secretory machinery. The FGF2 variant deficient for the binding to the Na^+,K^+-ATPase (FGF2 K54E/K60E/C77A) showed a narrow intensity distribution, which indicated the absence of high-order oligomers. The detailed stoichiometry analysis showed the presence of low-order oligomers: monomers (approx. 40 %) and dimers (approx. 60 %). The FGF2 variant deficient for the binding to the $PI(4,5)P_2$ lipids (FGF2 K127/R128/K133Q) showed a narrow intensity distribution as well, which indicated the absence of high-order oligomers. The detailed stoichiometry analysis showed the presence of low-order oligomers: monomers (approx. 20 %) and dimers (approx. 80 %). The FGF2 variant deficient for the interaction with the Na^+,K^+-ATPase and $PI(4,5)P_2$ (FGF2 K54E/K60E/C77A/K127Q/R128Q/K133Q) showed a narrow intensity distribution too, which corresponded to monomers (approx. 40 %) and dimers (approx. 60 %). And the addition of the C95A substitution to this last variant (FGF2 K54E/K60E/C77A/C95A/K127Q/R128Q/K133Q) again showed a narrow intensity distribution: monomers (approx. 20 %) and dimers (approx. 80 %) were the oligomeric species present.

The distributions were homogeneous for all single and combined binding-deficient variants to the elements of the secretion machinery at the inner leaflet of the plasma membrane. The distributions resemble the FGF2 C95A distribution. Low-order oligomers were predominant, while high-order oligomers were absent. Hence, FGF2 cis-elements for the interaction with the secretory machinery are central for the formation of FGF2 high-order oligomers. This suggests that the interaction with both the Na^+,K^+-ATPase and the $PI(4,5)P_2$ lipids at the plasma membrane are key for the formation of FGF2 high-order oligomers. Additionally, every studied FGF2 variant showed the

presence of the FGF2 dimer in the distribution. And the FGF2 dimer constituted the predominant oligomeric species. This phenomenon was observed independent of the presence or absence of the C95A substitution.

Ouabain inhibits the oligomerization of FGF2 into high-order oligomers

In the previous section I analyzed the oligomeric size distribution of various FGF2 variants. Of particular interest was the analysis on the variants binding-deficient to the FGF2 secretory machinery at the inner leaflet of the plasma membrane, specifically the Na^+,K^+-ATPase and $PI(4,5)P_2$. The single and combined binding-deficient variants (FGF2 K54E/K60E/C77A, FGF2 K127/R128/K133Q, FGF2 K54E/K60E/C77A/K127Q/R128Q/K133Q) showed a distribution similar to the FGF2 C95A, where the FGF2 dimer was observed, but high-order oligomers were absent. These results led to the hypothesis that the inner leaflet elements of the secretory machinery contribute to the formation of the FGF2 high-order oligomers. Since the Na^+,K^+-ATPase is the first contact of FGF2 to the inner leaflet of the plasma membrane[54], I decided to focus on the relevance of the interaction between FGF2 and the Na^+,K^+-ATPase in the formation of FGF2 high-order oligomers.

For that purpose, I studied the FGF2 oligomeric size distribution in U2OS cells upon treatment with ouabain (Fig. 12). I decided to use ouabain as a known inhibitor of the Na^+,K^+-ATPase[187–191]. And I decided to use U2OS cells, which are more sensitive to ouabain than CHO rodent cells[194].

I used single brightness stoichiometric analysis to determine FGF2 oligomeric size distribution in U2OS cells upon ouabain treatment (Fig. 13) in collaboration with Dr. Eleonora Margheritis from the group of Prof. Katia Cosentino at the University of Osnabrück. FGF2 WT was explored in the presence or absence of ouabain. FGF2 WT cells showed a wide-spread intensity distribution,

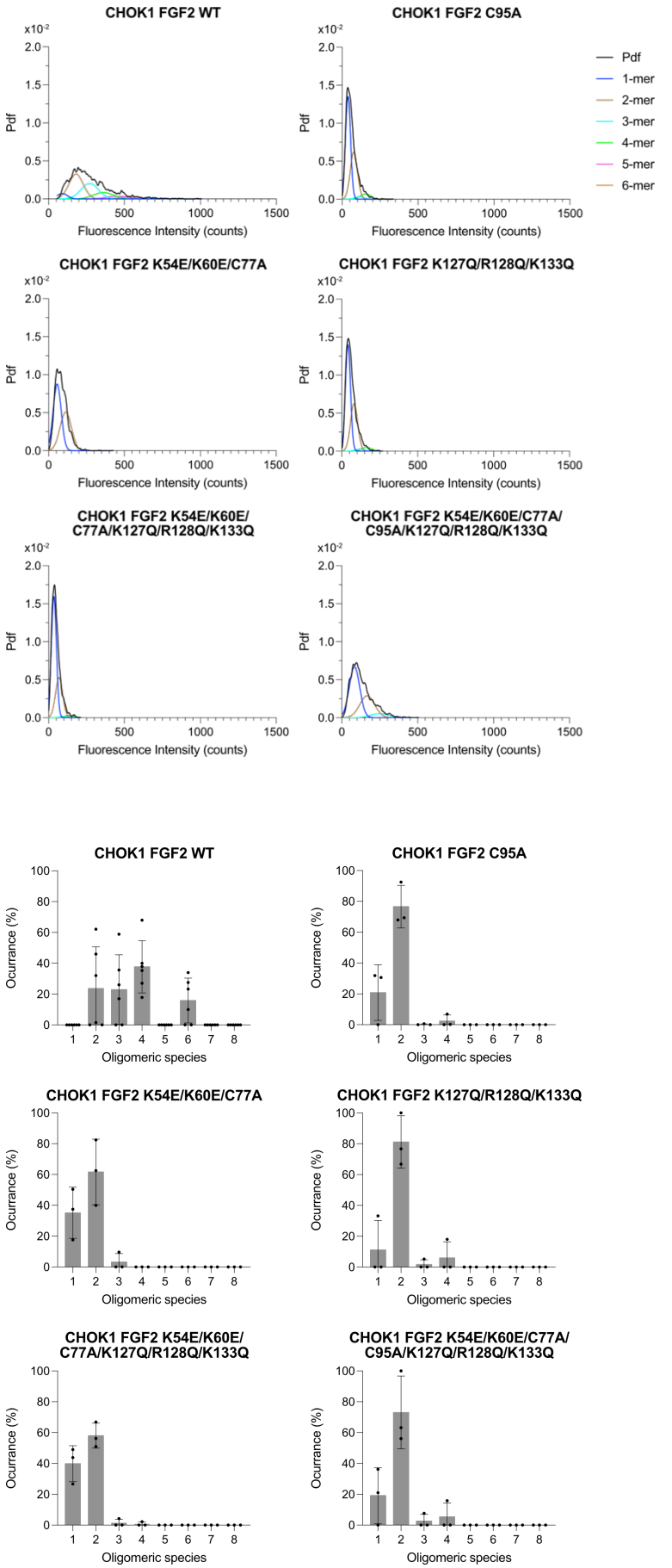

Figure 12. FGF2 oligomeric size distribution in FGF2-mGFP variants.

CHO K1 FGF2-mGFP cell lines were subjected to single-molecule brightness analysis using the Stoichiometry Analysis Software[269]. Plotted data correspond to three independent experiments with a total of 40-50 cells and a minimum of a total of 1500 particles being analysed per experiment.

A. Fluorescence intensity distributions of FGF2-mGFP oligomers for the different variants of FGF2 (WT, C95A, K54E/K60E/C77A, K127/R128/K133Q, K54E/K60E/C77A/K127Q/R128Q/K133Q, and K54E/K60E/C77A/C95A/K127Q/R128Q/K133Q). Brightness distributions of all values were plotted as probability density functions shown in black. Fit of Gaussians distributions representing the possible oligomeric states FGF2 can assume are shown in colours: monomer (dark blue), dimer (brown), trimer (turquoise), tetramer (green), pentamer (pink) and hexamer (orange).

B. Relative occurrence in % of oligomeric species of FGF2-mGFP. Error bars correspond to the standard deviation. (n=3)

Data produced jointly with Dr. Eleonora Margheritis. Part of the data present in Bayer, Fernández-Sobaberas and Griffo, 2025 [267].

indicating that a diverse set of oligomers were present. The detailed stoichiometry analysis showed the presence of high-order oligomers. This included: dimers (approx. 60 %), trimers (approx. 20 %), tetramers (approx. 20 %) and hexamers (below 5 %). Additionally, there was a lack of FGF2 monomers. Overall, the distribution of FGF2 WT in U2OS cells was similar as in CHO K1 cells. In comparison, the hexamer population was reduced while the dimer population increased, which are differences that can be explained by the general physiological differences of these cell lines.

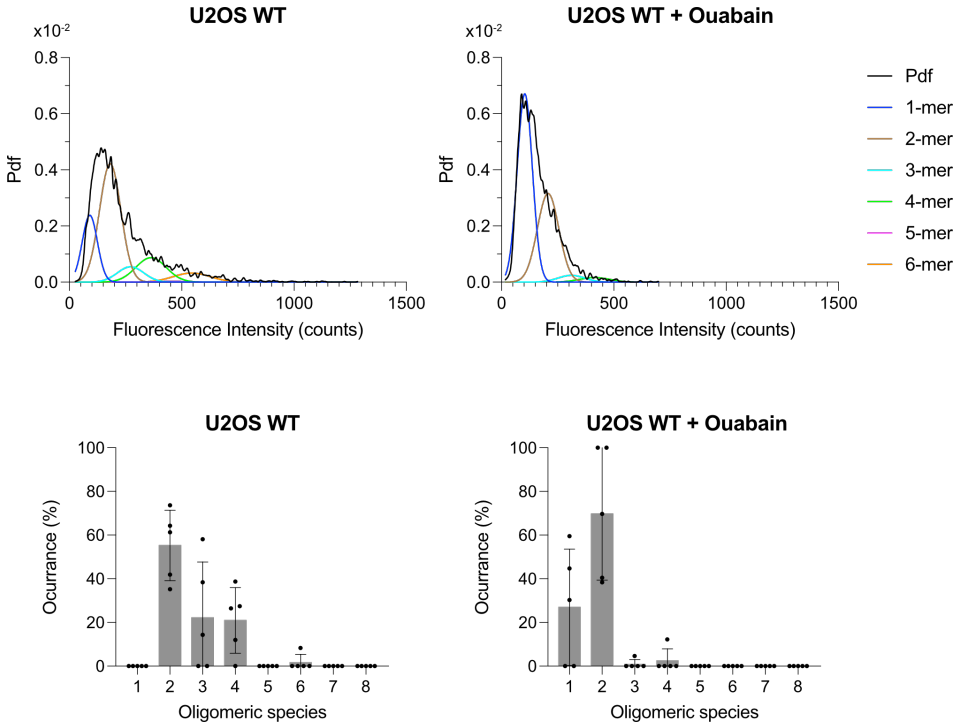

Figure 13. FGF2 oligomeric size distribution in U2OS FGF2-mGFP upon ouabain treatment.

U2OS FGF2-mGFP cell lines were subjected to single-molecule brightness analysis using the Stoichiometry Analysis Software[269] in the absence or presence of ouabain (50 μM). Plotted data correspond to five independent experiments with a total of 40-50 cells and a minimum of a total of 1500 particles being analysed per experiment.

A. Fluorescence intensity distributions of FGF2-mGFP oligomers. Brightness distributions of all values were plotted as probability density functions shown in black. Fit of Gaussians distributions representing the possible oligomeric states FGF2 can assume are shown in colours: monomer (dark blue), dimer (brown), trimer (turquoise), tetramer (green), pentamer (pink) and hexamer (orange).

B. Relative occurrence in % of oligomeric species of FGF2-mGFP. Error bars correspond to the standard deviation. (n=5)

Data produced jointly with Dr. Eleonora Margheritis.

Interestingly, when cells were treated with ouabain, the distribution of oligomers was shifted. A narrow intensity distribution was observed, which indicated the absence of high-order oligomers. The detailed stoichiometry analysis showed the absence of high-order oligomers: only monomers (approx. 30 %) and dimers (approx. 70 %) were present. Hence, the inhibition of the Na^+,K^+-ATPase by ouabain led to the absence of high-order oligomers. Instead, FGF2 remained as low-order oligomers, with the increase in the population of FGF2 dimers and monomers.

This distribution resembles the distribution in CHO K1 cells expressing FGF2 variant binding-deficient to the Na^+,K^+-ATPase. The inhibition of FGF2 interaction with the Na^+,K^+-ATPase, both by FGF2 residues substitution and by treatment with ouabain, prevented the formation of high-order oligomers. In opposition, the FGF2 monomer appeared in high proportion. These results further support that the interaction with the Na^+,K^+-ATPase promotes FGF2 high-order oligomerization.

ATP concentration in cells is reduced upon long-term treatment with ouabain

U2OS FGF2-Halo mutant cell lines are generated for the determination of Na^+,K^+-ATPase activity

Evidences showing the possible role of the Na^+,K^+-ATPase secretion have been several. The first evidence consisted on the inhibition of FGF2 secretion upon ouabain treatment, a Na^+,K^+-ATPase inhibitor[187–191]. The latest evidence was the identification of the Na^+,K^+-ATPase as the first contact of FGF2 at the inner leaflet of the plasma membrane[54]. However, the role of the Na^+,K^+-ATPase in FGF2 secretion is not clear. Na^+,K^+-ATPase is mainly known for its activity as an antiporter: for each molecule of ATP, three ions of Na^+ are exported and two ions of K^+ imported. This antiport of ions maintains the membrane potential in the cell, which is crucial for the correct concentration of ions and molecules across the cell. However, there are observations

suggesting the membrane potential does not play a role in FGF2 secretion. When the membrane gradient was altered by introducing different concentrations of Na^+ and K^+ in the medium, FGF2 secretion in cells was unaffected[137,275]. Hence, how the Na^+,K^+-ATPase facilitates FGF2 secretion and what is the relevance of the interaction between these two proteins is unclear.

In the previous section I provided evidence that the contact of FGF2 with the Na^+,K^+-ATPase is crucial for FGF2 to develop into high-order oligomers. When a FGF2 variant binding-deficient to the Na^+,K^+-ATPase was studied, FGF2 high-order oligomers were missing. When cells were treated with ouabain, FGF2 high-order oligomers were absent as well.

Several hypotheses explain the specific role of the Na^+,K^+-ATPase in FGF2 secretion. One hypothesis is that the activity of the Na^+,K^+-ATPase may be important for FGF2 secretion to maintain the integrity of the plasma membrane during translocation. Another hypothesis is the interaction between FGF2 and the Na^+,K^+-ATPase is a quality control check to select for FGF2 molecules functional for translocation. A final hypothesis, derived from the last results, is that Na^+,K^+-ATPase interaction may be important for FGF2 secretion, in particular, to facilitate the formation of the disulfide bridge.

In order to provide new evidences to clarify this topic, I decided to establish a method to study the activity of the Na^+,K^+-ATPase in cells. In order to measure the activity, the concentration of a substrate has to be monitored over time. Since the study of the activity is aimed at cells, this method had to be compatible with analyzing living cells, like for example using confocal microscopy. A series of fluorescent reporters have been established in this scope. The fluorescent properties vary depending on the concentration of the substrate. This allow the monitorization of several molecules in cells. Considering the experimental tools available, I decided to monitor the intracellular ATP concentration. For this approach, cells must express FGF2 with an expression

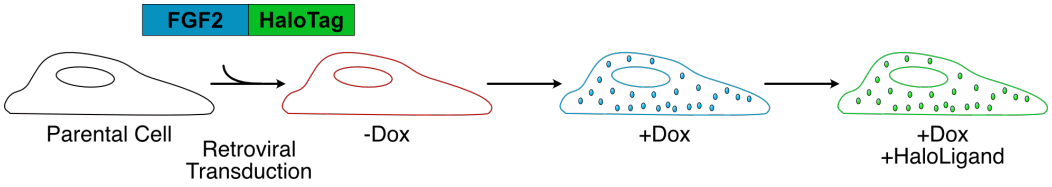

Figure 14. Schematic representation of the generation of the reporter cell lines U2OS FGF2-Halo and their biological characteristics.

U2OS cells were transduced with different mutant versions of FGF2 fused to the self-labelling protein tag Halo Tag. Reporter is expressed in a doxycycline-dependent manner. Reporter fluorescence detection is dependent upon Halo Ligand addition.

reporter that is compatible with the fluorescent reporter of the Na^+,K^+-ATPase substrates. Hence, U2O2 cells were generated that expressed FGF2 fused to the Halo Tag (Fig. 14). The Halo Tag captures the Halo Ligand, which contains a fluorophore. The fluorescent signal emitted as reporter will depend on the Halo Ligand introduced and its properties. Hence, the Halo Tag provides flexibility in the reporter characteristics. This allowed to generate and select cells based on the reporter Halo Ligand/Tag, and modify the fluorescent properties in favor of the assay.

Drastic changes in ATP concentrations are monitored in living cells with the ATeam sensor

As mentioned in the previous section, I decided to establish an assay to measure the Na^+,K^+-ATPase activity in cells by monitoring the ATP concentration in cells. For every cycle, where three ions of Na^+ are exported and two ions of K^+ are imported, an ATP molecule is consumed. It is estimated that the Na^+,K^+-ATPase consumes around 30 % of ATP levels in a cell[276]. Although ATP is a molecule required for many biochemical reactions in the cell, changes in ATP concentration can be attributed to the Na^+,K^+-ATPase due to the high consumption of ATP by the Na^+,K^+-ATPase.

For that purpose, I used the ATeam Sensor AT1.03_NL, a Förster resonance energy transfer (FRET)-based ATP sensor[261,262]. I intended to montior the concentration of ATP as a readout for the Na^+,K^+-ATPase activity and verify that changes in activity correlate with changes in FGF2

secretion. In that context, I first studied cells expressing FGF2 in several metabolic contexts. I studied ATP concentrations in the presence and absence of ouabain in order to understand the contribution of the Na^+,K^+-ATPase. I also studied ATP concentrations in the absence and presence of metabolic inhibitors, such as 2-deoxyglucose (2DG) and potassium cyanide (KCN). These compounds inhibit glycolysis and the respiratory chain respectively, which serve as a positive control[261].

I used the ATeam sensor to monitor ATP concentrations in living U2OS cells (Fig. 15). The initial pattern was studied on U2OS cells in the absence of FGF2. In the mock condition, ATP concentration levels are stable throughout the monitoring time period. Upon 2-deoxyglucose plus potassium cyanide addition, ATP concentration levels were drastically reduced in cells, approximately 50 % in less than 5 min, and remained low during the whole monitorization period. However, upon ouabain treatment, ATP concentration levels did not change in comparison to mock. In the presence of FGF2, ATP concentration levels remained stable. Upon the addition of 2-deoxyglucose plus potassium cyanide, ATP concentration levels dropped dramatically, approximately 40 % in less than 5 min and remained at that concentration level throughout the monitorization. Upon ouabain treatment, again no differences were observed compared to the mock condition.

Overall, the ATeam sensor was able to detect dramatic changes of ATP concentration levels, induced by severe alterations in the metabolic pathways of cells. However, no differences in ATP concentration levels were observed upon ouabain treatment.

ATP concentrations in living cells expressing FGF2 are monitored upon ouabain treatment

The effects of ouabain on FGF2 secretion in real time were not studied previously. Short to long incubations periods were used, ranging from several hours to complete days (2-48h)[54,137,207,275].

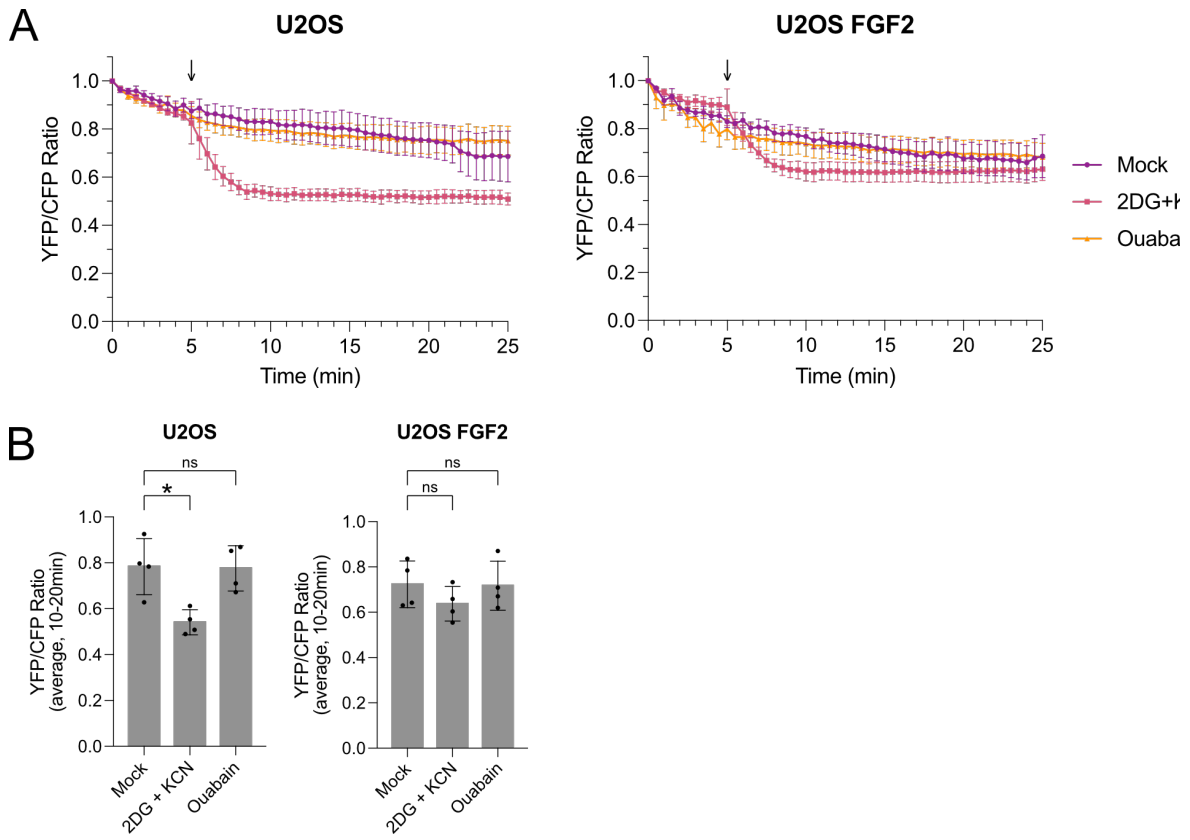

Figure 15. Monitoring of cytoplasmic ATP concentration levels in U2OS cells upon ouabain treatment.

A. Time courses of YFP/CFP emission ratio of cells expressing the ATP indicator AT1.03_NL. U2OS cells expressing or not FGF2 were treated with either mock (DMSO; 0,1 %), ouabain (50 µM) or the combination of 2-deoxyglucose (2DG, 10mM) and potassium cyanide (KCN, 1mM). The compounds were added to the medium at time 5 (min), indicated by an arrow. Data was quantified and normalized to time 0 (min) and set to 1 (n = 4). Error bars are standard deviations between measurements. Mock, purple romboids; 2DG and KCN, red squares; ouabain, orange triangles.

B. YFP/CFP emission ratio comparison upon treatments. YFP/CFP emission ratio from times 10 to 20 (min) were averaged for each compound (mock, ouabain or 2DG and KCN) in the presence or absence of FGF2 expression. Data was shown as mean ± SD (n = 4), not significant (ns) $p>0,05$; *$p\leq0,05$. The statistical analysis was based on a one-way ANOVA test. Data distribution was assumed to be normal, but this was not formally tested.

Taking this into consideration, I decided to study the effect of ouabain on ATP concentration levels in U2O2 with the ATeam sensor after incubation with ouabain.

ATP concentrations were studied with the ATeam sensor in U2OS cells upon treatment with ouabain for 6 h (Fig. 16). After a longer incubation with ouabain as in the above experiments, ATP

concentration levels were reduced (approx. 20 %). This reduction of ATP concentration was independent of the presence or absence of FGF2.

Overall, the experiments performed with the ATeam sensor showed that the ATP concentration levels were affected upon ouabain treatment. These effects were undetected upon direct treatment, but led to a gradual decrease of ATP concentration levels after incubation for several hours. However, ATP concentration levels in cells and the response to ouabain treatment was independent of the presence or absence of FGF2.

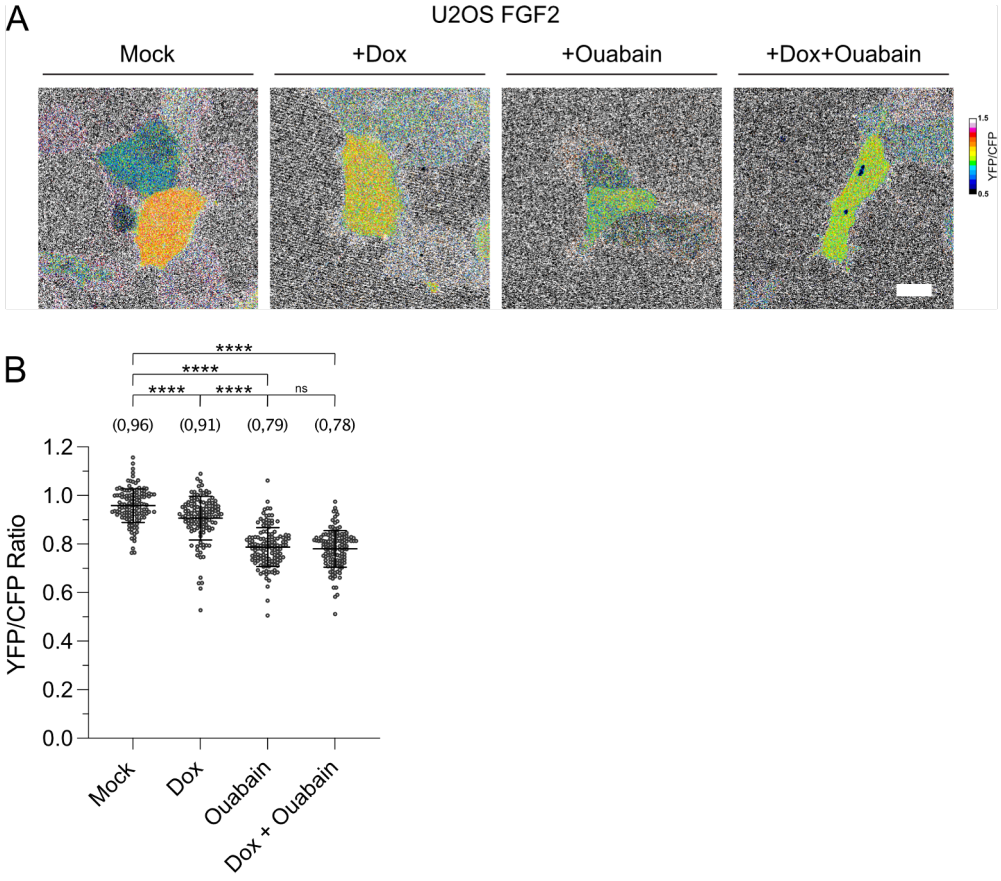

Figure 16. Cytoplasmic ATP concentration levels are reducd upon ouabain treatment.

A. Ratiometric pseudocolor images of U2OS cells expressing the ATP indicator AT1.03_NL in the presence or absence of FGF2 and/or ouabain. U2OS cells expressing FGF2-Halo cells were imaged after 6 h incubation with ouabain (50 µM). Scale bar 20 µm.

B. Quantification of YFP/CFP emission ratios. Data was quantified and normalized to average mock and set to 1 (n = 4), not significant (ns) p>0,05; ****p≤0,0001. Each dot represents a single cell. The statistical analysis was based on a one-way ANOVA test. Data distribution was assumed to be normal, but this was not formally tested.

The overexpression of membrane-attached variants of the cytosolic domains of the Na^+,K^+-ATPase facilitate FGF2 secretion by recruiting FGF2 to the plasma membrane

Cell lines expressing SH4-mCherry-α1 CD variants are generated to study Na^+,K^+-ATPase role in FGF2 recruitment

In order to further unravel the role of the Na^+,K^+-ATPase in FGF2 secretion, I continued with an alternative approach that could challenge most of the discussed hypotheses so far. The interaction site of FGF2 with the Na^+,K^+-ATPase is characterized. FGF2 interacts with the cytosolic domain (CD) of the Na^+,K^+-ATPase, particularly to the subCD3 domain (382-596) of the α1 subunit[54]. If the Na^+,K^+-ATPase simply acts as a docking platform for FGF2 to reach the plasma membrane, the expression of the interacting region at the inner leaflet of the plasma membrane could enhance the recruitment of FGF2 and promote FGF2 secretion or sequester FGF2 from the endogenous Na^+,K^+-ATPase and reduce the secretion. If the Na^+,K^+-ATPase performs a quality control check, the overexpression of the cytosolic domain may offer a bypass and move FGF2 particles on for secretion. If the activity of the Na^+,K^+-ATPase plays a role, the overexpression of the cytosolic domain should not influence FGF2 secretion.

In order to provide more evidences on the topic, I decided to overexpress the cytosolic domain of the Na^+,K^+-ATPase at the inner leaflet of the plasma membrane in cells. Specifically, the characterized subCD3, CD3 and CD1-3 cytosolic domains of the α1 subunit were selected for overexpression[54]. To visualize these constructs, the domains were fused to mCherry. In order to target the constructs back to the plasma membrane, the domains were fused to the SH4 domain[77,250,277]. Hence, I generated CHO K1, CHO 745 and U2OS cells that expressed these SH4-mCherry-α1 CD constructs (Fig. 17, 18). While FGF2-mGFP expressed in these cells is controlled

by a doxycycline-dependent promoter, the SH4-mCherry-α1 CD variants are expressed in a constitutive manner.

Prior to the experiments, I evaluated the expression of the SH4-mCherry-α1 CD variants in comparison to the Na^+,K^+-ATPase (Fig. 19). The western blot confirmed that the different constructs (SH4-mCherry-subCD3, SH4-mCherry-CD3, SH4-mCherry-CD1-3 and SH4-mCherry) were expressed homogenously. Likewise, Na^+,K^+-ATPase expression was homogenous and was unaltered by the expression of the constructs.

FGF2 secretion increases in cells expressing SH4-mCherry-α1 CD variants

First, I studied whether the overexpression of the SH4-mCherry-α1 CD variants have an effect on FGF2 secretion. With that purpose, I performed the cell surface biotinylation assay (Fig. 20). CHO K1, CHO 745 and U2OS cells expressing each SH4-mCherry-subCD3, SH4-mCherry-CD3,

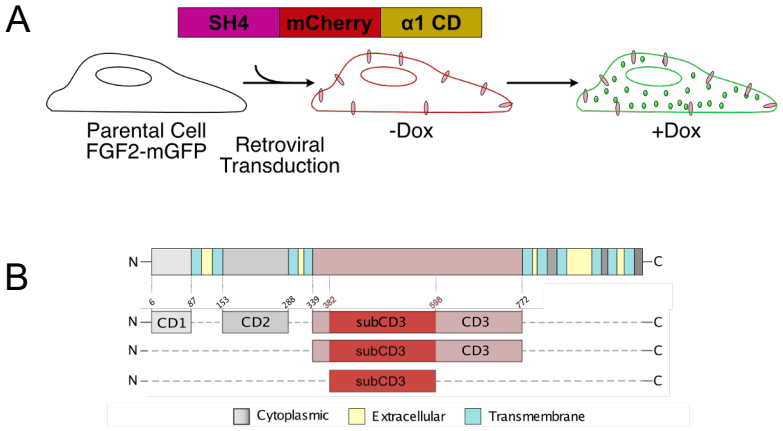

Figure 17. Schematic representation of the generation of the reporter cell lines expressing SH4-mCherry-α1 CD variants and their biological characteristics.

A. Cells expressing FGF2-mGFP were transduced with different cytosolic domains (CDs) of the α1 subunit of the Na^+,K^+-ATPase fused to the membrane-targeting domain SH4 and the fluorescent reporter mCherry. While the SH4-mCherry-α1 CD constructs are expressed constitutively, FGF2-mGFP is expressed in a doxycycline-dependent manner.

B. Schematic representation of the α1 protein sequence. The cytosolic domains are highlighted. *Adapted from Legrand et al., 2020* [54].

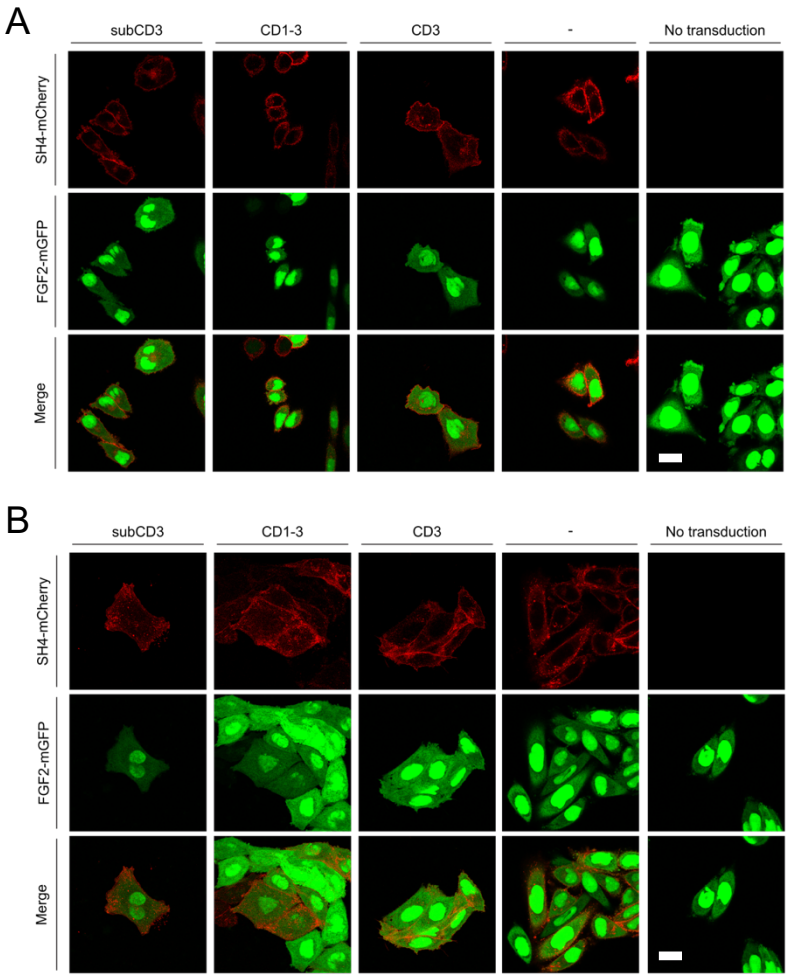

Figure 19. SH4-mCherry-α1 CD variants target the cytosolic domain of the α1 subunit of the Na^+,K^+-ATPase to the plasma membrane.

Representative fluorescence images on CHO K1 **(A)** and CHO 745 **(B)** cells expressing the different variants of the SH4-mCherry-α1 CDs construct (subCD3, CD3, CD1-3). FGF2-mGFP is shown in green, SH4-mCherry-α1 CDs in red (n=3). Scale bar 20 µm.

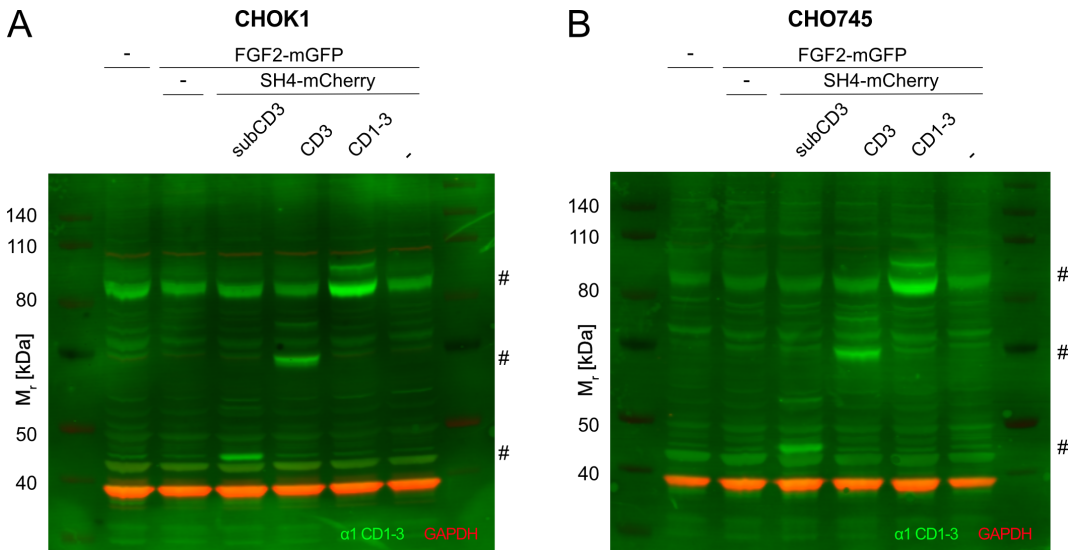

Figure 18. Na^+,K^+-ATPase and SH4-mCherry-α1 CD variants expression levels remained homogeneous in all overexpression cell lines.

Representative western blot on the expression levels of the α1 of the Na^+,K^+-ATPase and the SH4-mCherry-α1 CD variants in CHO K1 and CHO 745 cells. The analysis was conducted against α1 CD1-3 (green) and GAPDH (red) (n=3).

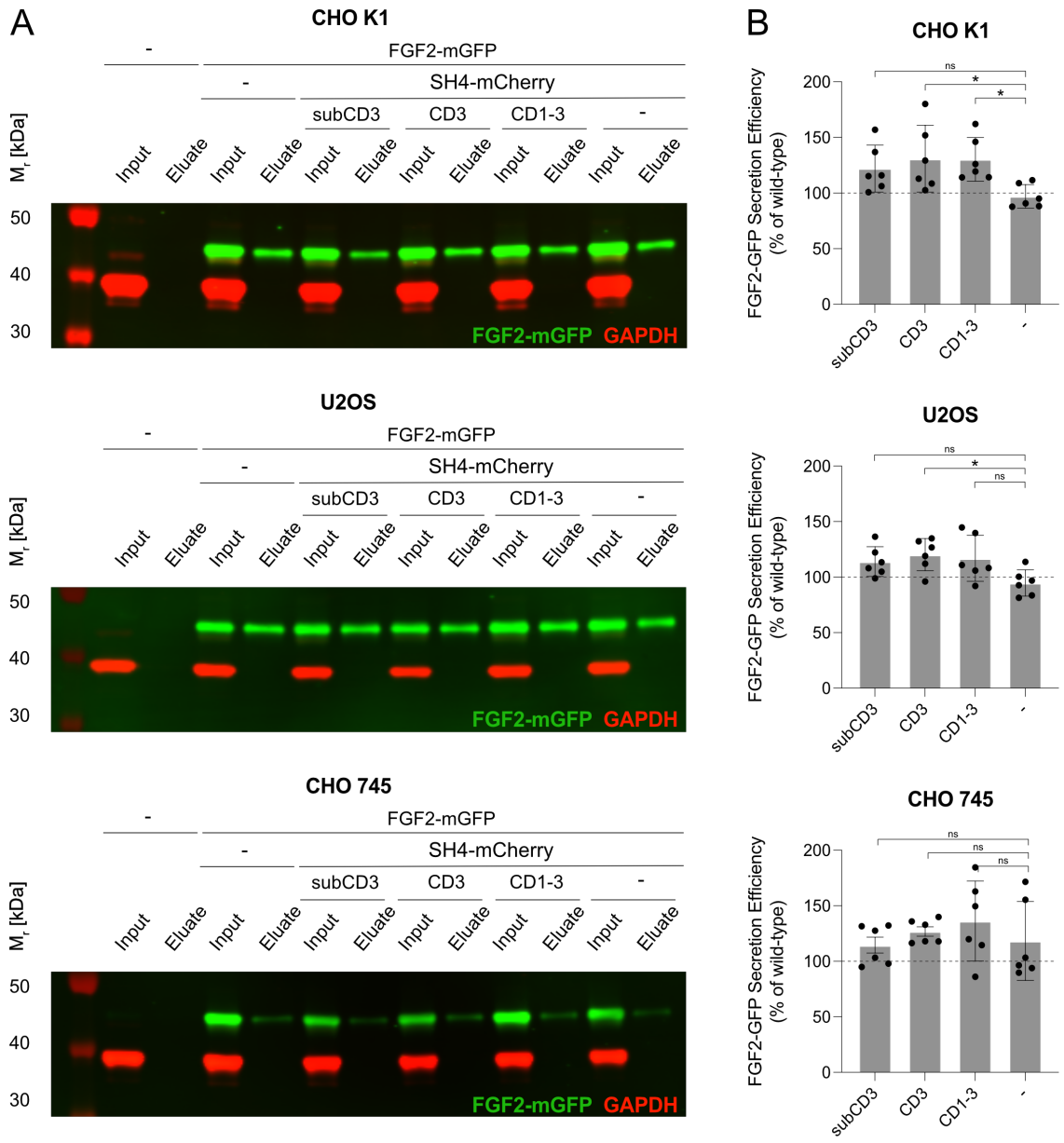

Figure 20. Efficient secretion of FGF2 from cells is enhanced with the overexpression of the cytosolic domains of the α1-subunit of the Na^+,K^+-ATPase.

Cell surface biotinylation experiments were conducted using stable CHO K1, CHO 745 and U2OS cell lines expressing FGF2-mGFP and several variants of the cytosolic domains of the α1-subunit of the Na^+,K^+-ATPase: subCD3, CD3, CD1-3. Total cell lysate (1,6 %) and biotinylated fraction (33,3 %) were analysed by western blotting using anti-GFP and anti-GAPDH antibodies.

A. Representative western blots for each cell line (CHO K1, CHO 745, U2OS). FGF2-mGFP is shown in green, GAPDH in red.

B. Quantification of FGF2-mGFP secretion efficiency. Data was quantified and normalized to the wild-type form (no SH4-mCherry-α1 CD overexpression) and set to 100 %. Data was shown as mean ± SD (n = 6), not significant (ns) $p>0,05$; *$p\leq0,05$. The statistical analysis was based on a one-way ANOVA test. Data distribution was assumed to be normal, but this was not formally tested.

SH4-mCherry-CD1-3 and SH4-mCherry were studied. Enhanced FGF2 secretion was observed in CHO K1 and U2OS when SH4-mCherry-α1 CD variants were expressed in comparison to SH4-mCherry. For every cytosolic domain of the α1 subunit variant overexpressed, FGF2 secretion increased. On the other hand, CHO 745, a cell line deficient in the synthesis of proteoglycans, and thus deficient in FGF2 secretion[278], showed no changes in FGF2 secretion. These results indicate the overexpression of the membrane-attached variants of the cytosolic domain of the Na^+,K^+-ATPase enhance FGF2 secretion.

Miss-localization of SH4-mCherry-α1 CD variants brings FGF2 secretion back to physiological levels

The SH4 domain provide an additional characteristic to the construct. The SH4 domain localizes at the plasma membrane due to post-translational modifications. It requires palmitoylation and myristylation for the correct localization[279]. When absent, the SH4 miss localizes. Hence, the SH4-mCherry-α1 CD constructs localization could be controlled by regulating its lipidation. I tested this phenomenon in the cells using fluorescence microscopy (Fig. 21). Upon treatment with of 2-bromopalmitate (2BP), a palmitoylation inhibitor, SH4-mCherry-α1 CD variants were depleted from the plasma membrane.

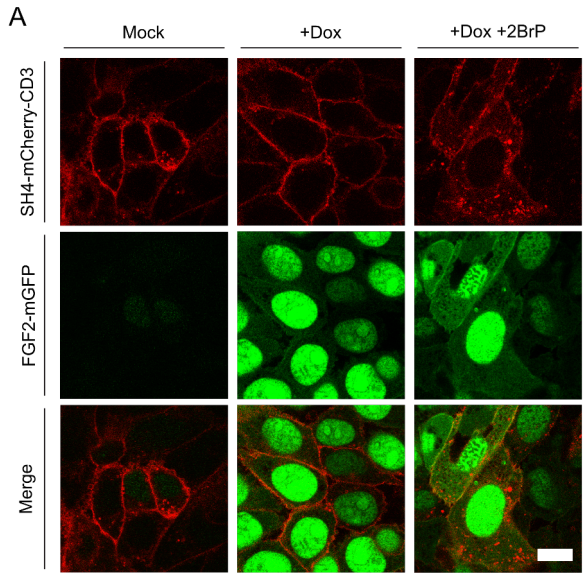

Figure 21. SH4-mCherry-α1 CD variants are displaced from the plasma membrane upon 2-bromopalmitate treatment.

Representative fluorescence images on CHO K1 cells expressing SH4-mCherry-CD3 in the absence or presence of 2-bromopalmitate (2BP, 50 μM). FGF2-mGFP is shown in green, SH4-mCherry-CD3 in red. (n=3). Scale bar 20 μm.

To challenge the first results obtained with the overexpression of the SH4-mCherry-α1 CD variants, I studied the effect on FGF2 secretion upon 2-bromopalmitate treatment. I performed cell surface biotinylation assay in CHO K1 expressing the SH4-mCherry-α1 CD variants (Fig. 22). All three cytosolic domain variants were studied, presenting homogeneous results. Interestingly, when cells were treated with 2-bromopalmitate, FGF2 secretion was dramatically reduced. That is consistent with the previous results, indicating the enhanced FGF2 secretion is directly dependent on the overexpression of the membrane-attached variants of the cytosolic domain of the Na^+,K^+-ATPase.

However, taking a further look to the cell surface biotinylation assay experiments in the presence of 2-bromopalmitate, I observed secretion did not increase in the mock condition as I observed in the first cell surface biotinylation assay experiments. The difference in conditions between these two sets of experiments was the presence of DMSO (0,1 %) in the mock treatment, while cells were untreated in the first experiment. To check if these differences were due to the addition of DMSO, I performed cell surface biotinylation assay comparing the conditions used in the previous experiments (untreated vs mock) in cells (Fig. 23). Only when SH4-mCherry-α1 CD variants overexpressing cells were untreated, FGF2 secretion increased. Thus, the concentration of DMSO used had an effect on the outcome of these experiments. And at the same time, the results confirm the differences in FGF2 observed in the two above experiments are dependent on the overexpression of the membrane-attached variants of the cytosolic domain of the α1 subunit of the Na^+,K^+-ATPase.

To sum up the outcome from the cell surface biotinylation experiments, the overexpression of the membrane-attached variants of the cytosolic domain of the α1 subunit of the Na^+,K^+-ATPase in cells led to an increase in FGF2 secretion. When these domains were displaced from the plasma

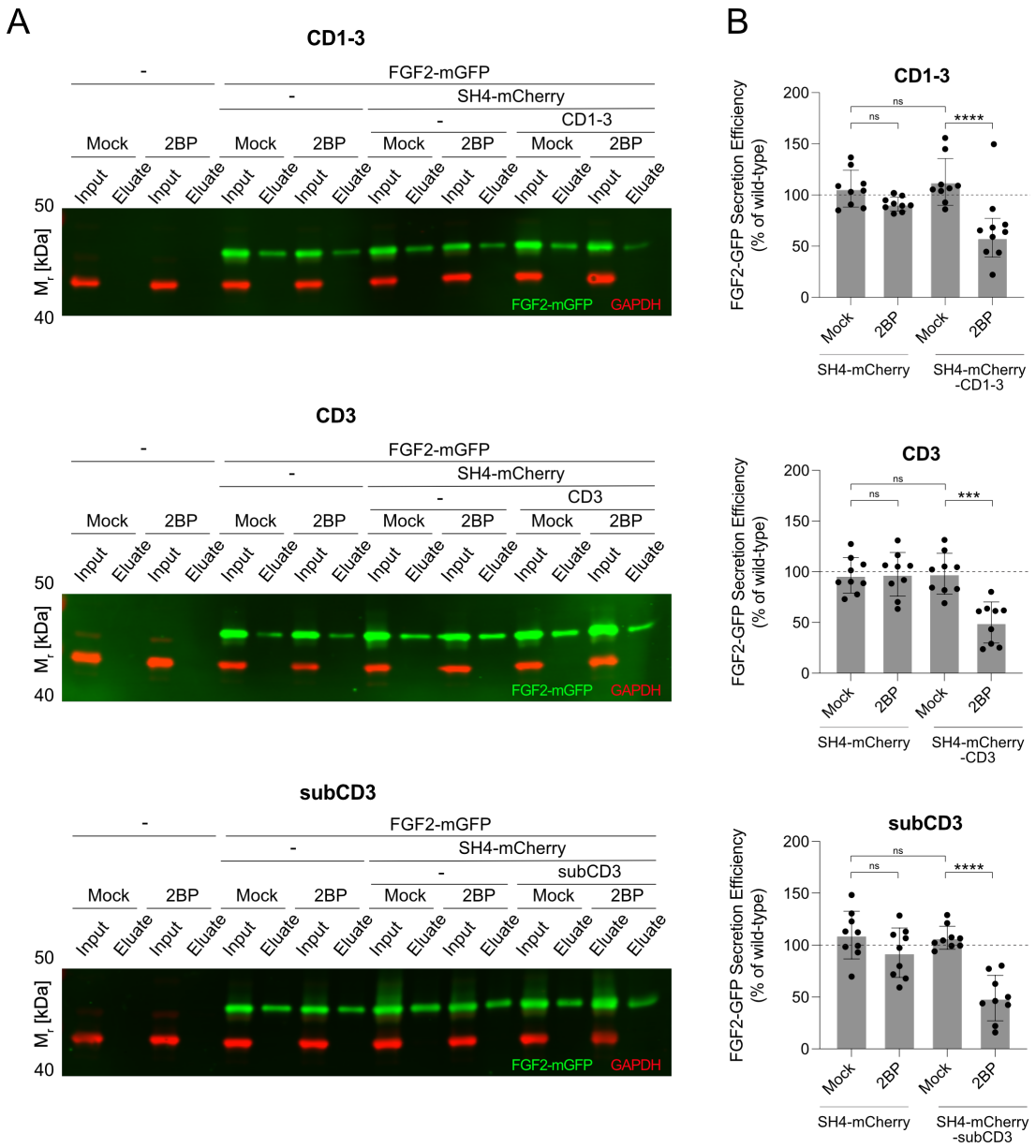

Figure 22. Efficient secretion of FGF2 from cells by the overexpression of the cytosolic domains of the α1-subunit of the Na^+,K^+-ATPase is reduced upon 2-bromopalmitate treatment.

Cell surface biotinylation experiments were conducted using stable CHO K1 cell lines expressing FGF2-mGFP and several variants of the cytosolic domains of the α1-subunit of the Na^+,K^+-ATPase: subCD3, CD3, CD1-3. The experiments were conducted in the absence or presence of 2-bromopalmitate (2BP, 50 μM). Total cell lysate (1,6 %) and biotinylated fraction (33,3 %) were analysed by western blotting using anti-GFP and anti-GAPDH antibodies.

A. Representative western blots for each overexpressed construct (CD1-3, CD3, subCD3). FGF2-mGFP is shown in green, GAPDH in red.

B. Quantification of FGF2-mGFP secretion efficiency. Data was quantified and normalized to the wild-type form (no SH4-mCherry-α1 CD overexpression) and set to 100 %. Data was shown as mean ± SD (n = 12), not significant (ns) p>0,05; ***p≤0,001; ****p≤0,0001. The statistical analysis was based on a one-way ANOVA test. Data distribution was assumed to be normal, but this was not formally tested.

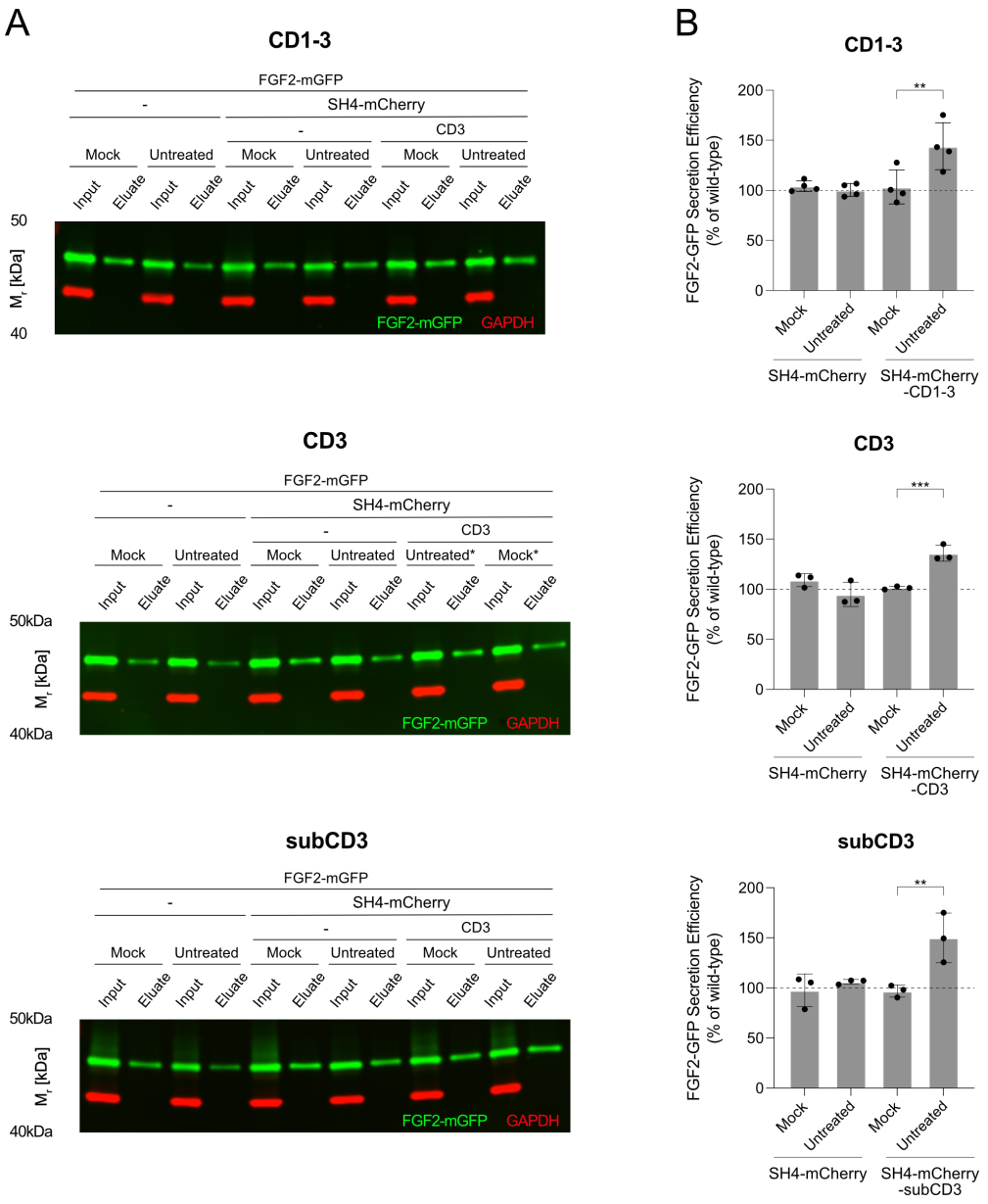

Figure 23. Enhanced secretion of FGF2 from cells by the overexpression of the cytosolic domains of the α1-subunit of the Na^+,K^+-ATPase is affected by the dissolvent.

Cell surface biotinylation experiments were conducted using stable CHO K1 cell lines expressing FGF2-mGFP and several variants of the cytosolic domains of the α1-subunit of the Na^+,K^+-ATPase: subCD3, CD3, CD1-3. The experiments were conducted in the absence or presence of DMSO (0,1 %). Total cell lysate (1,6 %) and biotinylated fraction (33,3 %) were analysed by western blotting using anti-GFP and anti-GAPDH antibodies.

A. Representative western blots for each overexpressed construct (CD1-3, CD3, subCD3). FGF2-mGFP is shown in green, GAPDH in red.

B. Quantification of FGF2-mGFP secretion efficiency. Data was quantified and normalized to the wild-type form (no SH4-mCherry-α1 CDs overexpression) and set to 100 %. Data was shown as mean ± SD (n = 3), **p≤0,01; ***p≤0,001. The statistical analysis was based on a one-way ANOVA test. Data distribution was assumed to be normal, but this was not formally tested.

membrane, FGF2 secretion decreased, with a stronger decrease than the WT secretion. These two phenomena supported further the hypothesis towards a role of the Na^+,K^+-ATPase focused on the recruitment of FGF2 as a docking platform to the membrane, with a less important contribution on the ion antiport activity of the pump.

FGF2 recruitment to the inner leaflet of the plasma membrane increases in cells expressing SH4-mCherry-α1 CD variants

To further support the hypothesis towards a role of the Na^+,K^+-ATPase focused on the recruitment of FGF2 as a docking platform to the membrane, I decided to study FGF2 recruitment upon the overexpression of the membrane-attached variants of the cytosolic domain of the α1 subunit of the Na^+,K^+-ATPase (SH4-mCherry-α1 CD) (Fig. 24). I used the TIRF recruitment assay to assess FGF2 recruitment to the plasma membrane in CHO K1 cells. 2-bromopalmitate was also used to compare the recruitment in the context of miss-localized SH4-mCherry-α1 CD variants. Cells expressing the SH4-mCherry-α1 CD constructs showed an increase recruitment in comparison to the WT cells. However, the degree of increased recruitment was not homogeneous for the constructs. While subCD3 induced a 133 % increase in FGF2 recruitment compared to WT, CD1-3 only led to a 5 % increase. Worth noticing is that the effect of FGF2 recruitment intensified as the constructs were shortened and specifically expressed FGF2 interaction sites. To displace the variants from the plasma membrane I treated cells with 2-bromopalmitate, generating two different outcomes. For CD3, the recruitment of FGF2 to the plasma membrane returned back to WT levels. For subCD3 and CD1-3, the increase in FGF2 secretion remained unaltered and did not decrease back to WT levels. WT cells showed no differences in the presence or absence of 2-bromopalmitate.

Overall, the TIRF recruitment assay showed an increase in FGF2 recruitment in cells expressing the membrane-attached variants of the cytosolic domain of the α1 subunit of the Na^+,K^+-ATPase. These results support the hypothesis that the SH4-mCherry-α1 CD constructs increase FGF2 secretion by the increase of FGF2 recruitment to the inner leaflet of the plasma membrane. However, FGF2 increased recruitment was not always recovered back to WT levels upon 2-bromopalmitate treatment. The additional docking platform provided by the SH4-mCherry-α1 CD constructs facilitated FGF2 to be recruited to the plasma membrane and FGF2 remained stably

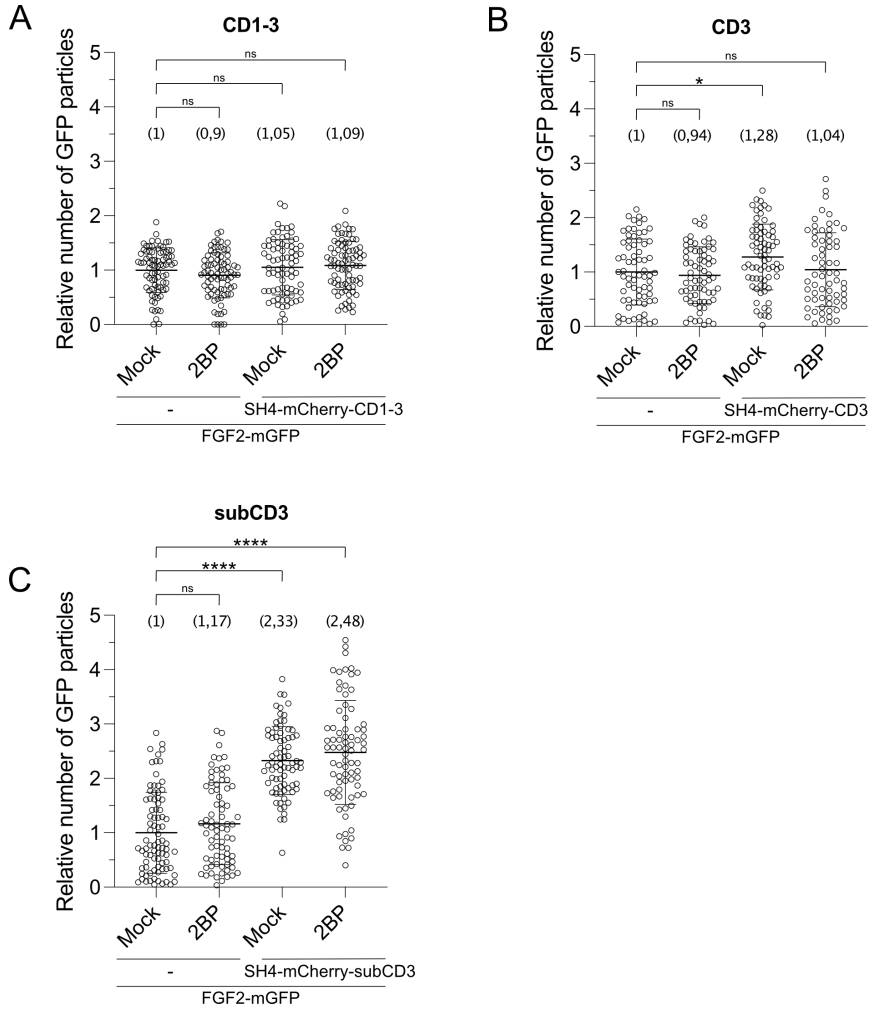

Figure 24. Small differences in FGF2-mGFP recruitment at the inner leaflet of the plasma membrane account for the increased secretion in cells overexpressing SH4-mCherry-α1 CD variants.

Quantification of real-time single-molecule TIRF recruitment assay for the CHO K1 cells expressing FGF2-mGFP and the different variants of the SH4-mCherry-α1 CD: CD1-3 **(A)**, CD3 **(B)** and subCD3 **(C)**. Cells were imaged in the presence or absence of 2-bromopalmitate (50 μM). Data was normalized to the mock condition and set to 1. Each dot represents a single cell. Data was shown as mean ± SD (n = 4). Statistical analysis was based on a one-way ANOVA test; not significant (ns) $p>0,05$; *$p\leq0,05$; ****$p\leq0,0001$.

attached to the plasma membrane after the overexpressed cytosolic domain of the α1 subunit of the Na^+,K^+-ATPase were detached from the membrane.

FGF2 dimer formation remains homogeneous in cells expressing SH4-mCherry-α1CD variants

As the above results concluded, the SH4-mCherry-α1 CD constructs led to an increase in FGF2 secretion. And this increase in FGF2 secretion was found together with an increase in FGF2 recruitment to the plasma membrane. Consequently, I wondered whether the SH4-mCherry-α1 CD variants would also lead to a change in FGF2 oligomerization.

First step I focused on FGF2 dimerization. To monitor FGF2 dimerization, I used the cross-linking assay, mentioned previously to visualize the FGF2 dimer in cells. I studied if FGF2 dimer formation was affected by the overexpression of the SH4-mCherry-α1 CD constructs (Fig. 25). BMH, BMOE and PMPI cross-linkers were used in CHO K1 cells expressing SH4-mCherry-CD3 (CD3 was chosen as the most representative domain among the SH4-mCherry-α1 CD constructs). The results were homogenous across the cross-linkers. FGF2 dimer was visible in all conditions in similar proportions. Overall, no differences in FGF2 dimer formation were observed between the SH4-mCherry construct with or without cytosolic domain.

FGF2 high-order oligomers are promoted in cells expressing SH4-mCherry-α1CD variants

After corroborating that FGF2 dimer formation was unaffected by the overexpression of the SH4-mCherry-α1 CD constructs, I wondered whether the overexpression of SH4-mCherry-α1 CD constructs would change FGF2 oligomeric size distribution at the plasma membrane.

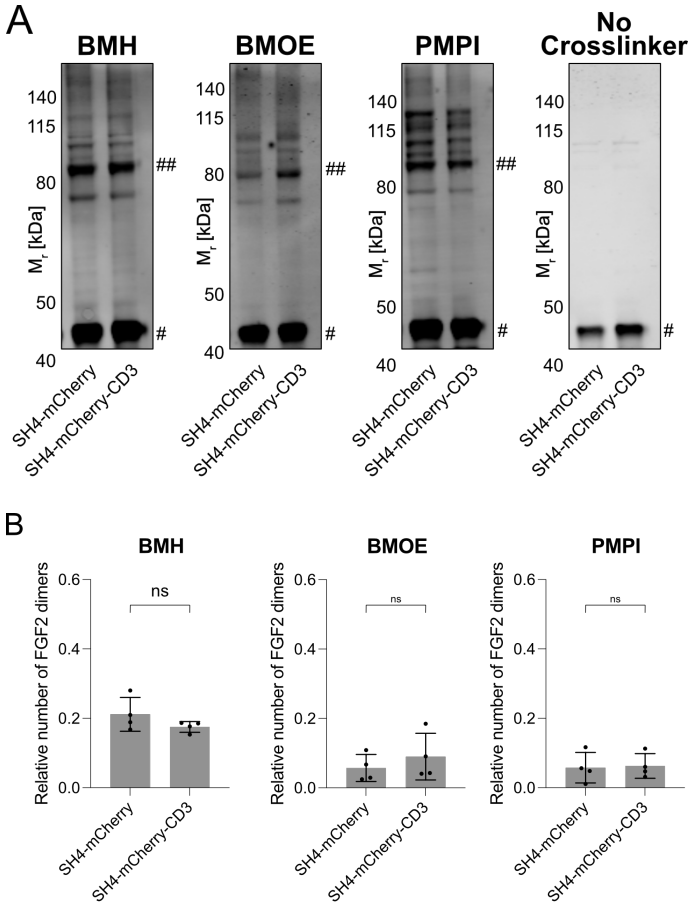

Figure 25. Fibroblast growth factor 2 (FGF2) dimer formation is robust in cells overexpressing SH4-mCherry-α1 CD3 as revealed by chemical cross-linking.

FGF2 dimer formation was analyzed by chemical cross-linking in cellular lysates. FGF2 was expressed as a FGF2-mGFP construct. FGF2 oligomers were analyzed by western blotting using polyclonal anti-FGF2 antibody. Three cross-linkers were used. N-p-maleimidophenylisocyanate (PMPI) contains a 8,7 Å length spacer between a maleimide (links to sulfhydryl groups) and isocyanate (links to hydroxyl groups) chemical groups. Bismaleimidoethane (BMOE) contains two maleimide groups separated by a 8 Å length spacer. Bismaleimidohexane (BMH) contains also two maleimide groups separated by a long 13 Å spacer.

A. Representative western blots for each cross-linkers (PMPI, BMOE, BMH). FGF2-mGFP monomers (45 kDa) are labeled with '#', FGF2-mGFP dimers (90 kDa) with '##'.

B. Quantification of FGF2-mGFP dimer to FGF2-mGFP monomer ratios. The FGF2-mGFP dimer to monomer ratios were shown as mean ± SD (n = 4), not significant (ns). The statistical analysis was based on a unpaired t-test. Data distribution was assumed to be normal, but this was not formally tested.

To check FGF2 oligomeric size distribution, I used the single brightness stoichiometry assay, mentioned previously to identify FGF2 oligomeric size distribution in living cells. I studied if FGF2 high-order oligomers formation was affected by the overexpression of the SH4-mCherry-α1 CD constructs (Fig. 26) in collaboration with Dr. Eleonora Margheritis from the group of Prof.

Katia Cosentino at the University of Osnabrück. CHO K1 cells expressing SH4-mCherry-CD3 were analyzed in the presence and absence of 2-bromopalmitate. Initially, both SH4-mCherry-CD3 in the presence and absence of 2BP showed a wide-spread intensity distribution, indicating that a diverse set of oligomers were present. Interestingly, as I took a closer analysis on the stoichiometry, I observed differences between the two. The SH4-mCherry-CD3 presented a combination of oligomers, including monomers, dimers, trimers, tetramers, hexamers and octamers. This is the first evidence of FGF2 octamers forming in living cells. In comparison to the WT, the overexpression of SH4-mCherry-CD3 led to a more extensive range of oligomers, allowing the formation from monomers to octamers, which were not previously found. On the contrary, upon 2-bromopalmitate treatment, the distribution shifted back to a similar distribution as observed in the WT cells. In the WT cells, the distribution remained homogenous in the presence and absence of 2-bromopalmitate. In conclusion, the overexpression of SH4-mCherry-CD3 enhanced the formation of FGF2 high-order oligomers. This is clear evidence supporting the role of the Na^+,K^+-ATPase in the formation of high-order oligomers required for pore formation and membrane translocation.

Na^+,K^+-ATPase abundance in the plasma membrane is reduced upon ouabain treatment

As mentioned above, inhibition of the Na^+,K^+-ATPase by ouabain leads to the inhibition of FGF2 secretion[130,137,275]. Also FGF2 loses interaction with the Na^+,K^+-ATPase when ouabain is present[54]. One consequence of ouabain inhibition of the Na^+,K^+-ATPase is the induction of Na^+,K^+-ATPase endocytosis[201,207]. I wondered, whether the FGF2 secretion inhibition by ouabain was partially due to the endocytosis of Na^+,K^+-ATPase.

For that reason, I decided to study the abundance of Na^+,K^+-ATPase in plasma membrane upon ouabain treatment. I used immunofluorescence microscopy to measure Na^+,K^+-ATPase

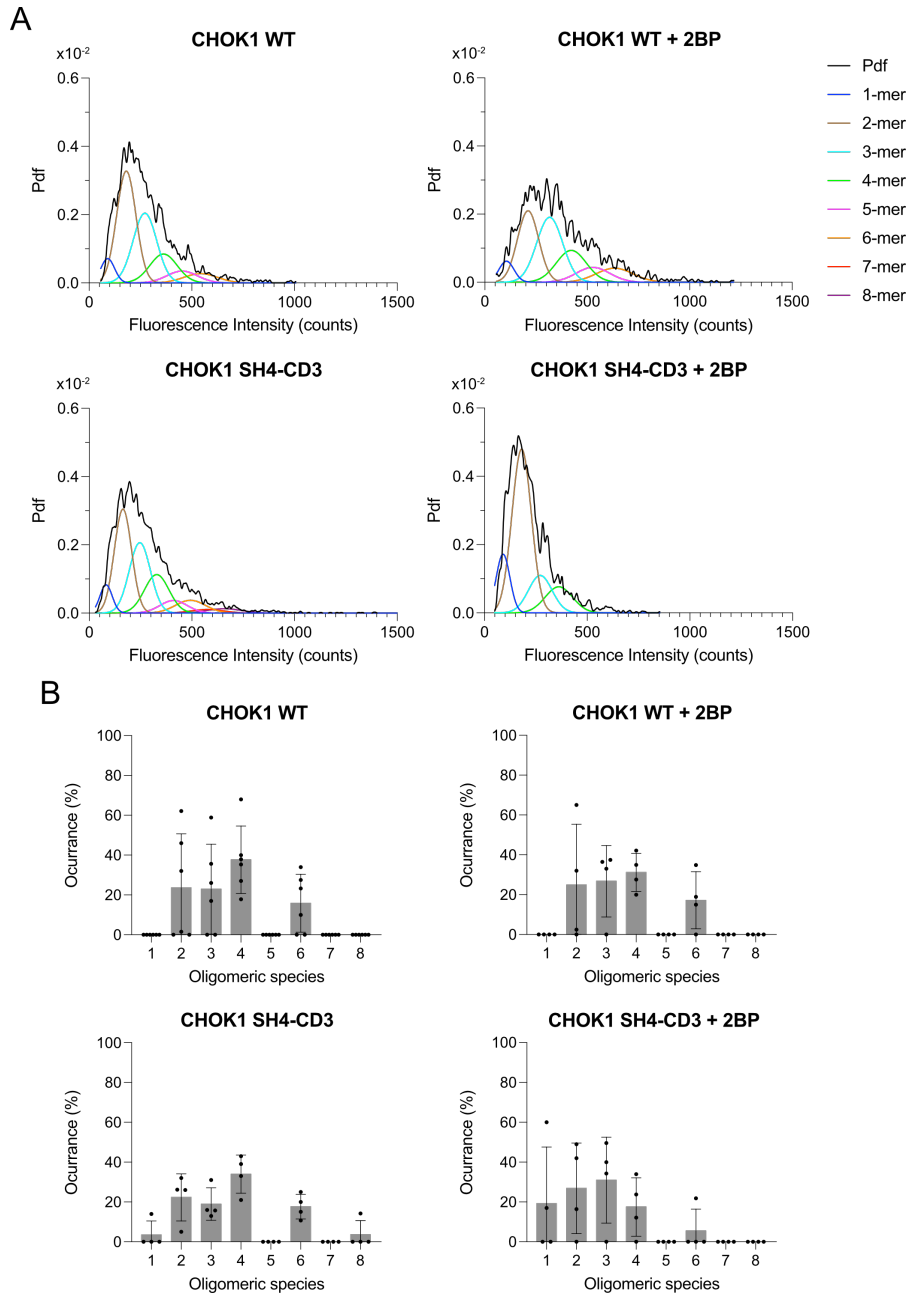

Figure 26. FGF2 oligomeric size distribution in size in SH4-mCherry-α1 CD3.

CHO K1 FGF2-mGFP SH4-mCherry-α1 CD3 and SH4-mCherry cell lines were subjected to single-molecule brightness analysis using the Stoichiometry Analysis Software[269] in the absence or presence of 2-bromopalmitate (2BP, 50 μM). Plotted data correspond to four independent experiments with a total of 40-50 cells and a minimum of a total of 1500 particles being analysed per experiment.

A. Fluorescence intensity distributions of FGF2-mGFP oligomers. Brightness distributions of all values were plotted as probability density functions shown in black. Fit of Gaussians distributions representing the possible oligomeric states FGF2 can assume are shown in colours: monomer (dark blue), dimer (brown), trimer (turquoise), tetramer (green), pentamer (pink), hexamer (orange), heptamer (red) and octamer (purple).

B. Relative occurrence in % of oligomeric species of FGF2-mGFP. Error bars correspond to the standard deviation. (n=4)

Data produced jointly with Dr. Eleonora Margheritis.

abundance upon ouabain treatment (Fig. 27). I used U2OS cells and induced FGF2 expression in the presence or absence of ouabain. Na^+,K^+-ATPase abundance in the plasma membrane was independent of FGF2 expression. When cells were treated with ouabain, Na^+,K^+-ATPase abundance in the plasma membrane was reduced, around 10 % less than in mock conditions. This provides evidence, one of the possible mechanisms contributing to the reduced secretion of FGF2 upon ouabain treatment is the endocytosis of the Na^+,K^+-ATPase, reducing the possibility to recruit FGF2 at the plasma membrane.

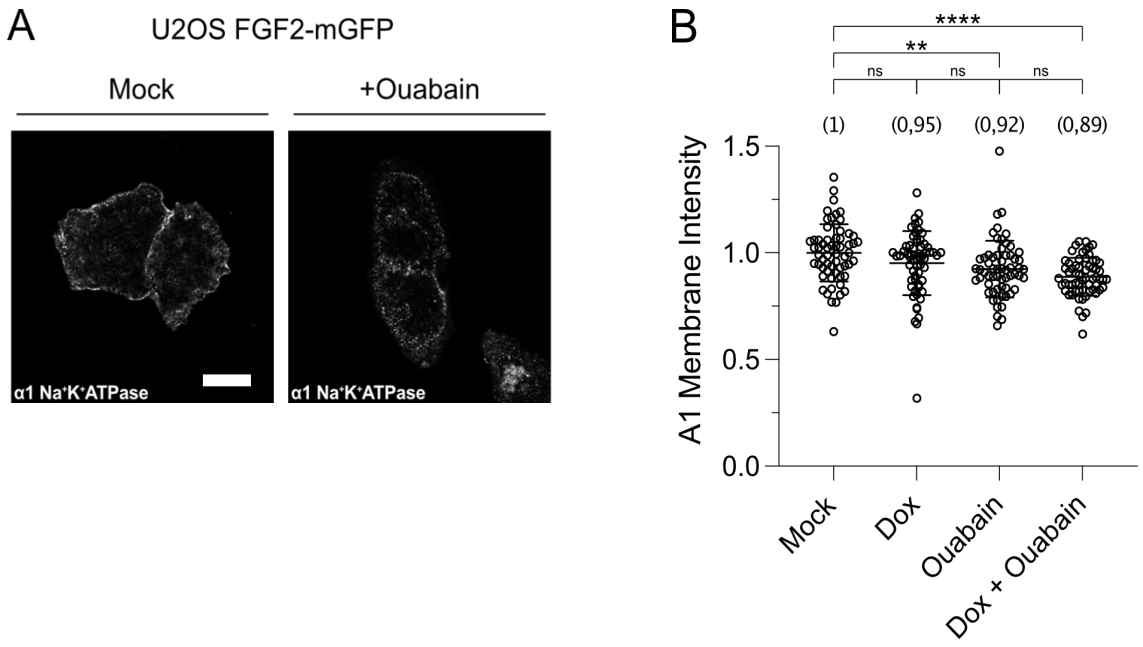

Figure 27. Na^+,K^+-ATPase abundance in plasma membrane is reduced upon ouabain treatment.

A. Representative immunofluorescence images of U2OS cells treated with ouabain (50 μM) for 6 h. Cells were imaged using anti- α1 antibody. Scale bar 20 μm.

B. Quantification of fluorescent signal at the plasma membrane of the cell relative to total surface cell. Data was quantified and normalized to average mock and set to 1 (n = 4), not significant (ns) $p>0,05$; $**p\leq0,01$; $****p\leq0,0001$. The statistical analysis was based on a one-way ANOVA test. Data distribution was assumed to be normal, but this was not formally tested.

Discussion

Great portion of FGF2 UPS pathway has been revealed in the recent years [6,51,254]. However, still several key aspects are unclear. One unknown aspect is the molecular mechanism of FGF2 oligomerization at the inner leaflet of the membrane. This aspect can be subdivided into several key points. It includes understanding the process of FGF2 assemby into complex structures, the chemical mechanism leading to the formation of disulfide bridges between FGF2 monomeres, the role of the cysteine residues in the disulfide bridge formation, and the steps in the pathway at which the intermediate oligomers form. Another unknown aspect is the functional role of the Na^+,K^+-ATPase in FGF2 UPS. As in the previous case, this aspect can be subdivided into several key points. It includes understanding the biological importance of the interaction between FGF2 and the Na^+,K^+-ATPase, the relevance of the Na^+,K^+-ATPase ion pump activity, and the relationship between the Na^+,K^+-ATPase and FGF2 oligomerization process.

Some hypotheses suggested an explanation to the mentioned scientific questions. The most prominent hypothesis suggests that the Na^+,K^+-ATPase acts as a landing platform, which recruits FGF2 into the inner leaflet of the plasma membrane. Another hypothesis suggests the interaction of FGF2 with the Na^+,K^+-ATPase would facilitate the formation of FGF2 dimers, which would later continue forward into the UPS pathway. A final hypothesis suggests that the interaction between these two proteins would be required for the maintenance of the plasma membrane potential during FGF2 membrane translocation.

In this thesis, I use a wide-range of experimental approaches to deepen the understanding on the role of the Na^+,K^+-ATPase in FGF2 secretory pathway and the relationship with FGF2 oligomerization. I provided new insights to identify the functional role of the residues C77 and

C95 and the contribution to disulfide bridge formation, together with further observations from other members in the group of Prof. Nickel[256]. I further showed that the Na^+,K^+-ATPase acts as a critical facilitator of the PI(4,5)P_2-dependent formation of high-order oligomers in a cellular context. And finally, I studied FGF2 recruitment at the inner leaflet of the plasma membrane and FGF2 secretion into the extracellular space in the context of the overexpression of a membrane-attached variant of the cytosolic domain of the α1 subunit of the Na^+,K^+-ATPase.

The cysteine residues C77 and C95 in FGF2 possess different roles in unconventional secretion

FGF2 undergoes secretion after oligomerization. FGF2 oligomerization is based on disulfide bridge formation. Previous studies have revealed that the residues C77 and C95 in FGF2 were crucial for both oligomerization and translocation[255]. However, some observations suggested a different contribution between both cysteine residues. Measuring secretion in single and double variants for the cysteine residues (C77A, C95A and C77/95A) resulted in impaired FGF secretion compared to WT. Interestingly, the double mutation had a stronger effect than the single mutation, and FGF2 C95A was less secreted than FGF2 C77A[255].

To further investigate this phenomenon and test the different contribution of the cysteine residues in FGF2 oligomerization, I decided to study dimer formation in FGF2 cysteine residues substitution variants. I used a cross-linker assay to quantify FGF2 dimer formation. I observed FGF2 C77A in the presence of cross-linker achieved dimer formation in similar proportions as compared to the WT. At the same time FGF2 C95A and FGF2 C77/95A were impaired in dimer formation.

These results support the hypothesis that the cysteine residues in FGF2 have different contribution. Specifically, the residue C95 is responsible for the formation of the disulfide bridge that produces FGF2 dimers. This result is coherent with further observations from other members in the group of Prof. Nickel, including *in sillico*, *in vitro*, and *in cellulo* experiments that support the residue C95 as the responsible residue for disulfide bride formation[256]. Indeed, these observations conclude that the FGF2 dimer is a result from the C95-C95 homo-disulfide bridge.

Complementarily, additional observations from other members in the group of Prof. Nickel suggest that the residue C77 is involved in the interaction with the Na^+,K^+-ATPase, together with the previously known residues lysines K54 and K60[54,256].

The above observations suggest the hypothesis of the FGF2 dimer as the basic unit from which FGF2 high-order oligomers (oligomers with more than 2 monomers) develop. This hypothesis was tested by studying FGF2 oligomeric size distribution in living cells. I used single brightness stoichiometric analysis in collaboration with the group of Prof. Cosentino. The results support the relevance of the residue C95 in FGF2 oligomerization, as the introduction of the C95A substitution in FGF2 led to the absence of high-order oligomers and correlated inversely with the increase in FGF2 low-order oligomers (monomer or dimer). These observations supported that the C95-C95 bond formation is essential for PI(4,5)P_2-dependent FGF2 oligomerization on membrane surface.

However, an important aspect to highlight from the stoichiometric analysis is the observation of FGF2 dimers in the FGF2 C95A. As mentioned previously, experimental observations from the group of Prof. Nickel and presented in this thesis showed that the FGF2 dimer is formed by the disulfide bridge C95-C95. Instead, this approach showed the formation of the FGF2 dimer independent of the C95-C95 disulfide bridge. Two possible hypotheses explain this observation.

One explanation relies on the fact that the single brightness stoichiometric analysis is unable to distinguish between oligomers resulting from covalent or non-covalent interactions. The FGF2 C95A would be able to form dimers by electrostatic interactions, which are unable to form a C95-C95A homo-disulfide bridge. A second explanation relies on the fact that FGF2 monomers must have several interaction interfaces in order to form high-order oligomers. The FGF2 C95A would be able to form a dimer with a different interface from the interface mediated by the residues C95-C95A interaction. Further experimental data on the formation of FGF2 high-order oligomers is required and is later discussed in this thesis.

The FGF2 dimer would also have a relevant function in the extracellular space. After translocation, experimental evidences promote the hypothesis that HSPGs disassemble FGF2 oligomers into FGF2 dimers. GPC1 was found to be a rate-limiting component of the FGF2 secretion machinery[145]. GPC1 interacts with high affinity with FGF2. The HSPGs chains that are present in GPC1 would favor the interaction with FGF2 in a dimer form. Additionally, the HSPGs chain stabilize the FGF/FGFR signaling complex, and is required for FGF binding to the receptor[112–114]. The FGF2 dimer was shown to be the functional conformation for binding the receptor[115]. Hence, it is reasonable to expect that the FGF2 C95-C95 homodimer is the primary ligand for FGFR and induce autocrine and paracrine signaling[273,274].

Taking into consideration all these observations, the current model for FGF2 oligomerization would start with the formation of the dimer as a result of the C95-C95 homo-disulfide bridge formation. The FGF2 dimer would serve as the building unit from which high-order oligomeric species can develop. The high-order oligomeric species accumulate and reach the functionality to translocate across the plasma membrane. Finally, FGF2 oligomers would disassemble post-translocation into the C95-C95 homo-disulfide bridge dimer to perform the cell signaling function.

The FGF2 tetramer and hexamer appear as important intermediate species to form functional oligomers for membrane translocation

Previous studies have shown the FGF2 dimer as the predominant oligomeric species in the plasma membrane of eukaryotic cells[131]. FGF2 was detected to form high-order (oligomers with more than 2 monomers) oligomeric species *in vitro*[255]. FGF2 oligomerization is crucial for pore formation and membrane translocation. However, the exact mechanism through which oligomerization provides the functionality for translocation to the FGF2 complex is still to be described.

In the pursuit to understand the oligomerization process, I performed in collaboration with the group of Prof. Cosentino a stoichiometric analysis of FGF2 in the plasma membrane of eukaryotic cells. This analysis, in contrast to the previous results, provided evidence for the existence of FGF2 tetramer and hexamer in living cells. FGF2 variants binding-deficient for the different components of the secretory machinery, as well as a dimer-deficient variant resulted in the lack of high-order oligomers. These FGF2 variants were restrained into monomers and dimers.

These observations are very interesting, as they expand over the previous knowledge on FGF2 oligomerization. Curiously the oligomeric distribution profiles correlate with the secretion rates of the FGF2 variants[54,144]. FGF2 variants that led to the absence of high-order oligomers showed reduced FGF2 secretion. These observations highlight the importance of FGF2 oligomerization for the efficient translocation across the plasma membrane and corroborate previous findings for the proposed FGF2 secretion mechanism by the group of Prof. Nickel[254].

The presence of tetramers and hexamers but not further oligomers suggest the hypothesis that the FGF2 tetramer or hexamer might be important intermediates to reach functional oligomers for

translocation. This is coherent with recent *in vitro* experiments, which determine tetramers and hexamers as the minimal oligomeric species capable of pore formation in liposomes[144,280]. Specifically, FGF2 hexamers were the most predominant oligomeric species linked to membrane pore formation. Additional on-going work from members of the group of Prof. Nickel shows that FGF2 tetramer and hexamer accumulate $PI(4,5)P_2$ locally in high abundance. This local high accumulation of $PI(4,5)P_2$ molecules would be sufficient for membrane remodeling events. These observations would support FGF2 tetramers and hexamers as functional for pore formation and translocation.

Taking into consideration all these observations, the current model for FGF2 oligomerization would start with the formation of FGF dimers. The FGF2 dimer would develop into high-order oligomeric species, including FGF2 tetramers and hexamers. FGF2 high-order oligomers interaction with the lipids in the membrane would correlate with a local accumulation of $PI(4,5)P_2$. Local accumulation of $PI(4,5)P_2$ is required for the remodeling of the plasma membrane and formation of a toroidal pore. The FGF2 tetramer and hexamer would be the minimal oligomeric species that accumulate sufficient $PI(4,5)P_2$ adequate for toroidal pore formation and FGF2 translocation.

Further experiments should be performed to determine the interface involve in the tetramer and hexamer formation and to determine the capacity for pore formation. Molecular dynamics simulations of FGF2 in interaction with the plasma membrane could provide insights on these aspects, both the potential FGF2 monomers interfaces and the accumulation of $PI(4,5)P_2$ in the membrane. The interfaces can be computed according to the thermodynamically most-favorable interface. The observations found from the simulations could be later be validated with the generation of FGF2 variants that substitute the residues involved in the formation of the newly

described interfaces. These FGF2 variants would be tested with *in vitro* and *in cellulo* experiments studying FGF2 oligomerization, recruitment and secretion.

The α1 subunit of the Na^+,K^+-ATPase contributes to the formation of FGF2 high-order oligomers

As previously discussed, FGF2 oligomerization is crucial for pore formation and membrane translocation. Previous experiments from the group of Prof. Nickel showed that FGF2 oligomerization was dependent on the residue C95, involved in FGF2 dimer formation, and the residues K127, R128, K133, involved in FGF2 interaction with $PI(4,5)P_2$ and FGF2 high-order oligomer formation[52,144,255,256]. In this thesis, experimental observations suggest that FGF2 interaction with the Na^+,K^+-ATPase may have a role in FGF2 oligomerization as important as the mentioned factors.

In order to deepen the understanding on the role of the Na^+,K^+-ATPase, I studied FGF2 oligomerization in relation to the secretory machinery. I used both the cross-linking assay and brightness stoichiometric analysis for that purpose. In both approaches I used the FGF2 variants binding-deficient for the secretory machinery at the inner leaflet of the plasma membrane, in particular, to the Na^+,K^+-ATPase and $PI(4,5)P_2$; as well as a dimer-deficient variant (C95A). The cross-linking assay provided insights on FGF2 dimer formation in these variants. FGF2 variants binding-deficient for the Na^+,K^+-ATPase and $PI(4,5)P_2$ showed reduced FGF2 dimer formation, with a stronger effect as the FGF2 dimer-deficient variant C95A. The stoichiometric analysis, performed in collaboration with the group of Prof. Cosentino, showed that FGF2 oligomeric size distribution presented high-order oligomers in the FGF2 WT variant. However, FGF2 variants binding-deficient for the different components of the secretory machinery, as well as a dimer-

deficient variant, resulted in the lack of high-order oligomers. These FGF2 variants were restrained into monomers and dimers.

The experimental results obtained with the FGF2 variants deficient for PI(4,5)P_2-binding and dimer formation corroborated the previous findings for the proposed FGF2 oligomerization mechanism by the group of Prof. Nickel. These results confirm the importance of the residues C95, K127, R128, K133 in FGF2 oligomerization.

Interestingly, the FGF2 variants binding-deficient for the Na^+,K^+-ATPase showed analogous results as the mentioned FGF2 variants deficient for PI(4,5)P_2-binding and dimer formation. These observations suggests that the Na^+,K^+-ATPase is also a crucial element in the formation of high-order FGF2 in cells. And these observations also suggest that FGF2 interaction with the Na^+,K^+-ATPase might be as important as the interaction with PI(4,5)P_2 for the formation of high-order oligomers. This indicates that both the Na^+,K^+-ATPase and PI(4,5)P_2 would work coordinately for a correct FGF2 oligomerization and efficient secretion of FGF2.

These observations are reinforced with the results obtained from the brightness stoichiometric analysis performed on cells overexpressing a membrane-attached variant of the cytosolic domain of the Na^+,K^+-ATPase. FGF2 high-order oligomeric population increased and even FGF2 octamers were observed. This further highlights the relevance of the Na^+,K^+-ATPase in FGF2 oligomerization.

Another observation that further highlights the relevance of the Na^+,K^+-ATPase in FGF2 oligomerization was obtained from the brightness stoichiometric analysis performed in cells treated with ouabain. FGF2 high-order oligomeric population was reduced upon ouabain treatment. This approach validated the result obtained from studying the FGF2 variant binding-

deficient for the Na^+,K^+-ATPase. And the observation also is coherent with previous findings from the group of Prof. Nickel[54,130].

Simultaneously, FGF2 dimer formation assessed by the cross-linking assay showed no differences in cells overexpressing a membrane-attached variant of the ATPase cytosolic domain of the Na^+,K^+-ATPase. This indicates that the overexpression of a membrane-attached variant of the ATPase cytosolic domain of the Na^+,K^+-ATPase stabilized the formation of high-order oligomers. Hence, this observation supports that FGF2 interaction with the Na^+,K^+-ATPase is relevant for the formation of FGF2 high-order oligomers.

Other experimental observations may support the hypothesis that the Na^+,K^+-ATPase is important for the formation of FGF2 high-order oligomers. These observations are related with the role of the Na^+,K^+-ATPase in the regulation of the redox potential[281] and intracellular ROS levels in cells[282]. FGF2 oligomerization is based on disulfide bridge formation[255], which requires the presence of oxidative agents to catalyze the reaction. The Na^+,K^+-ATPase has been recently linked to aquaporins or oxidases, which generate reactive oxygen species (ROS)[283]. ROS could be suggested as a potential oxidative agent that promotes disulfide bridge formation and FGF2 dimerization.

Taking into consideration all these observations, the outcome of these experiments support the hypothesis that FGF2 interaction with the Na^+,K^+-ATPase is relevant for the formation of FGF2 high-order oligomers. This adds an additional facet to the role of the Na^+,K^+-ATPase in FGF2 UPS. Further experimental data on the role of the Na^+,K^+-ATPase in the formation of FGF2 high-order oligomers is required and is later discussed in this thesis.

The cytosolic domain of the α1 subunit of the Na^+,K^+-ATPase facilitates FGF2 recruitment to the inner leaflet of the plasma membrane

Several evidences throughout the decades have suggested the Na^+,K^+-ATPase had a role in FGF2 UPS[54,130,137,275]. In the latest study from the group of Prof. Nickel, FGF2 direct interaction with the Na^+,K^+-ATPase was described[54]. The exact residues involved in the interaction were identified, and FGF2 variants with these residues substituted showed a small decrease in plasma membrane recruitment and secretion. From the experimental outcome, it was pointed out that the Na^+,K^+-ATPase was the first point of contact at the inner leaflet of the plasma membrane. However, the relevance of this interaction in FGF2 UPS remained unsolved.

One hypothesis proposed that the Na^+,K^+-ATPase could operate as a landing platform for FGF2, in order to reach the inner leaflet of the plasma membrane and advance into the secretory pathway. The hypothesis was tested though different approaches in this thesis, including advanced microscopy and biochemical techniques to measure the recruitment and secretion rates of FGF2. Additionally, membrane-attached variants of the cytosolic domain of the Na^+,K^+-ATPase were overexpressed in cells and studied with these experimental approaches. The TIRF recruitment assay showed that FGF2 recruitment increased upon the overexpression of the Na^+,K^+-ATPase cytosolic domains. Consequently, the biotinylation experiments showed that FGF2 secretion increased upon the overexpression of the Na^+,K^+-ATPase cytosolic domains. The increase in FGF2 recruitment and secretion withdrew when the overexpressed Na^+,K^+-ATPase cytosolic domain variants were displaced from the plasma membrane upon 2-bromopalmitate treatment.

These results support the hypothesis that the main role for the Na^+,K^+-ATPase in FGF2 UPS is to provide FGF2 a landing platform at the inner leaflet of the plasma membrane. Indeed, the

Na^+,K^+-ATPase would not be just the first contact of FGF2 to the plasma membrane, but rather would facilitate the recruitment of FGF2 to the inner leaflet. This function might be extremely relevant in the complex context of a biological cell membrane. While FGF2 has a high affinity toward the $PI(4,5)P_2$ lipids, as *in vitro* experiments with liposomes have shown[52,142], $PI(4,5)P_2$ represent a very small percentage of the lipid composition in eukaryotic plasma membranes[217]. Additionally, a high amount of membrane-related biological processes involve $PI(4,5)P_2$, which results in a high competition for the interaction with $PI(4,5)P_2$ between $PI(4,5)P_2$-binding proteins. Na^+,K^+-ATPase would facilitate that FGF2 overcomes the protein competition and interacts with the $PI(4,5)P_2$ lipids in the membrane. The Na^+,K^+-ATPase is abundantly present in the plasma membrane and the cytosolic domain extends outside of the membrane, facilitating the contact with the cytosolic FGF2.

Further experimental research is required to support the observations of the role of the Na^+,K^+-ATPase in the membrane recruitment of FGF2 and the formation of FGF2 high-order oligomers. *In vitro* reconstitution of the auxiliary machinery in liposomes would provide the experimental setup to study FGF2 recruitment and translocation, as well as FGF2 oligomerization. Another approach would be the use of genome editing techniques to mutate the endogenous Na^+,K^+-ATPase into a FGF2 binding-deficient variant and study FGF2 oligomerization, recruitment and secretion in cells. Further experiments can focus on studying the redox machinery at the plasma membrane and finding the relation to the secretory machinery of FGF2. Aquaporins or oxidases that have been previously described to interact with the Na^+,K^+-ATPase are good starting candidates. FGF2 secretion could be studied in conditions where redox machinery is altered by knock downs or chemical inhibition.

General effects of ouabain incubation may contribute indirectly to the inhibitory effect on FGF2 secretion in cells

Since the first evidences indicating a role of the Na^+,K^+-ATPase in FGF2 UPS, it was hypothesized the ion antiporter activity of the pump was required for the process. While approaches preventing the correct interaction of FGF2 with the Na^+,K^+-ATPase had an effect on FGF2 UPS, including Na^+,K^+-ATPase knockdowns, FGF2 binding-deficient variants or ouabain-dependent Na^+,K^+-ATPase inhibition; approaches disturbing the ion transport and membrane potential gradient showed no effect on FGF2 UPS[54,130,137,275] . Hence, the contribution of the ion pump activity on FGF2 UPS was unclear.

To clarify the relationship between FGF2 UPS and Na^+,K^+-ATPase ion antiporter activity, I monitored the concentration of ATP in cells as a readout for the activity of the Na^+,K^+-ATPase. Although ATP is substrate for many biochemical processes in the cell, the relationship between ATP and the Na^+,K^+-ATPase activity was established due to the high-rate of consumption of ATP by the Na^+,K^+-ATPase in cells[276]. The concentration of ATP was monitored using a Förster resonance energy transfer (FRET)-based sensor in different time scales, including real-time and time-point snapshot. Additionally, the effect of ouabain in the concentration of ATP was measured. The monitorization of the concentration of ATP in real-time resulted inadequate for the scope of the study. No differences in the concentration of ATP were observed in mock or ouabain-treated conditions. Changes in ATP concentration were observed only upon drastic metabolic conditions induced by the inhibition of the glycolysis and the respiratory chain with 2-deoxyglucose and potassium cyanide[261]. The monitorization of the concentration of ATP in time-point snapshots of longer incubation time showed that incubation with ouabain led to a decrease

in ATP concentration in cells. However, FGF2 expression produced no significant change in the concentration of ATP in cells.

There are two outcomes resulting from these experiments. One refers to the sensitivity of the FRET-based ATP sensor. During the monitorization of the concentration of ATP in real-time, no differences were observed upon ouabain treatment. This indicates that the effect of ouabain in the concentration of ATP in cells was undetected by the sensor. Hence, the effect of ouabain either requires longer incubation time as the time scale used in the real-time monitorization (25 min) to produce an effect; or produces a minor effect in ATP concentration, which are below than the sensitive range of the sensor (~ mM).

The other outcome refers to the effect of ouabain in the concentration of ATP in cells. In the conditions measured, 6 h incubation with 50 μM ouabain, the concentration of ATP was reduced. This result is coherent with the known canonical effect of ouabain[188–190]. The sustained inhibition of the Na^+,K^+-ATPase compromises the well-functioning of the cell due to the importance of the ion antiport activity in the homeostasis of the cell. In extreme case, the inhibition of the Na^+,K^+-ATPase compromises the cell metabolism and may lead to cytotoxic effects. Although this is an indirect effect, it may contribute to the inhibitory effect of ouabain in FGF2 secretion.

Another general consequence of the incubation with ouabain that may contribute to the inhibitory effect on FGF2 secretion is the internalization of the Na^+,K^+-ATPase. Inhibition of the Na^+,K^+-ATPase by ouabain can lead to the induction of Na^+,K^+-ATPase endocytosis[201,207]. I measured the abundance of Na^+,K^+-ATPase in plasma membrane upon ouabain treatment using immunofluorescence microscopy. Na^+,K^+-ATPase abundance in the plasma membrane was reduced around 10 % in cells treated with ouabain. This result supports that another possible

mechanism contributing to the reduced secretion of FGF2 upon ouabain treatment is the endocytosis of the Na^+,K^+-ATPase.

Overall, the outcomes observed in the above experiments corroborated the canonical effects of ouabain in cells. These general consequences may contribute to the inhibitory effect exerted by ouabain in FGF2 UPS. However, the experimental setup was unable to provide insights to the specific mechanism by which the ion antiport activity of the Na^+,K^+-ATPase is relevant for FGF2 secretion. Hence, further experimental work is required to tackle these two aspects. Molecular dynamic simulations may provide new perspective on the presence of conformational changes in the Na^+,K^+-ATPase upon the binding of ouabain. *In vitro* reconstitution of the Na^+,K^+-ATPase may provide a valuable setup to study the activity of the Na^+,K^+-ATPase.

A direct inhibitory effect of ouabain on FGF2 secretion in cells is based on the prevention of the formation of FGF2 high-order oligomers

More importantly, the experimental work in this thesis indeed reported a direct consequence of ouabain that contributes to the inhibitory effect of ouabain in FGF2 secretion. This direct effect is more relevant than the above mentioned effects and can contribute to the explanation of the inhibitory effect of ouabain in FGF2 UPS. Treatment with ouabain resulted in the reduction of FGF2 high-order oligomers in cells as assessed by the stoichiometric analysis. This result validated the observation that FGF2 high-order oligomers were reduced in a FGF2 variant deficient for the binding with the Na^+,K^+-ATPase. The result is also coherent with the observation that FGF2 interaction with the Na^+,K^+-ATPase was reduced upon ouabain treatment[54]. All these observations suggest a hypothesis describing the direct mechanism by which ouabain inhibits FGF2 secretion. The incubation of cells with ouabain would prevent the interaction between FGF2 and the

Na^+,K^+-ATPase. The lack of interaction between FGF2 and the Na^+,K^+-ATPase would prevent the formation of FGF2 high-order oligomers. Without the formation of high-order oligomers, FGF2 would lack the capacity to remodel the plasma membrane and would be unable to form the toroidal pore for efficient translocation. To validate this hypothesis further experimental work would be required with the focus on understanding the role of the Na^+,K^+-ATPase in the formation of FGF2 high-order oligomers, as previously discussed in this thesis.

Conclusion

In this thesis, I provided new insights in the role of the Na^+,K^+-ATPase in FGF2 UPS. Complementarily, I investigated FGF2 oligomerization and the dependance to the secretory machinery, in particular to the Na^+,K^+-ATPase and the $PI(4,5)P_2$ lipids. Additionally, I provided evidence that identify the functional role of the residues C77 and C95 and the contribution to disulfide bridge formation, together with further observations from other members in the group of Prof. Nickel. I further showed that the Na^+,K^+-ATPase acts as a critical facilitator of the $PI(4,5)P_2$-dependent formation of high-order oligomers in a cellular context. And finally, I studied FGF2 recruitment at the inner leaflet of the plasma membrane and FGF2 secretion into the extracellular space in the context of the overexpression of a membrane-attached variant of the cytosolic domain of the $\alpha 1$ subunit of the Na^+,K^+-ATPase.

These contributions improved the understanding on FGF2 UPS. The results provide an updated function to the Na^+,K^+-ATPase in FGF2 secretion as previously described. While the role as a protein docking platform for FGF2 gains relevance, a new role in the formation of FGF2 high-order oligomers appears.

Published Work and Contributions

Published work

Portions of the work described in this thesis were published at:

-Lolicato, Steringer. et al. Disulfide bridge-dependent dimerization triggers FGF2 membrane translocation into the extracellular space. eLife 12, RP88579 (2024).

-Bayer, Fernández-Sobaberas, Griffo, *et al.* Nanoscale PI(4,5)P_2 partitioning driven by FGF2 oligomerization triggers membrane pore formation. BioRxiv (2025) (*preprint*).

The methods "*Cross-linking experiments*" and "*Determination of the oligomeric size distribution of FGF2-mGFP by single particle brightness analysis*" were published in the original manuscript and inlcuded in this thesis.

The figures "*Figure 9. Fibroblast growth factor 2 (FGF2) dimer formation in cells depends on the residue C95 as revealed by chemical cross-linking.*" and "*Figure 12. FGF2 oligomeric size distribution in FGF2-mGFP variants.*" were published in the original manuscript and included in this thesis.

Contributions

Acknowledgment of the contribution to the presented work is given to:

The experiments and analysis for the determination of the oligomeric state of FGF2-mGFP were performed in collaboration with Dr. Eleonora Margheritis from the group of Prof. Katia Cosentino at the Department of Biology/Chemistry and Center for Cellular Nanoanalytics (CellNanOs) from the University of Osnabrück.

References

1. IUPAC-IUB Commission on Biochemical Nomenclature A One-Letter Notation for Amino Acid Sequences1–3. *J. Biol. Chem.* **243**, 3557–3559 (1968).
2. Palade, G. Intracellular Aspects of the Process of Protein Synthesis. *Science* **189**, 347–358 (1975).
3. Rothman, J. E. Mechanisms of intracellular protein transport. *Nature* **372**, 55–63 (1994).
4. Rothman, J. E. & Wieland, F. T. Protein Sorting by Transport Vesicles. *Science* **272**, 227–234 (1996).
5. Schekman, R. & Orci, L. Coat Proteins and Vesicle Budding. *Science* **271**, 1526–1533 (1996).
6. Pallotta, M. T. & Nickel, W. FGF2 and IL-1β – explorers of unconventional secretory pathways at a glance. *J. Cell Sci.* **133**, jcs250449 (2020).
7. Farhan, H. & Rabouille, C. Signalling to and from the secretory pathway. *J. Cell Sci.* **124**, 669–669 (2011).
8. Blobel, G. & Sabatini, D. Dissociation of Mammalian Polyribosomes into Subunits by Puromycin. *Proc. Natl. Acad. Sci.* **68**, 390–394 (1971).
9. Voeltz, G. K., Rolls, M. M. & Rapoport, T. A. Structural organization of the endoplasmic reticulum. *EMBO Rep.* **3**, 944–950 (2002).
10. Gorlich, D. Protein translocation into proteoliposomes reconstituted from purified components of the endoplasmic reticulum membrane. *Cell* **75**, 615–630 (1993).
11. Benham, A. M. Protein Secretion and the Endoplasmic Reticulum. *Cold Spring Harb. Perspect. Biol.* **4**, a012872–a012872 (2012).
12. Jackson, R. C. & Blobel, G. Post-translational cleavage of presecretory proteins with an extract of rough microsomes from dog pancreas containing signal peptidase activity. *Proc. Natl. Acad. Sci.* **74**, 5598–5602 (1977).
13. Gogala, M. *et al.* Structures of the Sec61 complex engaged in nascent peptide translocation or membrane insertion. *Nature* **506**, 107–110 (2014).
14. Pfeffer, S. *et al.* Structure of the native Sec61 protein-conducting channel. *Nat. Commun.* **6**, 8403 (2015).
15. Li, L. *et al.* Crystal structure of a substrate-engaged SecY protein-translocation channel. *Nature* **531**, 395–399 (2016).
16. McGilvray, P. T. *et al.* An ER translocon for multi-pass membrane protein biogenesis. *eLife* **9**, e56889 (2020).

17. Brodsky, J. L., Goeckeler, J. & Schekman, R. BiP and Sec63p are required for both co- and posttranslational protein translocation into the yeast endoplasmic reticulum. *Proc. Natl. Acad. Sci.* **92**, 9643–9646 (1995).

18. Loaeza-Reyes, K. J. *et al.* An Overview of Glycosylation and its Impact on Cardiovascular Health and Disease. *Front. Mol. Biosci.* **8**, 751637 (2021).

19. Schoberer, J., Shin, Y.-J., Vavra, U., Veit, C. & Strasser, R. Analysis of Protein Glycosylation in the ER. in *The Plant Endoplasmic Reticulum* (eds Hawes, C. & Kriechbaumer, V.) vol. 1691 205–222 (Springer New York, New York, NY, 2018).

20. Vembar, S. S. & Brodsky, J. L. One step at a time: endoplasmic reticulum-associated degradation. *Nat. Rev. Mol. Cell Biol.* **9**, 944–957 (2008).

21. Feige, M. J. & Hendershot, L. M. Disulfide bonds in ER protein folding and homeostasis. *Curr. Opin. Cell Biol.* **23**, 167–175 (2011).

22. Sato, K. COPII Coat Assembly and Selective Export from the Endoplasmic Reticulum. *J. Biochem. (Tokyo)* **136**, 755–760 (2004).

23. Sato, K. & Nakano, A. Mechanisms of COPII vesicle formation and protein sorting. *FEBS Lett.* **581**, 2076–2082 (2007).

24. Nakano, A. & Muramatsu, M. A Novel GTP-binding Protein, Sarlp, Is Involved in Transport from the Endoplasmic Reticulum to the Golgi Apparatus.

25. Barlowe, C. & Schekman, R. SEC12 encodes a guanine-nucleotide-exchange factor essential for transport vesicle budding from the ER. *Nature* **365**, 347–349 (1993).

26. Kuehn, M. J., Herrmann, J. M. & Schekman, R. COPII–cargo interactions direct protein sorting into ER-derived transport vesicles. *Nature* **391**, 187–190 (1998).

27. Saito, K. *et al.* TANGO1 Facilitates Cargo Loading at Endoplasmic Reticulum Exit Sites. *Cell* **136**, 891–902 (2009).

28. Malhotra, V. & Erlmann, P. Protein export at the ER: loading big collagens into COPII carriers. *EMBO J.* **30**, 3475–3480 (2011).

29. Peotter, J., Kasberg, W., Pustova, I. & Audhya, A. COPII-mediated trafficking at the ER/ERGIC interface. *Traffic* **20**, 491–503 (2019).

30. Appenzeller-Herzog, C. & Hauri, H.-P. The ER-Golgi intermediate compartment (ERGIC): in search of its identity and function. *J. Cell Sci.* **119**, 2173–2183 (2006).

31. Brandizzi, F. & Barlowe, C. Organization of the ER–Golgi interface for membrane traffic control. *Nat. Rev. Mol. Cell Biol.* **14**, 382–392 (2013).

32. Lucocq, J. M., Berger, E. G. & Warren, G. Mitotic Golgi fragments in HeLa cells and their role in the reassembly pathway. *J. Cell Biol.* **109**, 463–474 (1989).

33. Huang, S. & Wang, Y. Golgi structure formation, function, and post-translational modifications in mammalian cells. *F1000Research* **6**, 2050 (2017).

34. Cooper, G. M. The Golgi Apparatus. in *The Cell: A Molecular Approach* (Sinauer Associates: Sunderland (MA), 2000).

35. Arakel, E. C. & Schwappach, B. Formation of COPI-coated vesicles at a glance. *J. Cell Sci.* **131**, jcs209890 (2018).

36. Beck, R., Ravet, M., Wieland, F. T. & Cassel, D. The COPI system: Molecular mechanisms and function. *FEBS Lett.* **583**, 2701–2709 (2009).

37. Stornaiuolo, M. *et al.* KDEL and KKXX Retrieval Signals Appended to the Same Reporter Protein Determine Different Trafficking between Endoplasmic Reticulum, Intermediate Compartment, and Golgi Complex. *Mol. Biol. Cell* **14**, 889–902 (2003).

38. Goldberg, J. Structural Basis for Activation of ARF GTPase: Mechanisms of Guanine Nucleotide Exchange and GTP–Myristoyl Switching. *Cell* **95**, 237–248 (1998).

39. Ma, W. & Goldberg, J. Rules for the recognition of dilysine retrieval motifs by coatomer. *EMBO J.* **32**, 926–937 (2013).

40. De Matteis, M. A. & Luini, A. Exiting the Golgi complex. *Nat. Rev. Mol. Cell Biol.* **9**, 273–284 (2008).

41. Ponnambalam, S. & Baldwin, S. A. Constitutive protein secretion from the trans -Golgi network to the plasma membrane (Review). *Mol. Membr. Biol.* **20**, 129–139 (2003).

42. Jamora, C. Regulated secretion. *Genome Biol.* **1**, (2000).

43. Viotti, C. ER to Golgi-Dependent Protein Secretion: The Conventional Pathway. in *Unconventional Protein Secretion* vol. 1459 3–29 (Humana Press, 2016).

44. Rubartelli, A. & Sitia, R. Secretion of Mammalian Proteins that Lack a Signal Sequence. in *Unusual Secretory Pathways: From Bacteria to Man* (Springer, 1997).

45. Rabouille, C. Pathways of Unconventional Protein Secretion. *Trends Cell Biol.* **27**, 230–240 (2017).

46. Kim, J., Gee, H. Y. & Lee, M. G. Unconventional protein secretion – new insights into the pathogenesis and therapeutic targets of human diseases. *J. Cell Sci.* **131**, jcs213686 (2018).

47. Helms, J. B. & Rothman, J. E. Inhibition by brefeldin A of a Golgi membrane enzyme that catalyses exchange of guanine nucleotide bound to ARF. *Nature* **360**, 352–354 (1992).

48. Mollenhauer, H. H., James Morré, D. & Rowe, L. D. Alteration of intracellular traffic by monensin; mechanism, specificity and relationship to toxicity. *Biochim. Biophys. Acta BBA - Rev. Biomembr.* **1031**, 225–246 (1990).

49. Eilers, U., Klumperman, J. & Hauri, H. P. Nocodazole, a microtubule-active drug, interferes with apical protein delivery in cultured intestinal epithelial cells (Caco-2). *J. Cell Biol.* **108**, 13–22 (1989).

50. Zhao, L. *et al.* OutCyte: a novel tool for predicting unconventional protein secretion. *Sci. Rep.* **9**, 19448 (2019).

51. Dimou, E. & Nickel, W. Unconventional mechanisms of eukaryotic protein secretion. *Curr. Biol.* **28**, R406–R410 (2018).

52. Steringer, J. P. *et al.* Phosphatidylinositol 4,5-Bisphosphate (PI(4,5)P2)-dependent Oligomerization of Fibroblast Growth Factor 2 (FGF2) Triggers the Formation of a Lipidic Membrane Pore Implicated in Unconventional Secretion. *J. Biol. Chem.* **287**, 27659–27669 (2012).

53. Zeitler, M., Steringer, J. P., Müller, H.-M., Mayer, M. P. & Nickel, W. HIV-Tat Protein Forms Phosphoinositide-dependent Membrane Pores Implicated in Unconventional Protein Secretion. *J. Biol. Chem.* **290**, 21976–21984 (2015).

54. Legrand, C. *et al.* The Na,K-ATPase acts upstream of phosphoinositide PI(4,5)P2 facilitating unconventional secretion of Fibroblast Growth Factor 2. *Commun. Biol.* **3**, 141 (2020).

55. Agostini, S. *et al.* Inhibition of Non Canonical HIV-1 Tat Secretion Through the Cellular Na + ,K + -ATPase Blocks HIV-1 Infection. *EBioMedicine* **21**, 170–181 (2017).

56. Chang, H. C., Samaniego, F., Nair, B. C., Buonaguro, L. & Ensoli, B. HIV-1 Tat protein exits from cells via a leaderless secretory pathway and binds to extracellular matrix-associated heparan sulfate proteoglycans through its basic region: *AIDS* **11**, 1421–1431 (1997).

57. Nickel, W. The Unconventional Secretory Machinery of Fibroblast Growth Factor 2. *Traffic* **12**, 799–805 (2011).

58. La Venuta, G., Zeitler, M., Steringer, J. P., Müller, H.-M. & Nickel, W. The Startling Properties of Fibroblast Growth Factor 2: How to Exit Mammalian Cells without a Signal Peptide at Hand. *J. Biol. Chem.* **290**, 27015–27020 (2015).

59. Sparn, C. *et al.* Glypican-1 drives unconventional secretion of fibroblast growth factor 2. *eLife* **11**, e75545 (2022).

60. Martín-Sánchez, F. *et al.* Inflammasome-dependent IL-1β release depends upon membrane permeabilisation. *Cell Death Differ.* **23**, 1219–1231 (2016).

61. Latz, E., Xiao, T. S. & Stutz, A. Activation and regulation of the inflammasomes. *Nat. Rev. Immunol.* **13**, 397–411 (2013).

62. Heilig, R. *et al.* The Gasdermin-D pore acts as a conduit for IL-1β secretion in mice. *Eur. J. Immunol.* **48**, 584–592 (2018).

63. Liu, X. *et al.* Inflammasome-activated gasdermin D causes pyroptosis by forming membrane pores. *Nature* **535**, 153–158 (2016).

64. Ding, J. *et al.* Pore-forming activity and structural autoinhibition of the gasdermin family. *Nature* **535**, 111–116 (2016).

65. Katsinelos, T. *et al.* Unconventional Secretion Mediates the Trans-cellular Spreading of Tau. *Cell Rep.* **23**, 2039–2055 (2018).

66. Merezhko, M. *et al.* Secretion of Tau via an Unconventional Non-vesicular Mechanism. *Cell Rep.* **25**, 2027-2035.e4 (2018).

67. Goedert, M. *et al.* Assembly of microtubule-associated protein tau into Alzheimer-like filaments induced by sulphated glycosaminoglycans. *Nature* **383**, 550–553 (1996).

68. Holmes, B. B. *et al.* Heparan sulfate proteoglycans mediate internalization and propagation of specific proteopathic seeds. *Proc. Natl. Acad. Sci.* **110**, (2013).

69. Lolicato, F. *et al.* Cholesterol promotes clustering of PI(4,5)P2 driving unconventional secretion of FGF2. *J. Cell Biol.* **221**, e202106123 (2022).

70. Biadun, M. *et al.* Uncovering key steps in FGF12 cellular release reveals a common mechanism for unconventional FGF protein secretion. *Cell. Mol. Life Sci.* **81**, 356 (2024).

71. Locher, K. P. Structure and mechanism of ATP-binding cassette transporters. *Philos. Trans. R. Soc. B Biol. Sci.* **364**, 239–245 (2009).

72. Ketchum, C. J., Schmidt, W. K., Rajendrakumar, G. V., Michaelis, S. & Maloney, P. C. The Yeast a-factor Transporter Ste6p, a Member of the ABC Superfamily, Couples ATP Hydrolysis to Pheromone Export. *J. Biol. Chem.* **276**, 29007–29011 (2001).

73. Chen, W., Wang, S. & Xing, D. New Horizons for the Roles and Association of APE1/Ref-1 and ABCA1 in Atherosclerosis. *J. Inflamm. Res.* **Volume 14**, 5251–5271 (2021).

74. Kuchler, K. & Sterne, R. E. Saccharomyces cerevisiae STE6 gene product: a novel pathway for protein export in eukaryotic cells.

75. Claus, S., Jezierska, S. & Van Bogaert, I. N. A. Protein-facilitated transport of hydrophobic molecules across the yeast plasma membrane. *FEBS Lett.* **593**, 1508–1527 (2019).

76. Flieger, O. *et al.* Regulated secretion of macrophage migration inhibitory factor is mediated by a non-classical pathway involving an ABC transporter. *FEBS Lett.* **551**, 78–86 (2003).

77. Stegmayer, C. *et al.* Direct transport across the plasma membrane of mammalian cells of *Leishmania* HASPB as revealed by a CHO export mutant. *J. Cell Sci.* **118**, 517–527 (2005).

78. Ktistakis, N. T. & Tooze, S. A. Digesting the Expanding Mechanisms of Autophagy. *Trends Cell Biol.* **26**, 624–635 (2016).

79. Clague, M. J. & Urbé, S. Multivesicular bodies. *Curr. Biol.* **18**, R402–R404 (2008).

80. Kalluri, R. & LeBleu, V. S. The biology , function , and biomedical applications of exosomes. *Science* **367**, eaau6977 (2020).

81. Andrei, C. *et al.* The Secretory Route of the Leaderless Protein Interleukin 1b Involves Exocytosis of Endolysosome-related Vesicles.

82. Qu, Y., Franchi, L., Nunez, G. & Dubyak, G. R. Nonclassical IL-1β Secretion Stimulated by P2X7 Receptors Is Dependent on Inflammasome Activation and Correlated with Exosome Release in Murine Macrophages. *J. Immunol.* **179**, 1913–1925 (2007).

83. Zhang, M., Kenny, S. J., Ge, L., Xu, K. & Schekman, R. Translocation of interleukin-1β into a vesicle intermediate in autophagy-mediated secretion. *eLife* **4**, e11205 (2015).

84. Dupont, N. *et al.* Autophagy-based unconventional secretory pathway for extracellular delivery of IL-1β. *EMBO J.* **30**, 4701–4711 (2011).

85. Zhang, M. *et al.* A Translocation Pathway for Vesicle-Mediated Unconventional Protein Secretion. *Cell* **181**, 637-652.e15 (2020).

86. Grieve, A. G. & Rabouille, C. Golgi Bypass: Skirting Around the Heart of Classical Secretion. *Cold Spring Harb. Perspect. Biol.* **3**, a005298–a005298 (2011).

87. Kim, J. *et al.* Monomerization and ER Relocalization of GRASP Is a Requisite for Unconventional Secretion of CFTR. *Traffic* **17**, 733–753 (2016).

88. Gee, H. Y., Noh, S. H., Tang, B. L., Kim, K. H. & Lee, M. G. Rescue of ΔF508-CFTR Trafficking via a GRASP-Dependent Unconventional Secretion Pathway. *Cell* **146**, 746–760 (2011).

89. Jung, J. *et al.* The HSP70 co-chaperone DNAJC14 targets misfolded pendrin for unconventional protein secretion. *Nat. Commun.* **7**, 11386 (2016).

90. Schotman, H., Karhinen, L. & Rabouille, C. dGRASP-Mediated Noncanonical Integrin Secretion Is Required for Drosophila Epithelial Remodeling. *Dev. Cell* **14**, 171–182 (2008).

91. Tian, G. *et al.* An Unconventional Secretory Pathway Mediates the Cilia Targeting of Peripherin/rds. *J. Neurosci.* **34**, 992–1006 (2014).

92. Mohammadi, M., Olsen, S. K. & Ibrahimi, O. A. Structural basis for fibroblast growth factor receptor activation. *Cytokine Growth Factor Rev.* **16**, 107–137 (2005).

93. Eswarakumar, V. P., Lax, I. & Schlessinger, J. Cellular signaling by fibroblast growth factor receptors. *Cytokine Growth Factor Rev.* **16**, 139–149 (2005).

94. Tulin, S. & Stathopoulos, A. Extending the family table: Insights from beyond vertebrates into the regulation of embryonic development by FGFs. *Birth Defects Res. Part C Embryo Today Rev.* **90**, 214–227 (2010).

95. Popovici, C., Roubin, R., Coulier, F. & Birnbaum, D. An evolutionary history of the FGF superfamily. *BioEssays* **27**, 849–857 (2005).

96. Häcker, U., Nybakken, K. & Perrimon, N. Heparan sulphate proteoglycans: the sweet side of development. *Nat. Rev. Mol. Cell Biol.* **6**, 530–541 (2005).

97. Katoh, M. & Katoh, M. FGF signaling network in the gastrointestinal tract (Review). *Int. J. Oncol.* https://doi.org/10.3892/ijo.29.1.163 (2006) doi:10.3892/ijo.29.1.163.

98. Gospodarowicz, D. Localisation of a fibroblast growth factor and its effect alone and with hydrocortisone on 3T3 cell growth. *Nature* **249**, 123–127 (1974).

99. Gospodarowicz, D. & Moran, J. S. Mitogenic effect of fibroblast growth factor on early passage cultures of human and murine fibroblasts. *J. Cell Biol.* **66**, 451–457 (1975).

100. Gospodarowicz, D., Bialecki, H. & Greenburg, G. Purification of the fibroblast growth factor activity from bovine brain. *J. Biol. Chem.* **253**, 3736–3743 (1978).

101. Maciag, T., Cerundolo, J., Ilsley, S., Kelley, P. R. & Forand, R. An endothelial cell growth factor from bovine hypothalamus: identification and partial characterization. *Proc. Natl. Acad. Sci.* **76**, 5674–5678 (1979).

102. Prudovsky, I., Kumar, T., Sterling, S. & Neivandt, D. Protein-Phospholipid Interactions in Nonclassical Protein Secretion: Problem and Methods of Study. *Int. J. Mol. Sci.* **14**, 3734–3772 (2013).

103. Smallwood, P. M. *et al.* Fibroblast growth factor (FGF) homologous factors: new members of the FGF family implicated in nervous system development. *Proc. Natl. Acad. Sci.* **93**, 9850–9857 (1996).

104. Olsen, S. K. *et al.* Fibroblast Growth Factor (FGF) Homologous Factors Share Structural but Not Functional Homology with FGFs. *J. Biol. Chem.* **278**, 34226–34236 (2003).

105. Ornitz, D. M. & Itoh, N. The Fibroblast Growth Factor signaling pathway. *WIREs Dev. Biol.* **4**, 215–266 (2015).

106. Miyakawa, K. *et al.* A Hydrophobic Region Locating at the Center of Fibroblast Growth Factor-9 Is Crucial for Its Secretion. *J. Biol. Chem.* **274**, 29352–29357 (1999).

107. Jaye, M., Schlessinger, J. & Dionne, C. A. Fibroblast growth factor receptor tyrosine kinases: molecular analysis and signal transduction. *Biochim. Biophys. Acta BBA - Mol. Cell Res.* **1135**, 185–199 (1992).

108. Jimenez-Pascual, A., Mitchell, K., Siebzehnrubl, F. A. & Lathia, J. D. FGF2: a novel druggable target for glioblastoma? *Expert Opin. Ther. Targets* **24**, 311–318 (2020).

109. Yeh, B. K. *et al.* Structural basis by which alternative splicing confers specificity in fibroblast growth factor receptors. *Proc. Natl. Acad. Sci.* **100**, 2266–2271 (2003).

110. Kalinina, J. *et al.* The Alternatively Spliced Acid Box Region Plays a Key Role in FGF Receptor Autoinhibition. *Structure* **20**, 77–88 (2012).

111. Schlessinger, J. *et al.* Crystal Structure of a Ternary FGF-FGFR-Heparin Complex Reveals a Dual Role for Heparin in FGFR Binding and Dimerization. *Mol. Cell* **6**, 743–750 (2000).

112. Yayon, A., Klagsbrun, M., Esko, J. D., Leder, P. & Ornitz, D. M. Cell surface, heparin-like molecules are required for binding of basic fibroblast growth factor to its high affinity receptor. *Cell* **64**, 841–848 (1991).

113. Roghani, M. *et al.* Heparin increases the affinity of basic fibroblast growth factor for its receptor but is not required for binding. *J. Biol. Chem.* **269**, 3976–3984 (1994).

114. Pantoliano, M., Horlick, R. & Springer, B. Multivalent ligand-receptor binding interactions in the fibroblast growth factor system produce a cooperative growth factor and heparin mechanism for receptor dimerization. . 1994 Aug 30;33(34):10229-48. doi: 10.1021/bi00200a003. PMID: 7520751. *Biochemistry* **33**, 10229–10248 (1994).

115. Ullrich, A. & Schlessinger, J. Signal transduction by receptors with tyrosine kinase activity. *Cell* **61**, 203–212 (1990).

116. Yun, Y.-R. *et al.* Fibroblast Growth Factors: Biology, Function, and Application for Tissue Regeneration. *J. Tissue Eng.* **1**, 218142 (2010).

117. Presta, M. *et al.* Fibroblast growth factor/fibroblast growth factor receptor system in angiogenesis. *Cytokine Growth Factor Rev.* **16**, 159–178 (2005).

118. Xie, Y. *et al.* FGF/FGFR signaling in health and disease. *Signal Transduct. Target. Ther.* **5**, 181 (2020).

119. Schweigerer, L. *et al.* Capillary endothelial cells express basic fibroblast growth factor, a mitogen that promotes their own growth. *Nature* **325**, 257–259 (1987).

120. Seghezzi, G. *et al.* Fibroblast Growth Factor-2 (FGF-2) Induces Vascular Endothelial Growth Factor (VEGF) Expression in the Endothelial Cells of Forming Capillaries: An Autocrine Mechanism Contributing to Angiogenesis. *J. Cell Biol.* **141**, 1659–1673 (1998).

121. Korc, M. & Friesel, R. The Role of Fibroblast Growth Factors in Tumor Growth. *Curr. Cancer Drug Targets* **9**, 639–651 (2009).

122. Beenken, A. & Mohammadi, M. The FGF family: biology, pathophysiology and therapy. *Nat. Rev. Drug Discov.* **8**, 235–253 (2009).

123. Akl, M. R. *et al.* Molecular and clinical significance of fibroblast growth factor 2 (FGF2 /bFGF) in malignancies of solid and hematological cancers for personalized therapies. *Oncotarget* **7**, 44735–44762 (2016).

124. Bugler, B., Amalric, F. & Prats, H. Alternative Initiation of Translation Determines Cytoplasmic or Nuclear Localization of Basic Fibroblast Growth Factor. *MOL CELL BIOL*.

125. Claus, P. *et al.* Differential Intranuclear Localization of Fibroblast Growth Factor-2 Isoforms and Specific Interaction with the Survival of Motoneuron Protein. *J. Biol. Chem.* **278**, 479–485 (2003).

126. Sørensen, V., Nilsen, T. & Więdłocha, A. Functional diversity of FGF-2 isoforms by intracellular sorting. *BioEssays* **28**, 504–514 (2006).

127. Liao, S. *et al.* Biological functions of the low and high molecular weight protein isoforms of fibroblast growth factor-2 in cardiovascular development and disease. *Dev. Dyn.* **238**, 249–264 (2009).

128. Plotnikov, A. N., Hubbard, S. R., Schlessinger, J. & Mohammadi, M. Crystal Structures of Two FGF-FGFR Complexes Reveal the Determinants of Ligand-Receptor Specificity. *Cell* **101**, 413–424 (2000).

129. Kastrup, J., Eriksson, E., Dalbøge, H. & Flodgaard, H. X-ray structure of the 154-amino-acid form of recombinant human basic fibroblast growth factor. comparison with the truncated 146-amino-acid form. *Acta Crystallogr D Biol Crystallogr.* **53**, 160–168 (1997).

130. Zacherl, S. *et al.* A Direct Role for ATP1A1 in Unconventional Secretion of Fibroblast Growth Factor 2. *J. Biol. Chem.* **290**, 3654–3665 (2015).

131. Dimou, E. *et al.* Single event visualization of unconventional secretion of FGF2. *J. Cell Biol.* **218**, 683–699 (2019).

132. Schäfer, T. *et al.* Unconventional Secretion of Fibroblast Growth Factor 2 Is Mediated by Direct Translocation across the Plasma Membrane of Mammalian Cells. *J. Biol. Chem.* **279**, 6244–6251 (2004).

133. Jungnickel, B. & Kutay, U. PROTEIN TRANSPORT ACROSS THE EUKARYOTIC ENDOPLASMIC RETICULUM AND BACTERIAL INNER MEMBRANES. (2025).

134. Wienhues, U. *et al.* Protein folding causes an arrest of preprotein translocation into mitochondria in vivo. *J. Cell Biol.* **115**, 1601–1609 (1991).

135. Backhaus, R. *et al.* Unconventional protein secretion: membrane translocation of FGF-2 does not require protein unfolding. *J. Cell Sci.* **117**, 1727–1736 (2004).

136. Eilers, M. & Schatz, G. Binding of a specific ligand inhibits import of a purified precursor protein into mitochondria. *Nature* **322**, 228–232 (1986).

137. Florkiewicz, R. Z., Anchin, J. & Baird, A. The Inhibition of Fibroblast Growth Factor-2 Export by Cardenolides Implies a Novel Function for the Catalytic Subunit of Na+,K+-ATPase. *J. Biol. Chem.* **273**, 544–551 (1998).

138. Dahl, J. P., Binda, A., Canfield, V. A. & Levenson, R. Participation of Na,K-ATPase in FGF-2 Secretion: Rescue of Ouabain-Inhibitable FGF-2 Secretion by Ouabain-Resistant Na,K-ATPase α Subunits. *Biochemistry* **39**, 14877–14883 (2000).

139. Engling, A. *et al.* Biosynthetic FGF-2 is targeted to non-lipid raft microdomains following translocation to the extracellular surface of CHO cells. *J. Cell Sci.* **115**, 3619–3631 (2002).

140. Ebert, A. D. *et al.* Tec-Kinase-Mediated Phosphorylation of Fibroblast Growth Factor 2 is Essential for Unconventional Secretion. *Traffic* **11**, 813–826 (2010).

141. La Venuta, G. *et al.* Small Molecule Inhibitors Targeting Tec Kinase Block Unconventional Secretion of Fibroblast Growth Factor 2. *J. Biol. Chem.* **291**, 17787–17803 (2016).

142. Temmerman, K. *et al.* A Direct Role for Phosphatidylinositol-4,5-bisphosphate in Unconventional Secretion of Fibroblast Growth Factor 2. *Traffic* **9**, 1204–1217 (2008).

143. Zehe, C., Engling, A., Wegehingel, S., Schäfer, T. & Nickel, W. Cell-surface heparan sulfate proteoglycans are essential components of the unconventional export machinery of FGF-2. *Proc. Natl. Acad. Sci.* **103**, 15479–15484 (2006).

144. Steringer, J. P. *et al.* Key steps in unconventional secretion of fibroblast growth factor 2 reconstituted with purified components. *eLife* **6**, e28985 (2017).

145. Sparn, C. *et al.* Glypican-1 drives unconventional secretion of fibroblast growth factor 2. *eLife* **11**, e75545 (2022).

146. Müller, H.-M. *et al.* Formation of Disulfide Bridges Drives Oligomerization, Membrane Pore Formation, and Translocation of Fibroblast Growth Factor 2 to Cell Surfaces. *J. Biol. Chem.* **290**, 8925–8937 (2015).

147. Moscatelli, D. High and low affinity binding sites for basic fibroblast growth factor on cultured cells: Absence of a role for low affinity binding in the stimulation of plasminogen activator production by bovine capillary endothelial cells. *J. Cell. Physiol.* **131**, 123–130 (1987).

148. Bashkin, P. *et al.* Basic fibroblast growth factor binds to subendothelial extracellular matrix and is released by heparitinase and heparin-like molecules. *Biochemistry* **28**, 1737–1743 (1989).

149. Kaur, M., Lolicato, F. & Nickel, W. Plasma membrane transbilayer asymmetry of PI(4,5)P2 drives unconventional secretion of Fibroblast Growth Factor 2. *Nat. Commun.* **16**, 10816 (2025).

150. Skou, J. C. THE INFLUENCE OF SOME CATIONS ON AN ADENOSINE TRIPHOSPHATASE FROM PERIPHERAL NERVES.

151. Bublitz, M., Morth, J. P. & Nissen, P. P-type ATPases at a glance. *J. Cell Sci.* **124**, 3917–3917 (2011).

152. Axelsen, K. B. & Palmgren, M. G. Evolution of Substrate Specificities in the P-Type ATPase Superfamily. *J. Mol. Evol.* **46**, 84–101 (1998).

153. Pedersen, P. L. & Carafoli, E. Ion motive ATPases. I. Obiquity, properties, and significance to cell function.

154. Toyoshima, C. & Mizutani, T. Crystal structure of the calcium pump with a bound ATP analogue. *Nature* **430**, 529–535 (2004).

155. Anthonisen, A. N., Clausen, J. D. & Andersen, J. P. Mutational Analysis of the Conserved TGES Loop of Sarcoplasmic Reticulum Ca2+-ATPase. *J. Biol. Chem.* **281**, 31572–31582 (2006).

156. Gregersen, J., Mattle, D., Fedosova, N., Nissen, P. & Reinhard, L. Isolation, crystallization and crystal structure determination of bovine kidney Na+,K+-ATPase. *Acta Crystallographica Section:F Structural Biology Communications* **72**, 282–287 (2016).

157. Lopina, O. D., Tverskoi, A. M., Klimanova, E. A., Sidorenko, S. V. & Orlov, S. N. Ouabain-Induced Cell Death and Survival. Role of α1-Na,K-ATPase-Mediated Signaling and [Na+]i/[K+]i-Dependent Gene Expression. *Front. Physiol.* **11**, 1060 (2020).

158. Beggah, A. T., Jaunin, P. & Geering, K. Role of Glycosylation and Disulfide Bond Formation in the β Subunit in the Folding and Functional Expression of Na,K-ATPase. *J. Biol. Chem.* **272**, 10318–10326 (1997).

159. Tokhtaeva, E., Munson, K., Sachs, G. & Vagin, O. N-Glycan-Dependent Quality Control of the Na,K-ATPase β_2 Subunit. *Biochemistry* **49**, 3116–3128 (2010).

160. Figtree, G. A. *et al.* Reversible Oxidative Modification: A Key Mechanism of Na^+ -K^+ Pump Regulation. *Circ. Res.* **105**, 185–193 (2009).

161. Bibert, S. *et al.* FXYD Proteins Reverse Inhibition of the Na+-K+ Pump Mediated by Glutathionylation of Its β1 Subunit. *J. Biol. Chem.* **286**, 18562–18572 (2011).

162. Chow, D. & Forte, J. Functional significance of the beta-subunit for heterodimeric P-type ATPases. *The Journal of experimental biology* **198**, 1–17 (1995).

163. Chen, P.-X., Mathews, P. M., Good, P. J., Rossier, B. C. & Geering, K. Unusual degradation of α-β complexes in *Xenopus* oocytes by β-subunits of *Xenopus* gastric H-K-ATPase. *Am. J. Physiol.-Cell Physiol.* **275**, C139–C145 (1998).

164. Hilbers, F. *et al.* Tuning of the Na,K-ATPase by the beta subunit. *Sci. Rep.* **6**, 20442 (2016).

165. Noguchi, S., Mishina, M., Kawamura, M. & Numa, S. Expression of functional (Na^+ + K^+)-ATPase from cloned cDNAs. *FEBS Lett.* **225**, 27–32 (1987).

166. Horisberger, J. D., Jaunin, P., Good, P. J., Rossier, B. C. & Geering, K. Coexpression of alpha 1 with putative beta 3 subunits results in functional Na+/K+ pumps in Xenopus oocytes. *Proc. Natl. Acad. Sci.* **88**, 8397–8400 (1991).

167. Blanco, G., Koster, J. C. & Mercer, R. W. The alpha subunit of the Na,K-ATPase specifically and stably associates into oligomers. *Proc. Natl. Acad. Sci.* **91**, 8542–8546 (1994).

168. Beggah, A. T., Béguin, P., Bamberg, K., Sachs, G. & Geering, K. β-Subunit Assembly Is Essential for the Correct Packing and the Stable Membrane Insertion of the H,K-ATPase α-Subunit. *J. Biol. Chem.* **274**, 8217–8223 (1999).

169. Tokhtaeva, E., Sachs, G. & Vagin, O. Assembly with the Na,K-ATPase α_1 Subunit Is Required for Export of β_1 and β_2 Subunits from the Endoplasmic Reticulum. *Biochemistry* **48**, 11421–11431 (2009).

170. Sweadner, K. J. & Rael, E. The FXYD Gene Family of Small Ion Transport Regulators or Channels: cDNA Sequence, Protein Signature Sequence, and Expression. *Genomics* **68**, 41–56 (2000).

171. Scheiner-Bobis, G. The sodium pump: Its molecular properties and mechanics of ion transport. *Eur. J. Biochem.* **269**, 2424–2433 (2002).

172. Blanco, G. Na,K-ATPase Subunit Heterogeneity as a Mechanism for Tissue-Specific Ion Regulation. *Semin. Nephrol.* **25**, 292–303 (2005).

173. Garty, H. & Karlish, S. J. D. FXYD Proteins: Tissue-Specific Regulators of the Na,K-ATPase. *Semin. Nephrol.* **25**, 304–311 (2005).

174. Clausen, M. V., Hilbers, F. & Poulsen, H. The Structure and Function of the Na,K-ATPase Isoforms in Health and Disease. *Front. Physiol.* **8**, 371 (2017).

175. Marks, M. J. & Seeds, N. W. A heterogeneous ouabain-ATPase interaction in mouse brain. *Life Sci.* **23**, 2735–2744 (1978).

176. Shamraj, O. I. & LINGRELt, J. B. A putative fourth Na+,K+-ATPase a-subunit gene is expressed in testis.

177. Larsen, B. R. *et al.* Contributions of the Na^+ /K^+ -ATPase, NKCC1, and Kir4.1 to hippocampal K^+ clearance and volume responses. *Glia* **62**, 608–622 (2014).

178. Juhaszova, M. & Blaustein, M. P. Distinct Distribution of Different Na^+ Pump α Subunit Isoforms in Plasmalemma: Physiological Implications[a]. *Ann. N. Y. Acad. Sci.* **834**, 524–536 (1997).

179. Blom, H., Bernhem, K. & Brismar, H. Sodium pump organization in dendritic spines. *Neurophotonics* **3**, 041803 (2016).

180. Azarias, G. *et al.* A Specific and Essential Role for Na,K-ATPase α3 in Neurons Co-expressing α1 and α3. *J. Biol. Chem.* **288**, 2734–2743 (2013).

181. Hlivko, J. T., Chakraborty, S., Hlivko, T. J., Sengupta, A. & James, P. F. The human Na,K-ATPase alpha4 isoform is a ouabain-sensitive alpha isoform that is expressed in sperm. *Mol. Reprod. Dev.* **73**, 101–115 (2006).

182. Thundathil, J. C., Rajamanickam, G. D. & Kastelic, J. P. Na/K-ATPase and Regulation of Sperm Function. *Anim. Reprod.* **15**, 711–720 (2018).

183. Schneeberger, A. & Apell, H.-J. Ion Selectivity of the Cytoplasmic Binding Sites of the Na,K-ATPase: I. Sodium Binding is Associated with a Conformational Rearrangement. *J. Membr. Biol.* **168**, 221–228 (1999).

184. Stolz, M. *et al.* Structural Changes in the Catalytic Cycle of the Na+,K+-ATPase Studied by Infrared Spectroscopy. *Biophys. J.* **96**, 3433–3442 (2009).

185. Leone, F. A., Furriel, R. P. M., McNamara, J. C., Horisberger, J. D. & Borin, I. A. Cation transport coupled to ATP hydrolysis by the (Na, K)-ATPase: An integrated, animated model. *Biochem. Mol. Biol. Educ.* **38**, 276–279 (2010).

186. Castillo, J. P. *et al.* Mechanism of potassium ion uptake by the Na+/K+-ATPase. *Nat. Commun.* **6**, 7622 (2015).

187. Diefenbach, W. C. & Meneely, J. K. DIGITOXIN-A CRITICAL REVIEW.

188. Qiu, L. Y. *et al.* Reconstruction of the Complete Ouabain-binding Pocket of Na,K-ATPase in Gastric H,K-ATPase by Substitution of Only Seven Amino Acids. *J. Biol. Chem.* **280**, 32349–32355 (2005).

189. Qiu, L. Y. *et al.* Conversion of the Low Affinity Ouabain-binding Site of Non-gastric H,K-ATPase into a High Affinity Binding Site by Substitution of Only Five Amino Acids. *J. Biol. Chem.* **281**, 13533–13539 (2006).

190. Dostanic-Larson, I. *et al.* Physiological role of the α_1 - and α_2 -isoforms of the Na^+ -K^+ -ATPase and biological significance of their cardiac glycoside binding site. *Am. J. Physiol.-Regul. Integr. Comp. Physiol.* **290**, R524–R528 (2006).

191. Patel, S. Plant-derived cardiac glycosides: Role in heart ailments and cancer management. *Biomed. Pharmacother.* **84**, 1036–1041 (2016).

192. Bravený, P. Heart, calcium and time. *Exp Clin Cardiol* **7**, 3–6 (2002).

193. Kaplan, J. H. Biochemistry of Na,K-ATPase. *Annu. Rev. Biochem.* **71**, 511–535 (2002).

194. Underhill, D. A., Canfield, V. A., Dahl, J. P., Gros, P. & Levenson, R. The Na,K-ATPase α4 Gene (*Atp1a4*) Encodes a Ouabain-Resistant α Subunit and Is Tightly Linked to the α2 Gene (*Atp1a2*) on Mouse Chromosome 1. *Biochemistry* **38**, 14746–14751 (1999).

195. Haas, M., Askari, A. & Xie, Z. Involvement of Src and Epidermal Growth Factor Receptor in the Signal-transducing Function of Na+/K+-ATPase. *J. Biol. Chem.* **275**, 27832–27837 (2000).

196. Haas, M., Wang, H., Tian, J. & Xie, Z. Src-mediated Inter-receptor Cross-talk between the Na+/K+-ATPase and the Epidermal Growth Factor Receptor Relays the Signal from Ouabain to Mitogen-activated Protein Kinases. *J. Biol. Chem.* **277**, 18694–18702 (2002).

197. Yuan, Z. *et al.* Na/K-ATPase Tethers Phospholipase C and IP3 Receptor into a Calcium-regulatory Complex. *Mol. Biol. Cell* **16**, 4034–4045 (2005).

198. Aizman, O. & Aperia, A. Na,K-ATPase as a Signal Transducer. *Ann. N. Y. Acad. Sci.* **986**, 489–496 (2003).

199. Wang, H. *et al.* Ouabain Assembles Signaling Cascades through the Caveolar Na+/K+-ATPase. *J. Biol. Chem.* **279**, 17250–17259 (2004).

200. Tian, J. *et al.* Binding of Src to Na^+ /K^+ -ATPase Forms a Functional Signaling Complex. *Mol. Biol. Cell* **17**, 317–326 (2006).

201. Liu, L., Abramowitz, J., Askari, A. & Allen, J. C. Role of caveolae in ouabain-induced proliferation of cultured vascular smooth muscle cells of the synthetic phenotype. *Am. J. Physiol.-Heart Circ. Physiol.* **287**, H2173–H2182 (2004).

202. Wang, X. Q. *et al.* Apoptotic insults impair Na+, K+-ATPase activity as a mechanism of neuronal death mediated by concurrent ATP deficiency and oxidant stress. *J. Cell Sci.* **116**, 2099–2110 (2003).

203. Zhang, S. *et al.* Distinct Role of the N-terminal Tail of the Na,K-ATPase Catalytic Subunit as a Signal Transducer. *J. Biol. Chem.* **281**, 21954–21962 (2006).

204. Liang, M., Cai, T., Tian, J., Qu, W. & Xie, Z.-J. Functional Characterization of Src-interacting Na/K-ATPase Using RNA Interference Assay. *J. Biol. Chem.* **281**, 19709–19719 (2006).

205. Li, J., Zelenin, S., Aperia, A. & Aizman, O. Low Doses of Ouabain Protect from Serum Deprivation–Triggered Apoptosis and Stimulate Kidney Cell Proliferation via Activation of NF-κB. *J. Am. Soc. Nephrol.* **17**, 1848–1857 (2006).

206. Xie, Z. & Askari, A. Na^+ /K^+ -ATPase as a signal transducer. *Eur. J. Biochem.* **269**, 2434–2439 (2002).

207. Liu, J. *et al.* Ouabain Interaction with Cardiac Na+/K+-ATPase Initiates Signal Cascades Independent of Changes in Intracellular Na+ and Ca2+ Concentrations. *J. Biol. Chem.* **275**, 27838–27844 (2000).

208. White, C. N. *et al.* Activation of cAMP-dependent Signaling Induces Oxidative Modification of the Cardiac Na+-K+ Pump and Inhibits Its Activity. *J. Biol. Chem.* **285**, 13712–13720 (2010).

209. Liu, C.-C. *et al.* Susceptibility of β1 Na+-K+ Pump Subunit to Glutathionylation and Oxidative Inhibition Depends on Conformational State of Pump. *J. Biol. Chem.* **287**, 12353–12364 (2012).

210. Yan, Y. *et al.* Protein Carbonylation of an Amino Acid Residue of the Na/K-ATPase α1 Subunit Determines Na/K-ATPase Signaling and Sodium Transport in Renal Proximal Tubular Cells. *J. Am. Heart Assoc.* **5**, e003675 (2016).

211. Segall, L., Javaid, Z. Z., Carl, S. L., Lane, L. K. & Blostein, R. Structural Basis for α1 Versus α2 Isoform-distinct Behavior of the Na,K-ATPase. *J. Biol. Chem.* **278**, 9027–9034 (2003).

212. Cherniavsky-Lev, M., Golani, O., Karlish, S. J. D. & Garty, H. Ouabain-induced Internalization and Lysosomal Degradation of the Na+/K+-ATPase. *J. Biol. Chem.* **289**, 1049–1059 (2014).

213. Van Meer, G., Voelker, D. R. & Feigenson, G. W. Membrane lipids: where they are and how they behave. *Nat. Rev. Mol. Cell Biol.* **9**, 112–124 (2008).

214. Shimizu, T. Lipid Mediators in Health and Disease: Enzymes and Receptors as Therapeutic Targets for the Regulation of Immunity and Inflammation. *Annu. Rev. Pharmacol. Toxicol.* **49**, 123–150 (2009).

215. Nakamura, M. T., Yudell, B. E. & Loor, J. J. Regulation of energy metabolism by long-chain fatty acids. *Prog. Lipid Res.* **53**, 124–144 (2014).

216. Yamashita, A. *et al.* Acyltransferases and transacylases that determine the fatty acid composition of glycerolipids and the metabolism of bioactive lipid mediators in mammalian cells and model organisms. *Prog. Lipid Res.* **53**, 18–81 (2014).

217. Balla, T. Phosphoinositides: Tiny Lipids With Giant Impact on Cell Regulation. *Physiol. Rev.* **93**, 1019–1137 (2013).

218. Jiang, Z., Redfern, R. E., Isler, Y., Ross, A. H. & Gericke, A. Cholesterol stabilizes fluid phosphoinositide domains. *Chem. Phys. Lipids* **182**, 52–61 (2014).

219. Laux, T. *et al.* Gap43, Marcks, and Cap23 Modulate Pi(4,5)p2 at Plasmalemmal Rafts, and Regulate Cell Cortex Actin Dynamics through a Common Mechanism. *J. Cell Biol.* **149**, 1455–1472 (2000).

220. Stahelin, R. V., Scott, J. L. & Frick, C. T. Cellular and molecular interactions of phosphoinositides and peripheral proteins. *Chem. Phys. Lipids* **182**, 3–18 (2014).

221. Honigmann, A. *et al.* Phosphatidylinositol 4,5-bisphosphate clusters act as molecular beacons for vesicle recruitment. *Nat. Struct. Mol. Biol.* **20**, 679–686 (2013).

222. Levental, I. *et al.* Calcium-Dependent Lateral Organization in Phosphatidylinositol 4,5-Bisphosphate (PIP2)- and Cholesterol-Containing Monolayers. *Biochemistry* **48**, 8241–8248 (2009).

223. Rusinova, R., Hobart, E. A., Koeppe, R. E. & Andersen, O. S. Phosphoinositides alter lipid bilayer properties. *J. Gen. Physiol.* **141**, 673–690 (2013).

224. Lolicato, F., Nickel, W., Haucke, V. & Ebner, M. Phosphoinositide switches in cell physiology - From molecular mechanisms to disease. *J. Biol. Chem.* **300**, 105757 (2024).

225. Vance, D. E. & Vance, J. E. Biochemistry of lipids, lipoproteins, and membranes.

226. Crane, J. M. & Tamm, L. K. Role of Cholesterol in the Formation and Nature of Lipid Rafts in Planar and Spherical Model Membranes. *Biophys. J.* **86**, 2965–2979 (2004).

227. Ikonen, E. Cellular cholesterol trafficking and compartmentalization. *Nat. Rev. Mol. Cell Biol.* **9**, 125–138 (2008).

228. Ohvo-RekilÃ¤, H. Cholesterol interactions with phospholipids in membranes. *Prog. Lipid Res.* **41**, 66–97 (2002).

229. Radhakrishnan, A. & McConnell, H. M. Chemical Activity of Cholesterol in Membranes. *Biochemistry* **39**, 8119–8124 (2000).

230. Lange, Y., Ye, J. & Steck, T. L. How cholesterol homeostasis is regulated by plasma membrane cholesterol in excess of phospholipids. *Proc. Natl. Acad. Sci.* **101**, 11664–11667 (2004).

231. Yeagle, P. L. Modulation of membrane function by cholesterol. *Biochimie* **73**, 1303–1310 (1991).

232. Haines, T. H. Do sterols reduce proton and sodium leaks through lipid bilayers? *Prog. Lipid Res.* **40**, 299–324 (2001).

233. De Boer, J. F., Kuipers, F. & Groen, A. K. Cholesterol Transport Revisited: A New Turbo Mechanism to Drive Cholesterol Excretion. *Trends Endocrinol. Metab.* **29**, 123–133 (2018).

234. Rajendran, L. & Simons, K. Lipid rafts and membrane dynamics. *J. Cell Sci.* **118**, 1099–1102 (2005).

235. Carter, H. E., Glick, F. J., Norris, W. P. & Phillips, G. E. BIOCHEMISTRY OF THE SPHINGOLIPIDES. *J. Biol. Chem.* **170**, 285–294 (1947).

236. Gault, C., Obeid, L. & Hannun, Y. An Overview of Sphingolipid Metabolism: From Synthesis to Breakdown. in *Sphingolipids as Signaling and Regulatory Molecules* vol. 688 (Advances in Experimental Medicine and Biology, 2010).

237. Ichikawa, S. Expression cloning of a cDNA for human ceramide glucosyltransferase that catalyzes the first glycosylation step of glycosphingolipid synthesis.

238. Breiden, B. & Sandhoff, K. Ganglioside Metabolism and Its Inherited Diseases. in *Gangliosides: Methods and Protocols* (Springer, 2018).

239. Suzuki, J., Umeda, M., Sims, P. J. & Nagata, S. Calcium-dependent phospholipid scrambling by TMEM16F. *Nature* **468**, 834–838 (2010).

240. Parton, R. G. & Simons, K. Digging into Caveolae. *Science* **269**, 1398–1399 (1995).

241. Simons, K. & Van Meer, G. Lipid sorting in epithelial cells. *Biochemistry* **27**, 6197–6202 (1988).

242. Brown, D. & Rose, J. Sorting of GPI-anchored proteins to glycolipid-enriched membrane subdomains during transport to the apical cell surface. Cell 68, 533–544 (1992). *Cell* **68**, 533–544 (1992).

243. Simons, K. & Ikonen, E. Functional rafts in cell membranes. *Nature* **387**, 569–572 (1997).

244. Cebecauer, M. *et al.* Membrane Lipid Nanodomains. *Chem. Rev.* **118**, 11259–11297 (2018).

245. Sezgin, E., Levental, I., Mayor, S. & Eggeling, C. The mystery of membrane organization: composition, regulation and roles of lipid rafts. *Nat. Rev. Mol. Cell Biol.* **18**, 361–374 (2017).

246. Fantini, J., Garmy, N., Mahfoud, R. & Yahi, N. Lipid rafts: structure, function and role in HIV, Alzheimer's and prion diseases. *Expert Rev. Mol. Med.* **4**, 1–22 (2002).

247. Sargiacomo, M. & Sudol, M. Signal Transducing Molecules and Glycosyl-phosphatidylinositoMinked Proteins Form a Caveolin-rich Insoluble Complex in MDCK Cells.

248. Danielsen, E. M. & Van Deurs, B. A transferrin-like GPI-linked iron-binding protein in detergent-insoluble noncaveolar microdomains at the apical surface of fetal intestinal epithelial cells. *J. Cell Biol.* **131**, 939–950 (1995).

249. Chatterjee, S. & Mayor, S. The GPI-anchor and protein sorting: *Cell. Mol. Life Sci.* **58**, 1969–1987 (2001).

250. Simons, K. & Toomre, D. Lipid rafts and signal transduction. *Nat. Rev. Mol. Cell Biol.* **1**, 31–39 (2000).

251. Rajendran, L. *et al.* Asymmetric localization of flotillins/reggies in preassembled platforms confers inherent polarity to hematopoietic cells. *Proc. Natl. Acad. Sci.* **100**, 8241–8246 (2003).

252. Lucero, H. A. & Robbins, P. W. Lipid rafts–protein association and the regulation of protein activity. *Arch. Biochem. Biophys.* **426**, 208–224 (2004).

253. Lolicato, F. & Nickel, W. A Role for Liquid-Ordered Plasma Membrane Nanodomains Coordinating the Unconventional Secretory Pathway of Fibroblast Growth Factor 2? *Front. Cell Dev. Biol.* **10**, 864257 (2022).

254. Sparn, C., Meyer, A., Saleppico, R. & Nickel, W. Unconventional secretion mediated by direct protein self-translocation across the plasma membranes of mammalian cells. *Trends Biochem. Sci.* **47**, 699–709 (2022).

255. Müller, H.-M. *et al.* Formation of Disulfide Bridges Drives Oligomerization, Membrane Pore Formation, and Translocation of Fibroblast Growth Factor 2 to Cell Surfaces. *J. Biol. Chem.* **290**, 8925–8937 (2015).

256. Lolicato, F. *et al.* Disulfide bridge-dependent dimerization triggers FGF2 membrane translocation into the extracellular space. *eLife* **12**, RP88579 (2024).

257. Davis, M. W. & Jorgensen, E. M. ApE, A Plasmid Editor: A Freely Available DNA Manipulation and Visualization Program. *Front. Bioinforma.* **2**, 818619 (2022).

258. Schindelin, J. *et al.* Fiji: an open-source platform for biological-image analysis. *Nat. Methods* **9**, 676–682 (2012).

259. Urlinger, S. *et al.* Exploring the sequence space for tetracycline-dependent transcriptional activators: Novel mutations yield expanded range and sensitivity. *Proc. Natl. Acad. Sci.* **97**, 7963–7968 (2000).

260. Albritton, L. M., Tseng, L., Scadden, D. & Cunningham, J. M. A putative murine ecotropic retrovirus receptor gene encodes a multiple membrane-spanning protein and confers susceptibility to virus infection. *Cell* **57**, 659–666 (1989).

261. Imamura, H. *et al.* Visualization of ATP levels inside single living cells with fluorescence resonance energy transfer-based genetically encoded indicators. *Proc. Natl. Acad. Sci.* **106**, 15651–15656 (2009).

262. Spannl, S. *et al.* Glycolysis regulates Hedgehog signalling via the plasma membrane potential. *EMBO J.* **39**, e101767 (2020).

263. Mattheyses, A. L., Simon, S. M. & Rappoport, J. Z. Imaging with total internal reflection fluorescence microscopy for the cell biologist. *J. Cell Sci.* **123**, 3621–3628 (2010).

264. Tinevez, J.-Y. *et al.* TrackMate: An open and extensible platform for single-particle tracking. *Methods* **115**, 80–90 (2017).

265. Zacharias, D. A., Violin, J. D., Newton, A. C. & Tsien, R. Y. Partitioning of Lipid-Modified Monomeric GFPs into Membrane Microdomains of Live Cells. *Science* **296**, 913–916 (2002).

266. Ulbrich, M. H. & Isacoff, E. Y. Subunit counting in membrane-bound proteins. *Nat. Methods* **4**, 319–321 (2007).

267. Subburaj, Y. *et al.* Bax monomers form dimer units in the membrane that further self-assemble into multiple oligomeric species. *Nat. Commun.* **6**, 8042 (2015).

268. Griffo, A. *et al.* Nanoscale PI(4,5)P2 partitioning driven by FGF2 oligomerization triggers membrane pore formation.

269. Winkelmann, H., Richter, C. P., Eising, J., Piehler, J. & Kurre, R. Correlative single-molecule and structured illumination microscopy of fast dynamics at the plasma membrane. *Nat. Commun.* **15**, 5813 (2024).

270. Danial, J. S. H. *et al.* Systematic Assessment of the Accuracy of Subunit Counting in Biomolecular Complexes Using Automated Single-Molecule Brightness Analysis. *J. Phys. Chem. Lett.* **13**, 822–829 (2022).

271. López-Lastra, M., Rivas, A. & Barría, M. I. Protein synthesis in eukaryotes: The growing biological relevance of cap-independent translation initiation. *Biol. Res.* **38**, (2005).

272. Liu, Z. *et al.* Systematic comparison of 2A peptides for cloning multi-genes in a polycistronic vector. *Sci. Rep.* **7**, 2193 (2017).

273. Decker, C. G. *et al.* Fibroblast growth factor 2 dimer with superagonist in vitro activity improves granulation tissue formation during wound healing. *Biomaterials* **81**, 157–168 (2016).

274. Nawrocka, D., Krzyscik, M. A., Opaliński, Ł., Zakrzewska, M. & Otlewski, J. Stable Fibroblast Growth Factor 2 Dimers with High Pro-Survival and Mitogenic Potential. *Int. J. Mol. Sci.* **21**, 4108 (2020).

275. Florkiewicz, R. Z., Majack, R. A., Buechler, R. D. & Florkiewicz, E. Quantitative export of FGF-2 occurs through an alternative, energy-dependent, non-ER/Golgi pathway. *J. Cell. Physiol.* **162**, 388–399 (1995).

276. Voet, D. & Voet, J. G. ATP-Driven Active Transport. in *Biochemistry* (John Wiley & Sons, 2010).

277. Liang, X., Lu, Y., Wilkes, M., Neubert, T. A. & Resh, M. D. The N-terminal SH4 Region of the Src Family Kinase Fyn Is Modified by Methylation and Heterogeneous Fatty Acylation. *J. Biol. Chem.* **279**, 8133–8139 (2004).

278. Zehe, C., Engling, A., Wegehingel, S., Schäfer, T. & Nickel, W. Cell-surface heparan sulfate proteoglycans are essential components of the unconventional export machinery of FGF-2. *Proc. Natl. Acad. Sci.* **103**, 15479–15484 (2006).

279. Rawat, A. & Nagaraj, R. Determinants of membrane association in the SH4 domain of Fyn: Roles of N-terminus myristoylation and side-chain thioacylation. *Biochim. Biophys. Acta BBA - Biomembr.* **1798**, 1854–1863 (2010).

280. Šachl, R. *et al.* Functional Assay to Correlate Protein Oligomerization States with Membrane Pore Formation. *Anal. Chem.* **92**, 14861–14866 (2020).

281. Figtree, G. A., Keyvan Karimi, G., Liu, C.-C. & Rasmussen, H. H. Oxidative regulation of the Na+–K+ pump in the cardiovascular system. *Free Radic. Biol. Med.* **53**, 2263–2268 (2012).

282. Boldyrev, A., Bulygina, E., Yuneva, M. & Schoner, W. Na/K-ATPase Regulates Intracellular ROS Level in Cerebellum Neurons. *Ann. N. Y. Acad. Sci.* **986**, 519–521 (2003).

283. Zhang, H., Lai, F., Cheng, X. & Wang, Y. Involvement of NADPH oxidases in the Na/K-ATPase/Src/ROS oxidant amplification loop in renal fibrosis. *Mol. Med. Rep.* **28**, 161 (2023).